Design of a conveyance device based on a digital actuators array and structured plate

Jing Xu

Par **Jing XU**

Design of a conveyance device based on a digital actuators array and structured plate

Thèse présentée
pour l'obtention du grade
de Docteur de l'UTC

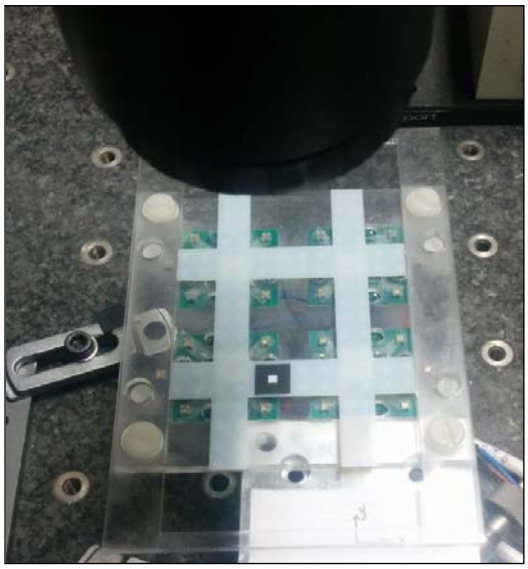

Soutenue le 17 mai 2016
Spécialité : Advanced Mechanics

D2273

PhD THESIS
Submitted of the degree of
DOCTOR
in
UNIVERSITÉ DE TECHNOLOGIE DE COMPIÈGNE

Speciality: Advanced Mechanics
by
Jing XU

Design of a conveyance device based on a digital actuators array and structured plate

17 may 2016

Yassine Haddab
Professeur à l'Université de Montpellier (Rapporteur)

Jacques Lottin
Professeur à l'Université de Savoie Mont Blanc, Polytech Annecy-Chambéry, Annecy (Rapporteur)

Michaël Gauthier
Directeur de Recherche, FEMTO-ST, Besançon (Examinateur)

Emmanuel Doré
Maître de conférences à l'Université de Technologie de Compiègne (Examinateur)

Laurent Petit
Maître de conférences à l'Université de Technologie de Compiègne (Co-encadrant de Thèse)

Christine Prelle
Professeur à l'Université de Technologie de Compiègne (Directrice de Thèse)

Laboratoire Roberval, UMR 7337, UTC / CNRS

Thèse Présentée pour obtenir le
grade de DOCTEUR
De
UNIVERSITÉ DE TECHNOLOGIE DE COMPIÈGNE

Spécialité Mécanique Avancée

Par
Jing XU

Conception d'un système de déplacement basé sur un réseau d'actionneurs numériques et d'un plateau structuré

17 mai 2016

Yassine Haddab
Professeur à l'Université de Montpellier (Rapporteur)

Jacques Lottin
Professeur à l'Université de Savoie Mont Blanc, Polytech Annecy-Chambéry, Annecy (Rapporteur)

Michaël Gauthier
Directeur de Recherche, FEMTO-ST, Besançon (Examinateur)

Emmanuel Doré
Maître de conférences à l'Université de Technologie de Compiègne (Examinateur)

Laurent Petit
Maître de conférences à l'Université de Technologie de Compiègne (Co-encadrant de Thèse)

Christine Prelle
Professeur à l'Université de Technologie de Compiègne (Directrice de Thèse)

Laboratoire Roberval, UMR 7337, UTC / CNRS

Acknowledgement

Firstly, I would like to express my sincere gratitude to my PhD supervisor Pr. Christine Prelle and Mr. Laurent Petit for their continuous support of my Ph.D study and related research, for their patience, motivation and immense knowledge. Their guidance helped me in all the time of research and the completion of this thesis.

I would also like to thank all the members of the jury (Pr. Yassine Haddab, Pr. Jacques Lottin, Mr. Michaël Gauthier, Mr. Emmanuel Doré). Thanks for their valuable time and advices.

My sincere thanks also goes to Dr. Erwan Dupont, Dr. Muneeb Khan, Mr. Phillipe Pouille and all the other staff members of Laboratoire Roberval to provide me their precious support and advices.

I have to thank my colleagues and my friends, Xingxing Liu, Yinfan HOU, Zeina El Rawashdeh, Neha ARORA, Zineb Yanha etc. We have passed four years togoter as a family, thanks for their kindly help and spiritual support.

At last, I owe my gratitude to my family, especially, to my husband, Qiaochu Li, for their support, their help, and their encouragement to finish my thesis.

Table of contents

Introduction

Nowadays, mechanical and mechatronical systems tend to become more compact and complex due to the need of increasing functionalities with reduced size. To add functionalities in these systems, actuators and sensors are generally integrated to ensure high reliability level. Classical integrated actuators are based on analogical principle. These actuators can reach any position between the extreme positions of their stroke. They are generally controlled in closed loop with sensory components to ensure high performances. However, in case of compact or highly integrated systems, the added sensory components make the integration of these functionalities complex or not always possible. The control also becomes more difficult to be implemented. Moreover, continuous energy supply is necessary to keep the mobile part in a given position to counteract disturbances. The continuous supplied energy can also generate heating or deterioration of the system.

An alternative to these actuators can be found with the use of digital actuators. Digital actuators are composed of a mobile part which can switch between several precise and repeatable discrete positions. All the intermediate positions, located between the discrete positions, correspond only to transient states which cannot be held in normal functioning. The control of these actuators is very simple and realized in open loop without feedback sensors. The integration of these actuators in mechatronical system becomes then much easier. To switch the mobile part between the discrete positions, energy pulses are only needed and no external energy is consumed to hold the mobile part in discrete position. The energy consumption of digital actuators is then minimized. However, the main drawback of digital actuators is their discrete strokes defined during the manufacturing step. Using several digital actuators, variable strokes can however be obtained. Another important property of digital actuator is that the manufacturing quality of these actuators is very important because manufacturing errors cannot be compensated using the control as for analogical actuators.

In previous work realized in Roberval laboratory of the Université de Technologie de Compiègne, a digital electromagnetic actuator has been studied and developed [PETI 2009]. The architecture composed of four discrete positions distributed in the plane represents the main originality of this actuator. In this thesis, a single digital actuator has been firstly designed, simulated and manufactured. Then, the performances of an experimental digital actuator have been characterized (switching time along two displacement axes, energy consumption,

positioning repeatability error, displaceable mass, etc.). In this study, a good accordance has been observed between simulated and experimental results. An array composed of 25 elementary actuators arranged in 5 × 5 matrix has then been designed. During the designing step, the magnetic and electromagnetic interactions between the elementary actuators have been considered. Based on this design, a prototype of the array has been manufactured and assembled.

In the continuity of this thesis, another thesis focused on the characterization of the existing actuators array and its application to realize a planar conveyance device has been realized by P. Huyan [HUYA 2015]. In this thesis, a static model of the actuators array has been simulated and the planar conveyance application, based on a flat plate placed above the actuators array, has been proved. The influence of some parameters (controlling currents value and form, conveyed mass, etc.) on the conveyance task has been quantified. Then, an optimization of the actuators array design has been realized using genetic algorithm in order to obtain a new actuators array design which maximize the performances and minimize its size.

This present thesis is a continuation of the two previous theses and has two main objectives. Firstly, a dynamic model of the conveyance application studied in the thesis of P. Huyan has been carried out and compared with experimental results. In previous work, the planar conveyance device has been realized with a flat plate. The second objective was to design a new planar conveyance device based on actuators array with a structured plate in order to reduce the sliding between the conveyed plate and the fixed part of the device. The present thesis is divided into five chapters.

In the first chapter, a state of art of digital actuation is proposed. A definition and the properties of digital actuators are firstly given. Then, the switching and holding functions are described and the technical solutions and physical principles used in literature to obtain these functions are described. Then, applications of digital actuators are presented.

The purpose of the second chapter is to present the dynamic model of the planar conveyance with a flat plate based on the existing actuators array. The principles of elementary digital actuator and actuators array are firstly presented. The dynamic model is then described and simulation results obtained in different conditions are shown. Finally, simulation and experimental results are compared.

In the third chapter, a new planar conveyance device is proposed and designed based on an actuators array with a structured plate. Firstly, the elementary digital actuator is presented and designed. Then, an actuators array is sized considering the magnetic and electromagnetic effects. Finally, a 3D model of the device is presented.

The objective of the forth chapter is to experimentally validate the conveyance application of the proposed device. The manufacturing of a prototype is firstly presented. Then, the control system is described. Finally, experimental and theoretical results are presented and compared.

In the fifth chapter, a conclusion of the work realized in this thesis is given. Then, perspectives in several aspects are proposed.

Chapter 1: State of the art of digital actuator

The work presented in this thesis is focused on the study of a planar conveyance device based on a digital actuators array (DAA). In the first chapter, a literature review in the field of digital actuation is then realized. Firstly, a definition of the digital actuation is given then a classification of the digital actuators is proposed. The two key functions of digital actuators are then presented, switching and holding, and the solutions to realize these functions are described. Finally, the applications of digital actuators correspond to different functions are presented.

I.1 Introduction

I.1.1 Digital actuator

Mechatronic systems become more and more complex because they integrate an increased number of features. These features are generally obtained by integrating sensors or actuators. In case of advanced features, the classical actuators used are based on an analogical behavior. They can realize continuous actions within their working stroke limits (Figure I- 1). In order to achieve a high performance level, a closed loop control is generally used to reach precisely and rapidly the objectives. An advantage of the closed loop control is that the manufacturing errors of the actuators can be compensated using correction factors. Furthermore, to hold the mobile part in a given position and to limit the influence of external disturbances, analogical actuators generally need to be continuously supplied. However, due to the control theory, the integration of sensors is needed, which makes the control of analogical actuators become very complex to ensure high performances.

An alternative to analogical actuators can be found with digital actuators. Digital actuators are composed of a mobile part which can switch between several precise and repeatable discrete positions (Figure I- 1). During the switching between two discrete positions, the intermediate positions between the discrete positions are only transient positions that cannot be kept by the mobile part. Due to the working principle of digital actuators, energy is only needed to switch the mobile part between the discrete positions. The control of these actuators is then very simple and realized in open loop using energy pulses without feedback sensors because the discrete positions are well known and repeatable. The unnecessary of sensors makes system integration much more convenient as compared to analogical actuators. Moreover, energy consumption is united because energy pulses are only needed to switch the mobile part and no energy is consumed to hold it in discrete positions. The main drawback of digital actuators is their stroke

fixed at the manufacturing step. Large strokes can however be found by assembling several digital actuators. A crucial point is the need of a high manufacturing quality to ensure the performances of digital actuators (e.g. the stroke value). A manufacturing error can indeed not be compensated using the simple control of digital actuators. The comparison between the analog actuators and digital actuators is given in Table I- 1.

There are two parts of the objectives of this thesis. Firstly, the work is the continuation of the previous model based on the 25 DAA with a flat plate. Then, a new model based on DAA with a structured plate is designed and studied. The following parts of this chapter will focus on the literatures related to digital actuators, including the actuation principles and the applications.

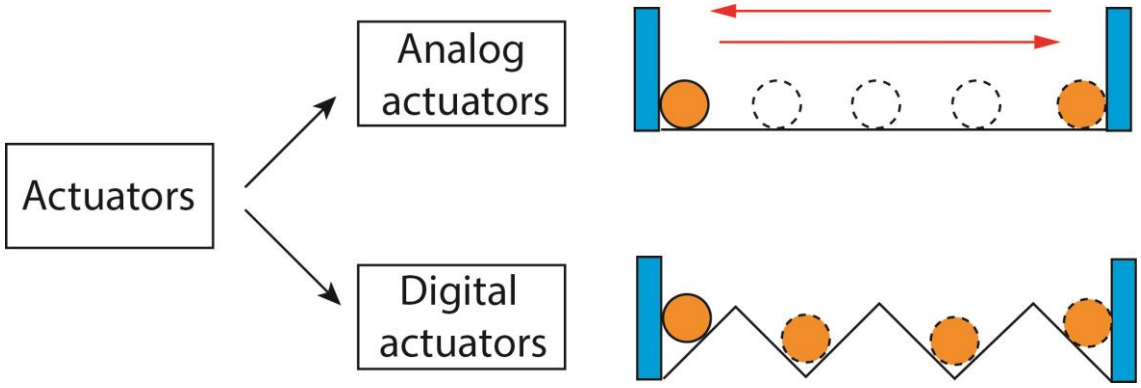

Figure I- 1 : Illustration of analog actuator and digital actuator

Table I- 1: Comparison between analog and digital actuators

Properties	Analogical actuators	Digital actuators
Stroke	Continuous	Discrete / Multi-discrete
Manufacturing constraints	Low	High
Control	May be complex	Simple
Need of sensors	Yes (closed loop control)	No (open loop control)
Integration	May be complex	Simple
Energy consumption	Continuous supply	Pulsed mode control

I.2 Actuation principles and applications

In digital actuators, two main functions are needed: the switching and the holding functions. The switching function ensures the switching of the mobile part between the discrete positions thanks to energy supply. The holding function ensures the holding of the mobile part in discrete position without energy input. In the next paragraphs, the solutions used in literature to obtain these two functions are described.

I.2.1 Switching function

The switching function produces a driving exerted on the mobile part to switch it between the discrete positions. According to the literature, the switching function can be obtained thanks to several physical principles: electrothermal, electrostratic, electromagnetic and piezoelectric.

I.2.1.1 Electrothermal principle

An electrothermal driving force can be generated using several techniques. The main techniques are increasing the pressure due to a temperature increase to generate thermal expansion by membrane, by bimetal or bimorph actuators on one hand, and using actuators made of Shape Memory Alloys (SMA) on the other hand.

I.2.1.1.1 Membrane actuation

Digital actuators based on a membrane actuation are equipped with either an integrated electrical resistive heater or an external heat source to increase the temperature of the entrapped gas or liquids in a sealed cavity. The active element is a membrane or a diaphragm which is deflected upon expansion/contraction of the gas or liquids when temperature increases or decreases, respectively.

Based on this principle, a phase-change valve has been developed by Song *et al*. [SONG 2007]. This digital actuator has two heating and cooling thermoelectric modules. The cooling and heating modules are located on the top and bottom sides, respectively. When a positive charge is applied to the lower thermoelectric module, the working fluid is heated to evaporate from liquid into vapor phase within the sealed cavity. The increasing evaporation raises the pressure of the vapors which moves the bistable membrane to the upper position. When a negative charge is applied to the lower and upper thermoelectric modules, the fluid becomes cool. Decrease in temperature condensates vapors to liquid. As a result, the membrane switches to the lower position. This device prototype has been fabricated with membrane made of 100 µm polyethylene terephthalate film and 30 mm×30 mm×8 mm sealed cavity (Figure I- 2(a)).

Unlike the previous thermal actuator that is actuated with liquid, Goll *et al*. [GOLL 1996] have used air to move the membrane. The valve is composed of a resistive heater, an actuator chamber, a fluid chamber, an inlet and an outlet. A swing polyimide diaphragm is placed between the actuator chamber and the fluid chamber. If the resistive heater is supplied the temperature increases due to Joule effect that generates an expansion of the trapped air in the

actuator chamber. The membrane can be switched from open position to closed position by increasing the pressure of air in the actuator chamber and vice versa (Figure I- 2 (b)).

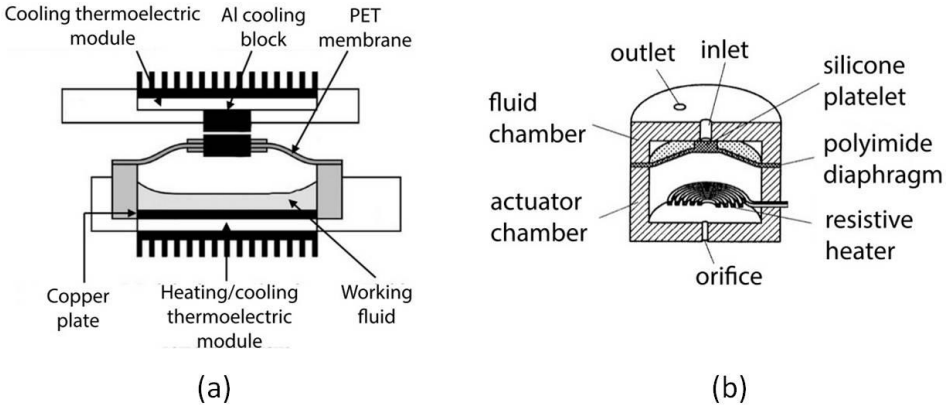

Figure I- 2 : Thermal actuator with bistable membrane: (a) [SONG 2007] (b) [GOLL 1996]

Based on the thermal actuation principle, Wijngaart *et al*. [WIJN 2006] have designed a new micro valve with a thermo-pneumatic gas bubble (Figure I- 3). The device is equipped with a resistive heater which is used for thermo-pneumatic actuation. An air pocket is trapped in the actuation chamber (Figure I- 3(a)). When the temperature rises, the air in the actuation chamber inflates, the pressure of the gas increases to introduce a gas bubble into the liquid channel, which blocks the flow of the liquid (Figure I- 3(b)).

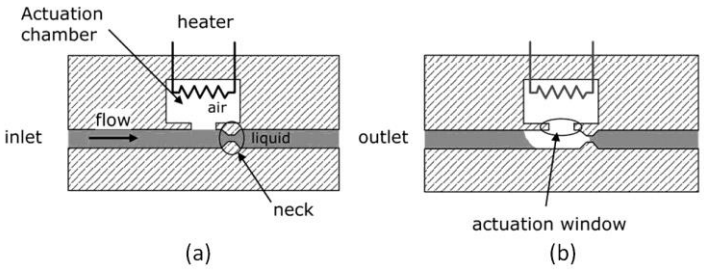

Figure I- 3: Thermo-pneumatic gas bubble valve [WIJN 2006]

I.2.1.1.2 Bimetal thermal actuator

Electrothermal driving force can also be generated using different coefficients of thermal expansion of materials. In this way, a beam composed of two same sized layers assembled together can be considered (Figure I- 4). When the beam is heated, the layer composed of the material with the higher thermal expansion coefficient will expand more as compared with the other one. A force can then be generated. This kind of actuator is called bimetal actuator.

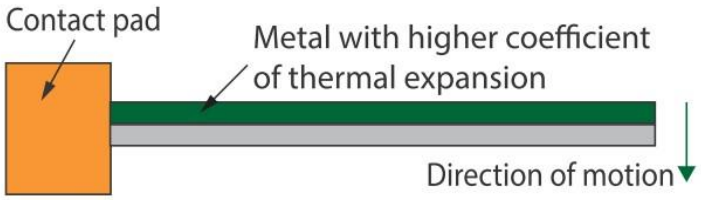

Figure I- 4: Principle of bimetal thermal actuator

Based on this principle, Mao *et al*. [MAO 2010] have developed a bistable micro switch based on a dual-beam structure. The bistable micro switch is composed of two identical bimorph electrothermal actuators, conductive electric and metal contacts pair and a separation block to keep the two contacts apart from each other initially. The bottom and top layers of the bimorph actuator are made of silicon oxide and nickel, respectively. According to Figure I- 5, this bistable micro switch can stay latched in two states (ON and OFF states) and power is only needed to change the state. At first, the switch is OFF (Figure I- 5 (a)), then the actuator A (placed at the left) is heated, it bends down and the left contact goes below the right contact (Figure I- 5 (b)). After cooling actuator A, the contact pair overlaps each other, the switch is at ON state (Figure I- 5 (c)). Similarly, when the actuator B (placed at the right) is heated, the right contact goes below the left upper contact (Figure I- 5 (d)). The switch switches then from ON to OFF state (Figure I- 5 (e)). The tip deflection of actuators is about 50 µm and the total actuation force is about 2 mN.

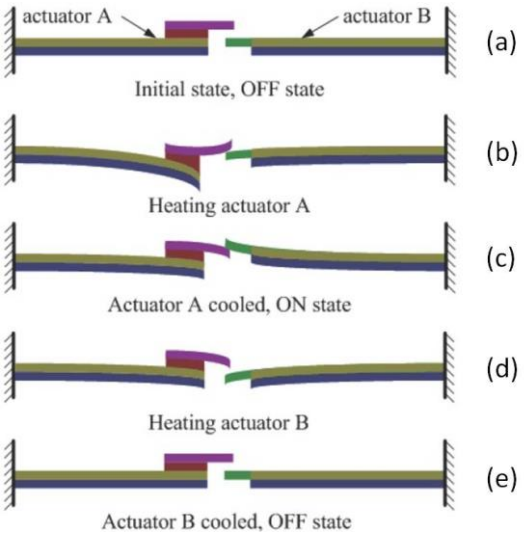

Figure I- 5: An electrothermal dual-beam bistable micro switch [MAO 2010]

I.2.1.1.3 Bimorph thermal actuator

A bimorph actuator is another type of electrothermal actuation which consists of two metallic arms (made with the same material) with different widths as shown in Figure I- 6. The thinner and wider arms are called “hot arm” and “cold arm”, respectively. The higher cross section of the wider arm results in lower electrical resistance in comparison with the thinner arm. The heat generated in the cold arm is then less than in the hot arm when an electric current passes through the actuator. Due to the temperature gradient between hot and cold arms, the actuator will bend towards the cold arm due to larger expansion in the hot arm [SUMA 2012].

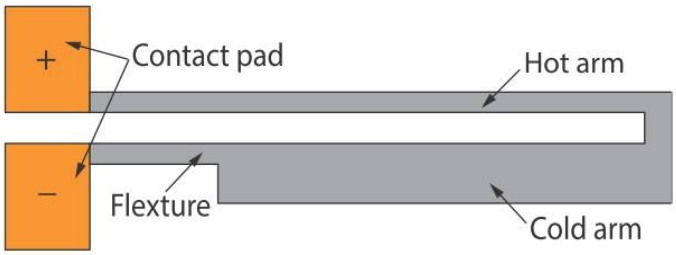

Figure I- 6: Principle of bimorph thermal actuator [SUMA 2012]

Khazaai and Slicker have developed an electro-thermal MEMS switch using V-shaped actuators [KHAZ 2010]. This switch is composed of two sets of actuators, one set is used to drive the movable contact and the other set is used for the lateral latching system (see Figure I- 7). The switch has two states. The actuator stays at “OFF” state without actuation, and the actuator is switched to “ON” state when it is actuated. The two sets of electro-thermal MEMS actuators with opposite directional displacements are designed to meet the contact and latching requirements, and are fabricated using PolyMUMPS technology. The actuator combines a “chevron” beam actuator and a bimorph actuator with unequal hot beams. The contacts and latching mechanism using two sets of the 4-arm V-shape actuators can provide locking/unlocking of the micro switch to allow a desired “On” and “Off” state of the signal path Figure I- 7 (a). When the actuator is switched to one of the positions, it can be maintained by the latching mechanism without extra input energy.

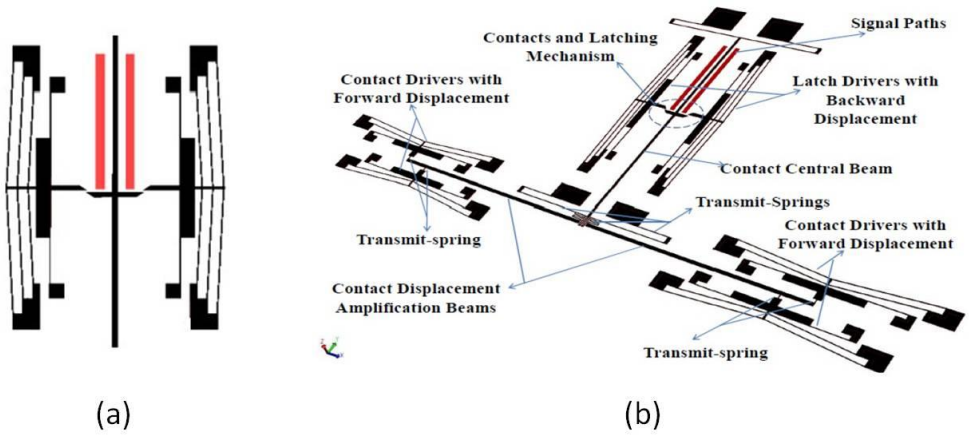

Figure I- 7: A V-shape electrothermal switch [KHAZ 2010]

I.2.1.1.4 Shape Memory Alloys actuator

Besides the actuators presented before which are widely used, another typical thermal actuators based on SMA can be found in literature. The actuators made of this material are always fabricated with a pre-deformed shape. The SMA material "remembers" its original shape and it has the property to return to the pre-deformed shape when heated. For these actuators, two ways of energy source are employed to generate a temperature rise: using Joule effect with a current which passes through the SMA part and using light illumination.

A dynamic Braille display has been developed by Haga et *al.* [HAGA 2005] using SMA digital actuators (see Figure I- 8). Each pin of the device is inserted into a magnetic material tube and a SMA micro-coil is placed around. SMA micro-coil actuators are fixed between two printed circuit boards. The SMA coils are firstly compressed from the length of the memorized shape. The SMA coils twine an insulated metal pin, and each SMA coil is grounded at the middle of the pin. The electric current flows to the upper or lower half of the SMA coil independently through the printed circuit boards. When a current is injected, the SMA coil is heated, so the compressed SMA extends, thus the pin will move up or down. The magnetic material tube is attracted to the upper iron plate when the pin moves upward. The upper position is then held magnetically without extra energy. In reverse, the pin is pushed down when the upper half of the SMA coil is activated.

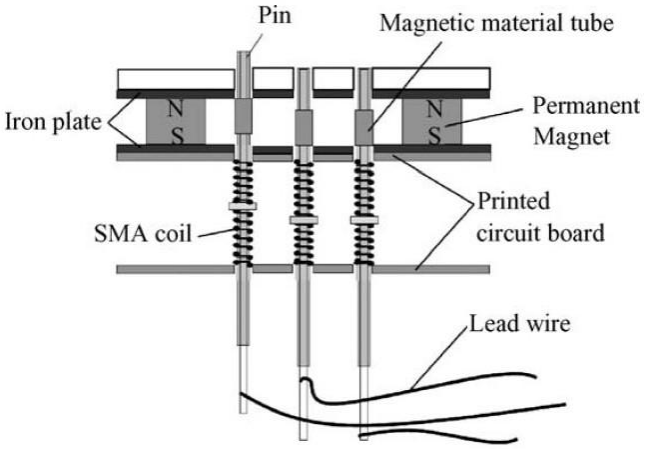

Figure I- 8: SMA coil actuator [HAGA 2005]

Unlike the previous actuator which is actuated by Joule effect, Zaidi *et al*. [ZAID 2011] have proposed a novel bistable actuator based on SMA heated by light illumination (see Figure I- 9). This wireless actuator makes its integration easy and simple in a mechatronic system. In their study, two SMA samples are used to switch a bistable curved beam between two stable positions. Two laser sources, infrared and red laser, are used as thermal input energy. The thickness of each SMA layer is different. So SMA "1" responds only to red layer but not to the infrared laser, while SMA "2" responds to infrared laser not to the red laser. The bistable curved beam is placed between the two SMA samples (Figure I- 12). At first, the SMA "1" is deformed to contact the beam, while the SMA "2" is flat; the beam stays at one of the stable position. When the SMA "1" is heating by an infrared source, no change of SMA "1" was observed. When the SMA "1" is heating by a red source, the initially deformed SMA "1" regains its predefined flat shape. The generated force is applied on the beam which switches the beam to the second stable position. In this position, the SMA "2" is deformed so that the initial position can be reached when the SMA "2" is heated by a red laser.

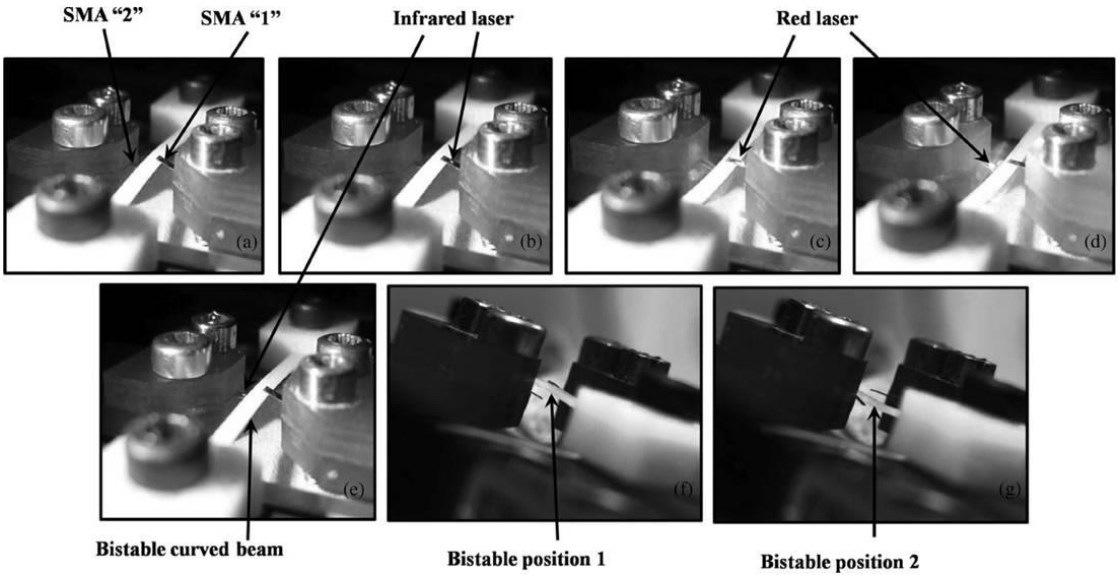

Figure I- 9: A SMA with a Bistable curved beam actuator [ZAID 2011]

I.2.1.2 Electrostatic principle

The electrostatic principle is one of the most frequently used actuation principle in micro-electromechanical systems. The electrostatic effect is a function of the distance between facing charged electrodes, the facing surface and the supply voltages. To illustrate this principle, a parallel-plate micro-actuator which consists of two facing electrodes (one movable and the other is fixed) are considered (Figure I- 10). When the electrodes are energized, the gap between the two electrodes will increase or decrease due to the attractive or repulsive electrostatic force between them. The electrostatic force between the two electrodes can be mathematically computed using equation (I.1). There are many applications with electrostatic actuation, such as optical grates and shutters, micro-mirrors, variable capacitors, micro accelerometers, comb-drive actuators etc. [DONG 2010, HUWE 2010]

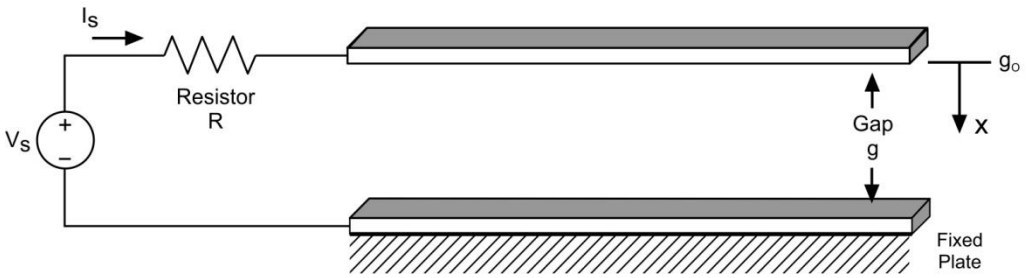

Figure I- 10: Principle of electrostatic actuator

$$C = \frac{\varepsilon b(l-x)}{d}$$
$$W = \frac{1}{2}CU^2 \qquad \text{(I.1)}$$
$$f_x = \frac{\partial W}{\partial X} = -\frac{\varepsilon b}{2d}U^2$$

ε : The dielectric constant of the material between the gap (F/m)

b : Width of the plates (m)

l : Overlap length of the plates (m)

x : Displacement of the moveable plate

d : Gap between the two electrodes (m)

W : The static energy (J)

C : Capacitance (F)

U : Tension (V)

I.2.1.2.1 Facing electrodes

Many digital actuators based on the electrostatic principle have been developed in literature. Oberhammer *et al*. [OBER 2006] have developed a tri-stable switch based on electrostatic actuators (see Figure I- 11). The switch is composed of one input cantilever, two ground electrodes, two common stoppers and two output cantilevers. The cantilevers are made of silicon layer with gold coating. The process of the switching is presented in Figure I- 12. Initially, the input cantilever is placed at the center of the switch. When a voltage is supplied on one of the ground electrodes and the input cantilever, the generated electrostatic force makes the input cantilever to contact the corresponding output cantilever. The hooks at the end of the cantilevers help maintain the state of the switch without extra energy. Thus the energy is only needed to change the state.

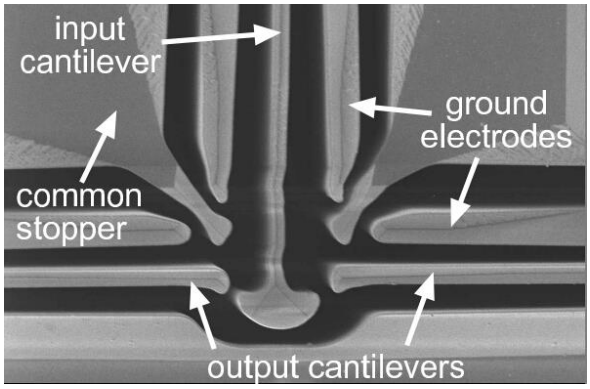

Figure I- 11: Tri-stable switch based on electrostatic actuator [OBER 2006]

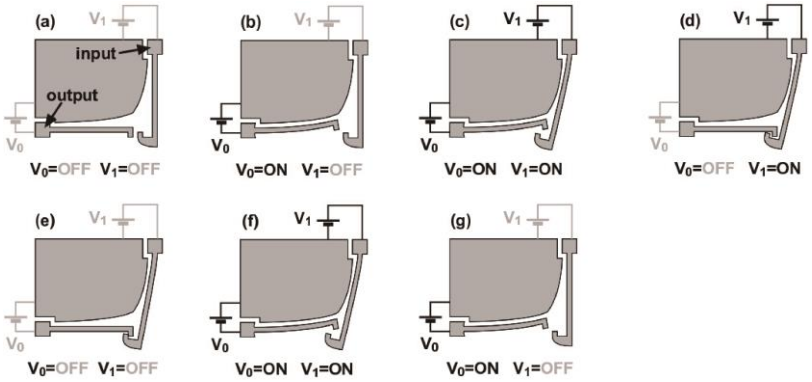

Figure I- 12: Switching process [OBER 2006]

I.2.1.2.2 Comb-drive actuators

Another solution found in literature to generate an electrostatic force is the use of comb-drive electrodes. Freudenreich et *al*. [FREU 2004] have presented a micromechanical bistable switch based on comb-drive actuators to switch between the stable positions (see Figure I- 13). The switch is composed of two parts: two comb-drive electrodes and a central bistable toggle-lever structure. A stiff beam connects the electrostatic drives and the toggle-lever structure. The structure is initially in a non-compressed configuration (I). Then, the flexible structure is compressed in x-direction so that an unstable central position (II) is reached and the structure has two stable positions (IIIa and IIIb). When a current is employed, the switch can be moved in y-direction between the two stable positions.

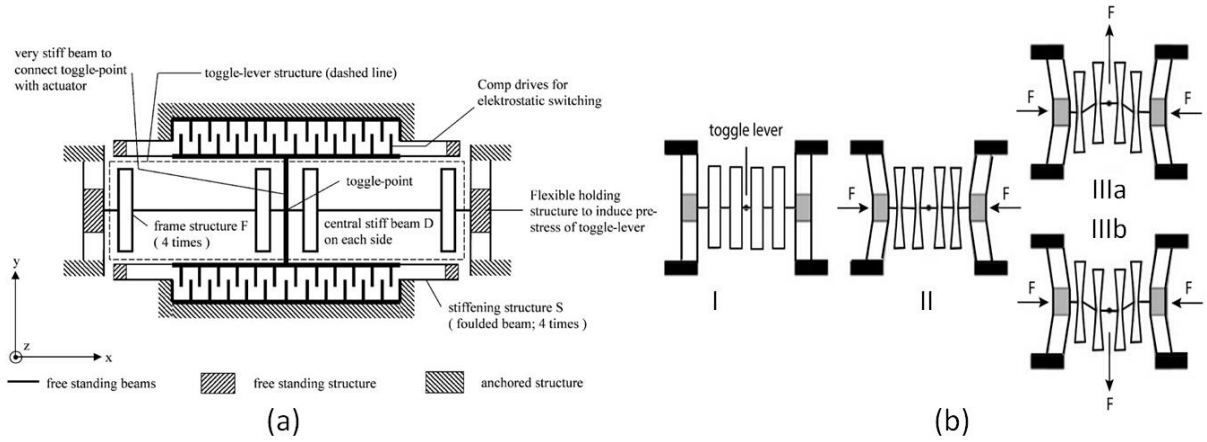

Figure I- 13: A bistable switch using comb-drive actuators [FREU 2004]

I.2.1.3 Electromagnetic principle

The electromagnetic principle has been widely used to generate the driving force for digital actuators. This principle is indeed well adapted for this type of actuators because a non-extra energy consuming holding force can be easily obtained using Permanent Magnets (PMs). In literature, the digital actuators based on electromagnetic principle present some interest as high speed, fast response, simple design and low cost. Three manners of generated magnetic force are presented in this part.

1.2.1.3.1 Reluctance force

The magnetic reluctance is analogous to the resistance in an electrical circuit. An electric field causes an electric current to follow the path of least resistance; similarly, a magnetic field causes magnetic flux to follow the path of least magnetic reluctance. When a coil of the magnetic circuit is energized, a reluctance force appears in order to minimize the overall reluctance of the magnetic circuit. The expression of the electromagnetic reluctance force as function of the magnetic gap is given in equation (I.2).

$$F_m = \frac{d\left(\frac{R_m}{\Phi}\right)}{de} \qquad \text{(I.2)}$$

R_m : Reluctance (H^{-1}),

Φ : Magnetic flux (Wb),

F_m : Magnetomotive force (V),

e : Magnetic gap (m).

Based on this principle, Zhang et *al*. [ZHAN 2007] have developed a bistable electromagnetic switch (see Figure I- 14). This actuator is composed of a cantilever beam with two free ends linked to the fixed part by two torsional beams, two PMs and two planar coils. When a 70 mA current pulse is injected through the coils, the reluctance force is generated. One of the ends of the movable cantilever beam is then attracted by the planar coil and it rotates to a stable position. The stroke of the end of the cantilever beam is about 17 µm and the switching time is about 20 µs.

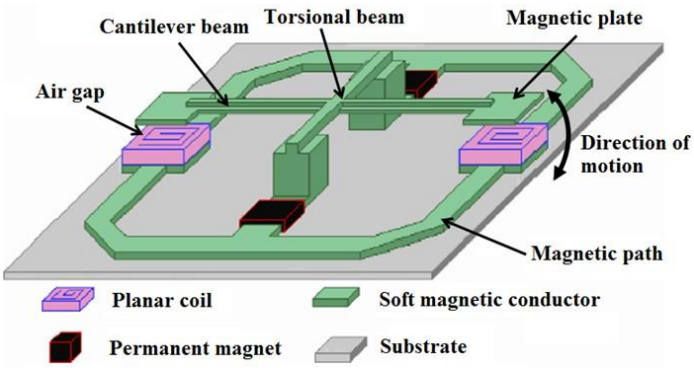

Figure I- 14: Electromagnetic bistable actuator [ZHAN 2007]

Luharuka et *al*. [LUHA 2008] have developed a compliant bistable electromagnetically actuated rotary gate microvalve (see Figure I- 15). This microvalve is composed of a suspended gate mass, a bistable mechanism, two electromagnetic actuation posts and four orifices etched into substrate. The bistable mechanism ensures two stable positions of the gate (ON and OFF states). The suspended gate is made of soft magnetic material, such as NiFe alloy and can rotate around its axis between two stable positions. The four electromagnetic actuation posts ensure the switch between the two states. When the posts are supplied, a reluctance force appears to generate the rotation of the mobile part. Two types of microvalves have been developed with the bistable mechanisms placed outside (Figure I-20 a) and inside (Figure I-20 b), respectively. For the inside structure, the diameter is 3 mm, the rotational angles are 12° or 18° and the maximum torque generated is 1.0 – 1.6 µNm. For the outside structure, the diameter is 2 mm, the rotational angles are 8° and 6° and the torque is up to 0.4 µNm. The switching time is less than 10 ms.

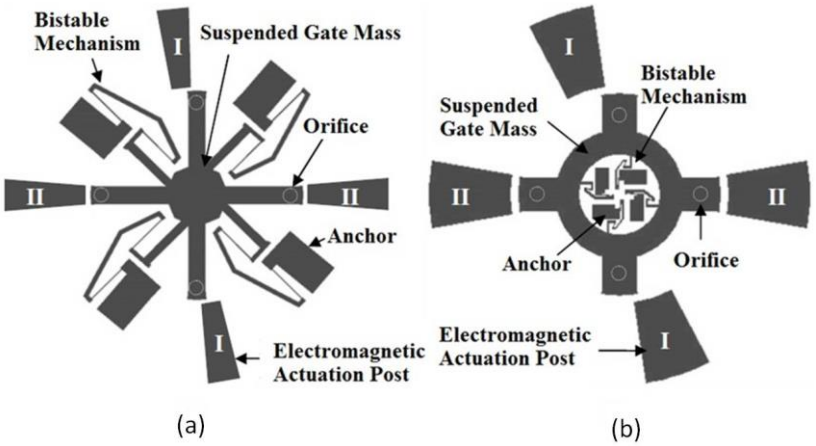

Figure I- 15: Electromagnetic rotary micro valve: (a) Inside (b) Outside [LUHA 2008]

1.2.1.3.2 Lorentz force

The second principle for magnetic actuation is based on the Lorentz Force principle. A Lorentz force is generated when an electric current passes through a conductor placed in a magnetic field. The expression of this force is given by equation (I.3).

$$\vec{F} = I \times \vec{l} \wedge \vec{B} \qquad \text{(I.3)}$$

$\vec{F}$: Lorentz force (N),

I : Current passing through the conductor (A),

$\vec{l}$: Length of the conductor (m),

$\vec{B}$: Magnetic flux density (T).

One of the applications of Lorentz force found in the literature is to develop digital actuators for micro relay purpose. Wu *et al*. [WUYI 2010] have presented a bistable microcantilever actuator based on the Lorentz force driving (see Figure I- 16). The actuator is composed of a cantilever beam with two free ends; a circular-shaped support linked to the fixed part a magnetic circuit and an external electric circuit. A PM is placed beside the anchors to generate a uniform static magnetic field. The cantilever beam is made of magnetic material and connected by the circular-shaped support. The support is connected to the anchors by two torsion flexures. When a current passes through the external electric circuit, the Lorentz force is generated and the cantilever beam can then rotate clockwise or counter clockwise around the torsion flexure to contact the circuit. The switch between the two stable positions can be obtained by switching the current between the two external electric circuits.

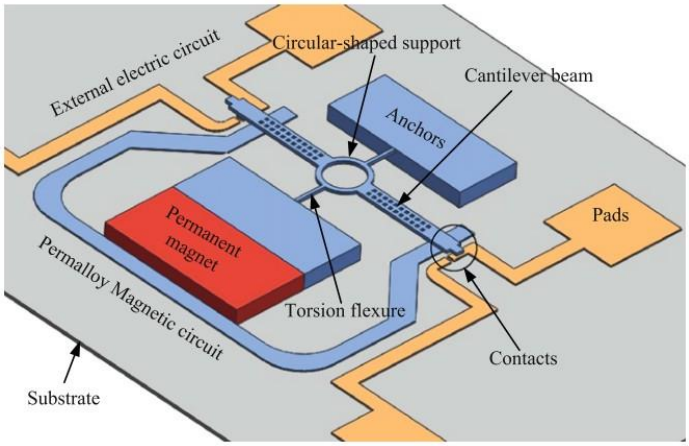

Figure I- 16: Bistable microcantilever-based Micro relay [WUYI 2010]

1.2.1.3.3 Induction force

The third principle for electromagnetic actuation is based on the generation of an induction force using the Faraday's law. In an electromagnetic system, an induced current appears in a coil due to the variation of magnetic flux density around it. The variable magnetic flux within the coil creates an electromotive force due to the induced current (equation (I.4)). The electromotive force is opposite to the change of the magnetic flux density.

$$F_{EM}(t) = -\frac{d\Phi(t)}{dt} \qquad \text{(I.4)}$$

F_{EM} : Electromotive force (V),

Φ : Magnetic flux (Wb).

Based on the generated induction force principle, Liao *et al*. [LIAO 2010] and Chia *et al*. [CHIA 2010] have developed a 2×2 electromagnetic optical switch based on this kind of digital actuators. The switch is illustrated in Figure I- 17, which consists of two pairs of output and out system. Each pair has one input collimator, one output collimator, one movable mirror, one fixed mirror and an actuation module. The actuation module is composed of a ferromagnetic seesaw, a PM, an electromagnetic coil and two stoppers. It is connected with the mirror structure via an L-shape arm. This arm is employed for bistable mirror switching. Initially, the actuator is not in contact with the cantilever, the optical signal is then reflected by the movable mirror to be output by its own output fiber (Figure I- 17(a)). When a current passes through the induction force generated pushes the cantilevers upward and then, the optical signals pass under

the movable mirror and are reflected by the fixed mirror to the other pair of output channels (Figure I- 17(b)). The switching time is less than 10 ms.

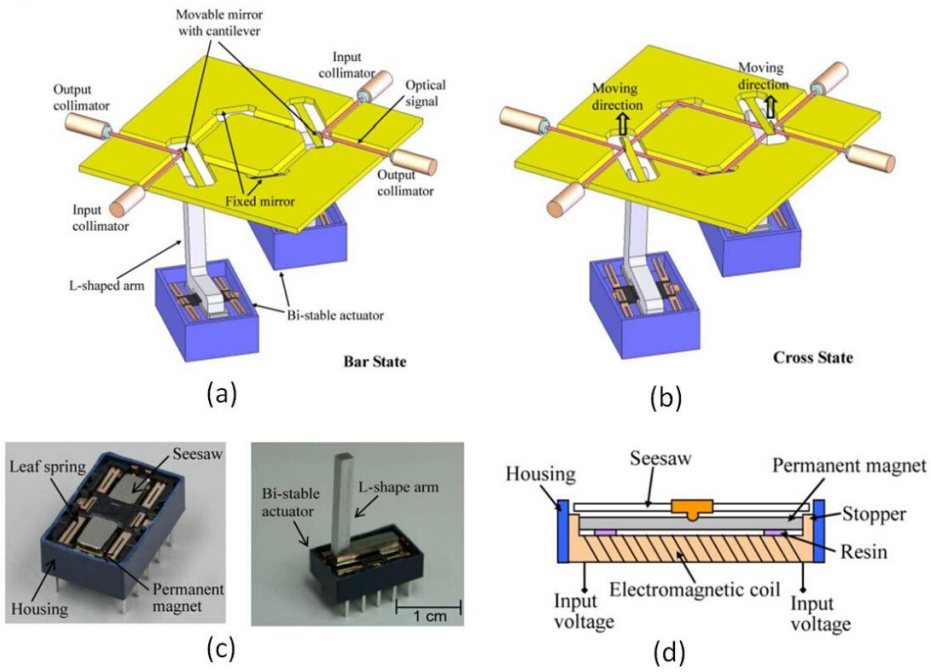

Figure I- 17: An optical switch based on induction force [CHIA 2010]

I.2.1.4 Piezoelectric principle

Smart materials are a special class of materials which can be used to generate a force or motion thanks to external stimuli. As it is nominated, piezoelectricity means electricity resulting from pressure. Electric charge is accumulated in some materials (such as crystals, certain ceramics, and biological matter such as bone, DNA and various proteins) in response to applied mechanical stress. The effect is related to the appearance of an electric dipole density within the material's volume and also reversible. When a stress is applied on a piezoelectric material, the surface densities on the electrodes change. Vice versa, when it is under the charge of different electric potential, the stress or the strain occurs in the material [KHAN 2014]. There are many advantages for piezoelectric actuators, such as rapid response, precise positioning, high energy conversion etc. Eq. (I.5) gives the relation between the mechanical constraint applied on a piezoelectric material (p_t), the electrical polarization (σ) and the applied force (F).

$$\sigma = \frac{p_t}{K \cdot \boldsymbol{E}} \qquad Q = \frac{F}{K \cdot \boldsymbol{E}} \tag{I.5}$$

σ : Electrical polarization ($C.m^{-2}$),

p_t : Mechanical constraint (Pa),

K : Piezoelectrical module,

F : Force (N),

E : Induction electrical field ($V.m^{-1}$),

Q : Electrical charge (C).

One drawback of piezoelectric materials is that they tend to come back to the initial state when the applied power is removed. In literature, the most common way to actuate digital actuators is to integrate piezoelectric material into bistable structures. Cazottes *et al*. [CAZO 2008] have associated a bistable system with a MFC (Macro Fiber Composite) piezo-based actuator shown in Figure I- 18 (a). A buckled beam is firstly pre-compressed and reaches one of the stable positions. When an external electric charge is applied, the MFC, attached on the buckle beam, generates an extension all along the beam. The buckle beam is then pushed downward to the other stable position. The energy should be sustained to keep this stable position, when the external energy is removed, the buckled beam moves upward to the initial position. The stroke can reach up to 0.5% of the length of the system. The extension of the buckled beam leads to a distributed torque along the actuator, which is used to switch the mechanism. Giddings *et al*. [GIDD 2007] and Portela *et al*. [PORT 2008] have also presented bistable laminates actuated by MFC actuators (Figure I- 18 (b) and (c)). The MFC is directly placed on the laminate. The bistable structure is made of carbon fiber composites which can keep one of the stable positions without the need of a constant holding force. The laminate length is 150 mm.

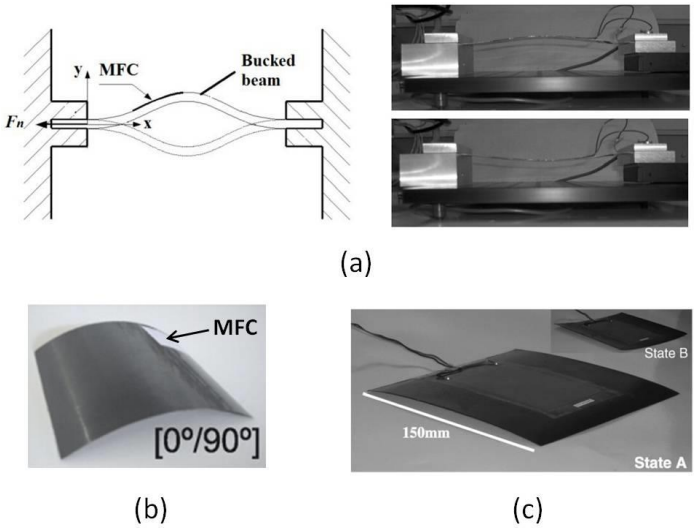

**Figure I- 18: Piezoelectric actuators: (a) [CAZO 2008]
(b) [PORT 2008] (c) [GIDD 2007]**

I.2.2 Holding function

The holding function represents the second important function of digital actuators. This function ensures the holding of the mobile part of digital actuators in discrete positions. As for the switching function, the solutions used in literature to realize the holding function are presented in this section and can be categorized as: magnetic holding, locking structures, compliant structures and hinged mechanisms.

I.2.2.1 Magnetic holding

The electromagnetic principle is one of the most used principles to realize the switching function of digital actuators. Based on this principle, the magnetic holding solution is also widely used in digital actuators because a non-consuming force can be easily obtained using PMs. Ahn *et al*. [AHNH 2014] have developed an electrical switch based on digital actuators (see Figure I- 19 (a)). The actuator is composed of a static yoke, two PMs, two pairs of trip coils and a movable plunger. The plunger is firstly held by the PMs. When a current passes through the coils, the plunger moves upwards or downwards. After the plunger reaches one of the stable positions (fully open or closed position), it is held by PMs.

Staab *et al*. [STAA 2011] have developed an electrothermally actuated magnetostatic bistable microrelay based on bimorph actuation with cold and hot beams (see Figure I- 19 (b)). This microrelay is composed of a magnetic circuit, a nickel spring which guides the electrical nickel contact and two electrothermal actuators. The nickel contact is deposited by micro

electroplating with magnetic flux guiding material which can generate a magnetic field as holding force to draw the nickel contact to one of the pole shoes without additional electrical energy. The dimension of the two PMs is 3.0 × 3.0 × 0.5 mm^3. The dimension of the relay is 3.60 × 5.80 × 0.25 mm^3, the switching time is less than 8 ms. The magnetostatic holding force is 12.4 mN, the nominal deflection is 74 µm with a 17 mN blocking force.

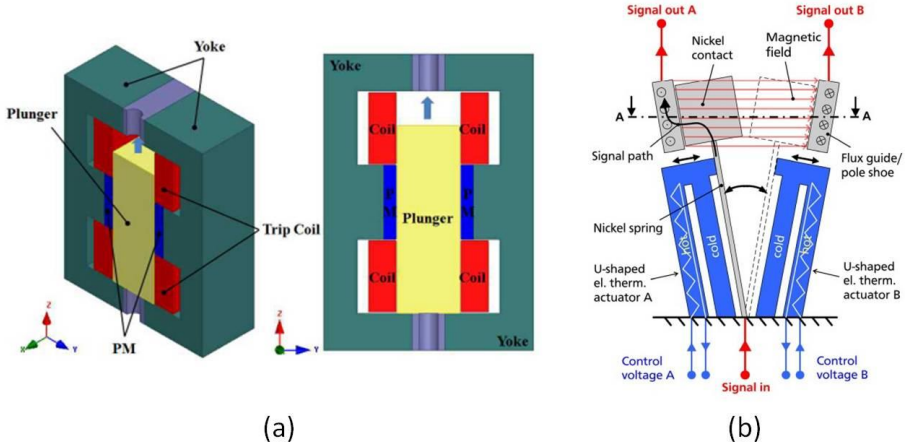

Figure I- 19: Magnetic holding force: (a) Magnetic interrupter [AHNH 2014] (b) Bistable microrelay [STAA 2011]

I.2.2.2 Locking structures

The holding function can also be obtained using locking structures. Roodenburg *et al*. [ROOD 2008] have presented a switch based on the induction actuation principle. The switch consists of a fixed inductor, a pawl to keep the states of the actuator, a fixed contact part and a movable contact part. The movable contact is equipped with a copper plate and connected by a contact force spring. When a current (i_q) flows in the inductor, a magnetic field (B) is generated and produces an induced current in the copper plate (i_p). The induced current in the copper plate is opposite to the current in the inductor, and then a repulsion force between the inductor and the copper plate is generated. The movable part moves downward and reaches the lower stable position which is locked by the pawl. To reach the upper stable position, a spring placed below the mobile part is used.. The stroke of this actuator is about 25 mm, the maximum force is 200 kN with an 8 kA current supplying and the switching time is about 2 ms.

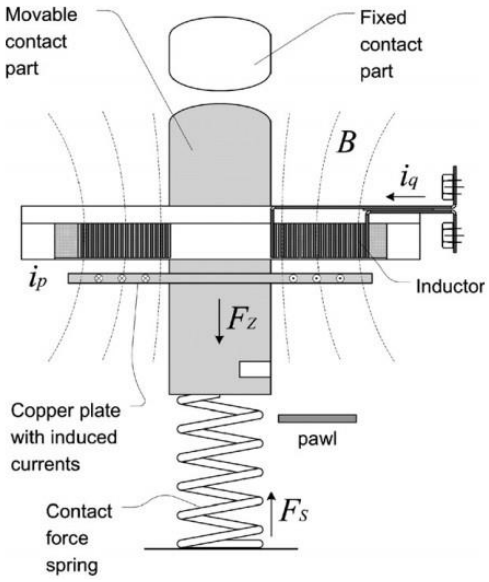

Figure I- 20 : Holding by Pawl [ROOD 2008]

I.2.2.3 Compliant structures

Besides the mentioned holding function, compliant structure is also used importantly. The compliant structure can make the actuators obtain several discrete positions. A comb-drive actuator based on electrostatic actuation has been presented developed by Freudenreich et *al*. [FREU 2004]. They have designed a micromechanical bistable switch by using a compliant structure. To obtain two stable positions, the structure has to be compressed (Figure I- 21(a)). The holding force of this actuator is obtained by elastic deformation.

Chen *et al*. [CHEN 2005] have developed a 2×2 optical switch also based on a compliant structure shown in Figure I- 21 (b). The switch is composed of an H-beam actuator based on electrothermal actuation. The actuator is connected with two buckled springs (buckled beams) by a movement link structure and a reflective micro-mirror. The switch is switched between two states obtained by the buckled beams. The two ends of each buckled spring beam are anchored. The switching time is 5 ms under a 25V dc pulse.

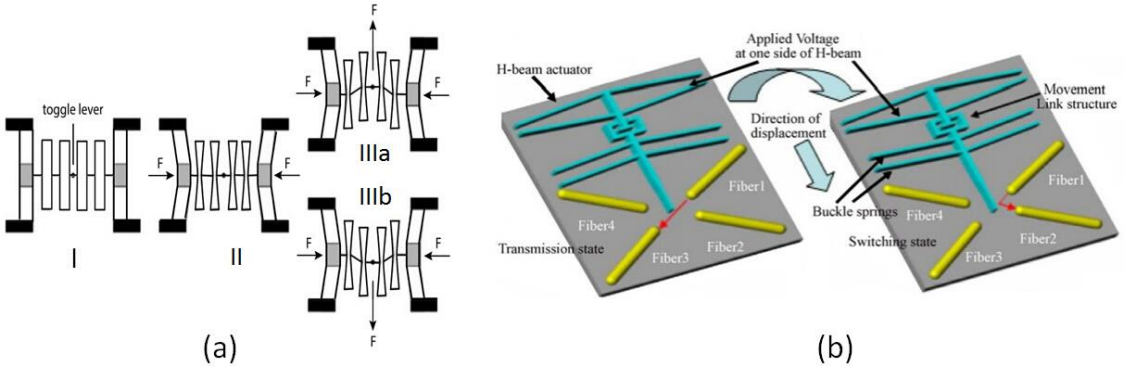

Figure I- 21: Holding by compliant structures (a) [FREU 2004] (b) [CHEN 2005]

I.2.2.4 Hinged mechanism

Hinged mechanism is another holding function used to realize the stable positions of the actuators. Usually, the beams are hinged with a shuttle, and then the hinged mechanism can have two pre-stabled positions. Wang *et al*. [WANG 2009] have presented a compliant bistable mechanism driven by electromagnetic force (see Figure I- 22). The device is made of PM which can generate a magnetic field. The bistable actuator is connected to the substrate by the contact pads. A shuttle mass is connected to the lateral springs by hinged beams (Figure I- 22 (a)). The actuator has two stable positions (Figure I- 22 (b) and (c)), the holding force of this actuator is provided by the flexible hinges.

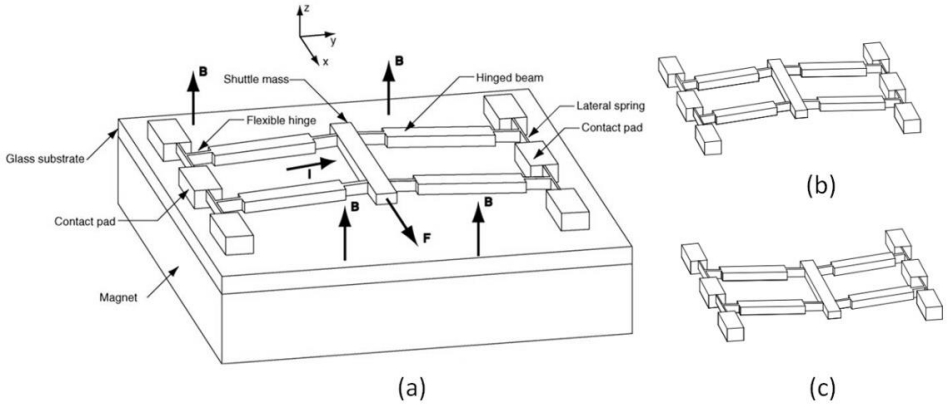

Figure I- 22: A bistable mechanism held by hinged mechanism [WANG 2009]

I.3 Digital Actuators applications

Digital actuators are widely used in different domains. The applications can be divided into two groups according to the number of applied actuators: single actuation applications and multiple actuation applications. Single actuation applications use only one single actuator. Multiple

actuators applications are based on several actuators that are integrated together to realize complex tasks. In this section, the applications of these two groups are presented with examples

I.3.1 Single actuation applications

The single actuators are typically used for discrete displacement output and switches. In this part, the applications are illustrated with their functionalities.

I.3.1.1 Discrete displacement output

Digital actuators have been used as discrete displacement output according to their characteristics: they can assure a fixed output displacement between the discrete positions and the displacement has a high repeatability.

Chalvet *et al*. [CHAL 2013] have developed a digital microrobot based on bistable modules to realize micropositioning tasks. This bistable module consists of three main elements: a mechanical bistable structure, two pairs of electrothermal actuators and two stop blocks. The mechanism of the bistable structure is composed of two curved beams and is connected to the borders and the shuttle by hinges (Figure I- 23 (a)). The actuation is based on electrothermal principle. When the actuators are actuated, the bistable structure is pushed forth and back to reach each one stable position limited by the two stop blocks. The stop blocks are locking structures to providing the holding force after the bistable structure reaching the stable positions. The power is only needed when the bistable structure is switched between the states. The distance between two stable positions is 30 µm and the blocking fore is 1.54 mN.

Meneroud *et al*. [MENE 2006] developed a bistable micro actuator for a discrete displacement output, shown in Figure I- 23 (b). The actuator is composed of coils, moving magnets, electromagnets. This actuator has two functioning states; each state corresponds to the position of the mobile part. When a current passed through the coil, the movable pin with magnets is switched by generated electromagnetic force between the two states. The diameter of this actuator is 5 mm with a 0.62 mm stroke. The switching time is 0.7 ms and the energy consumption is about 20 mJ.

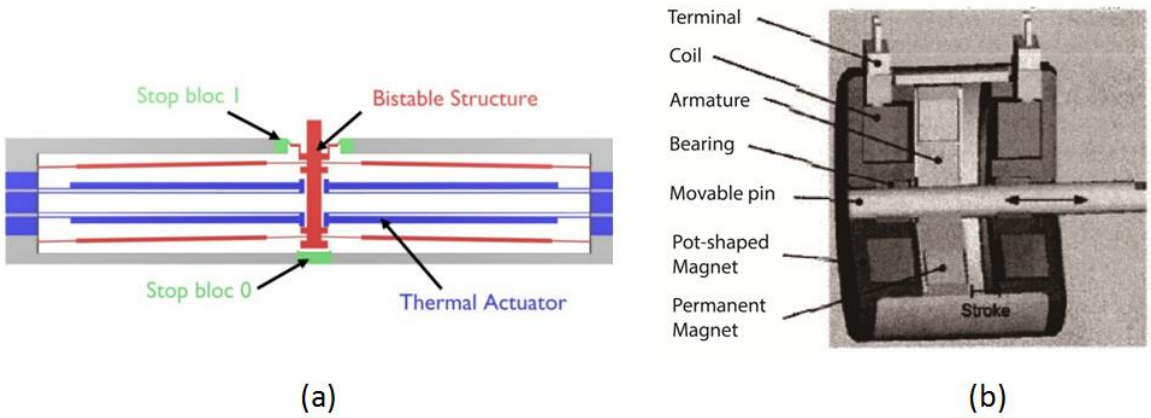

Figure I- 23: (a) A digital microrobot [CHAL 2013] (b) A bistable micro actuator [MENE 2006]

I.3.1.2 Switches

Another application of single actuation is used as switches or valves. Digital actuators have been used as different switches, such as fluidic switch, optical switch and electrical switch. Several switches are presented in this part.

I.3.1.2.1 Fluidic switch

Fluidic switch can be widely found in literature, it can be realized by different switching principles, and several examples of fluidic switches based on digital actuators are presented.

Carlen et al. have presented a micro-valve based on the thermal expansion of a thin layer of paraffin wax [CARL 2000]. The substrate is 1 mm thick; the inlet hole is 500 µm-diameter connected to a 200 × 20 μm^2 tank. A channel leads to a circular reservoir where the actuator and the outlet hole located. A 100 µm-diameter outlet hole is 2 µm above the actuator (see Figure I- 24). When the heater is heated, the actuator is activated, the paraffin expands; the diaphragm is then deflected vertically to press against the valve seat to seal the outlet hole. The paraffin can deliver very high actuation forces to achieve a good seal even at low actuation power. The deflection distance was 3 µm in about 20 ms, with a power less than 50 mW.

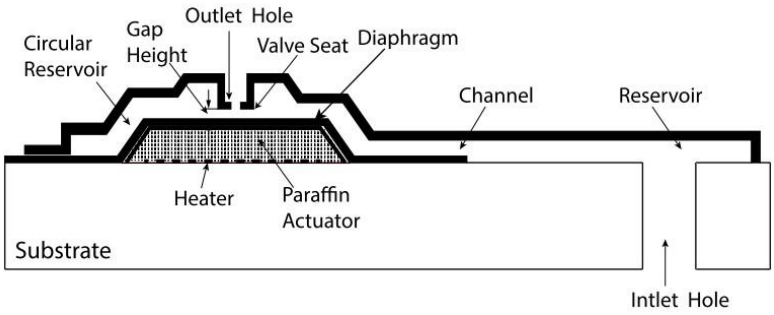

Figure I- 24: Paraffin actuated microvalve [CARL 2000]

A silicon on/off valve based on a bistable electromagnetic actuator has been developed by Böhm *et al.* [BOHM 2000] (Figure I- 25). This actuator is composed of a spring-biased soft iron armature and a soft iron housing composed of a PM and a coil. In the open position, the armature is held in contact with the top of the housing by the magnet, so the valve closing boss is pulled to allow fluid flow. To close the valve, an electric current of appropriate direction and amplitude is injected into the coil. A magnetic flux is then generated and if the counteracting flux is large enough to reach a certain threshold, the force of the spring pushes the armature downwards to close the valve. The dimension of this silicon valve part is 7×7×1 mm^3 and the actuator stroke is 200 µm.

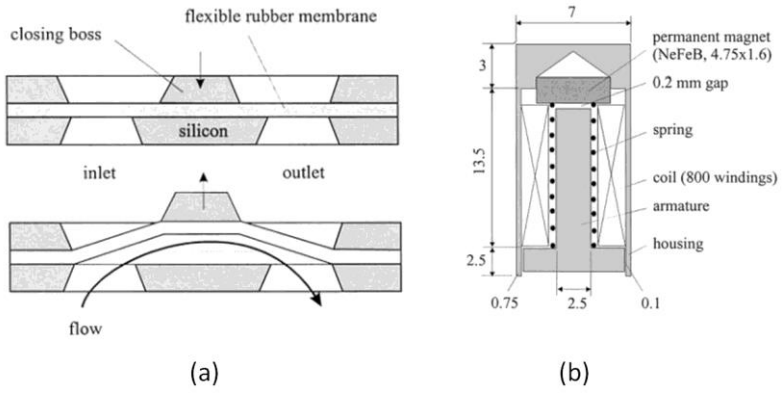

Figure I- 25: A bistable electromagnetic valve: (a) Cross-section of the valve part (b) Cross-section of the cylindrical electromagnetic actuator [BOHM 2000]

I.3.1.2.2 Optical switch

Besides the fluidic switches, digital actuators are also used as optical switch. Cochran *et al*. [COCH 2005] have developed an optical microswitch based on electrothermal actuation (Figure I- 26). This switch is realized by the direct actuation of optical fibers, a pair of input and output optical fiber is actuated from an out-of-line and in-line position. The holding function is realized by a spring-supported slider and a locking actuator. When the optical fiber is switched at one

of the position, it can be maintained at the stable position by the locking structure. The length of the actuator is 5500 µm and the height of beams is 125 µm. The maximum unloaded actuator stroke is 136 µm with a 125 mA current. The switching time is 40 ms and the resolution of measurement is 2 µm.

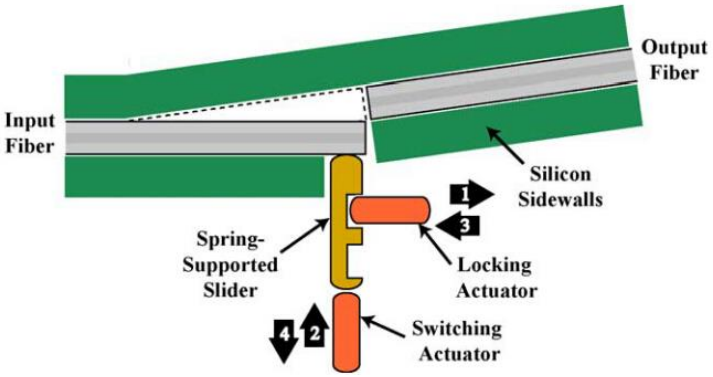

Figure I- 26: Optical switch based on electrothermal actuator [COCH 2005]

Liu et al. [LIU 2015] has developed an optical wireless bistable micro-actuator. This actuator is composed of two fixed mirror, two SMAs and a bistable beam (Figure I- 27 (a)). The length of the bistable beam is 8 mm, the thickness is 25 µm and the depth is 400 µm. The bistable mechanism is wirelessly actuated by laser heated SMA element. The laser can heat SMA 1 directly, while the laser should be reflected two times by fixed mirrors to heat SMA 2. So the switching time of SMA 1 is about 1.5s and 2s for SMA 2. The two stable positions are illustrated in (Figure I- 27 (b) and (c)). From the zoom figure, it is shown that a small gap is between SMA, so there is no load effect from SMA elements. The stroke of this bistable actuator is 300 µm.

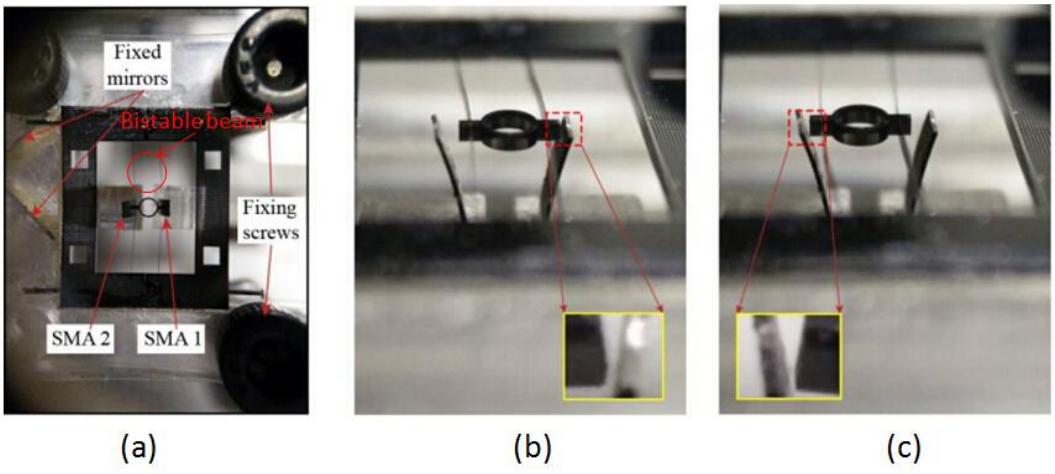

Figure I- 27: Optical wireless bistable micro-actuator [LIU 2015]

Herding et al. [HERD 2004] also developed an optical switch based on electrostatic principle (see Figure I- 28). This optical switch is composed of an input fiber, two output fibers and two fixed electrodes placed on both sides of the input fiber. The input fiber is covered with a conductive metal layer and firstly located at the center of the substrate. When a voltage is applied on one of the two electrodes and the metal layer, the input fiber will be switched to one of the positions of the output fibers due to the electrostatic force. For this optical switch, no it can be maintained at the position by continuous applied voltage, if the voltage is removed, the input fiber will return to the center position. The stroke of the input fiber is 65 µm and the switching time is 7 ms.

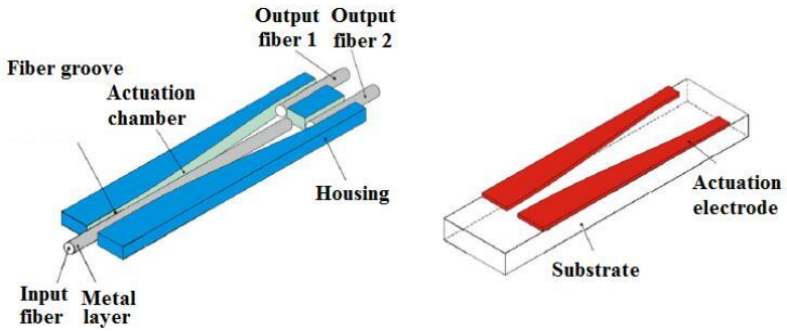

Figure I- 28: Optical switch based on electrostatic actuator [HERD 2004]

I.3.1.2.1 Electrical switch

Digital actuators have been developed to realize electrical switches. These switches have the advantages of low cost, highly stable and low energy consuming. Several electrical switches have been realized based on different switching principles.

Plotz *et al*. [PLOT 2001] have proposed an electrical switch based on electrostatic actuation (Figure I- 29). The switch is composed of a movable torsional part, two actuators and two contacts. A torsional axis is positioned at the middle of the movable part and two actuator electrodes are placed below the movable structure at the left and the right. The right side actuator is in the "off" state while the right one is in the "on" state. When a voltage is applied between the movable plate and one of the actuator electrodes, the torsional axis will switch the stated by the generated electrostatic force. The initial gap distance in the closed position is doubled to ensure the bistable operation which avoids the sensitive disturbance. But a sustaining power is needed at the opened position to provide holding force. The standard structure has a width of 100 µm and a length of 120 µm, the switching time is 10 µs.

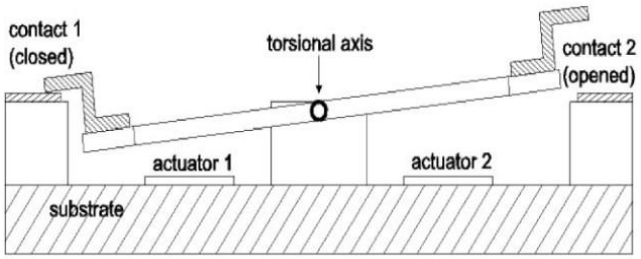

Figure I- 29: Electrical switch based on electrostatic actuator [PLOT 2001]

Dieppedale et al. [DIEP 2004] have developed an electrical switch based on electromagnetic actuation. This bistable actuator is composed of one mobile PM, four fixed PMs and an actuation coil. The electromagnetic Lorentz force is generated when a current passes through the coil. If the Lorenz force is higher than the magnetic force generated by the fixed magnets, the mobile magnet switches between the stable positions and contact the fixed magnets. Then one of the electric circuits will be closed when the other one is open. The fixed magnets provide the holding force for the mobile magnet. A device prototype has been micro fabricated with a 5 µm × 40 µm × 100 µm mobile magnets, the total dimension is 5µm × 40µm × 100µm. The width of the coil is 20 µm, the actuation time is about 30 µs, the energy needed to switch is 48 µJ and the maximum current is 4 A.

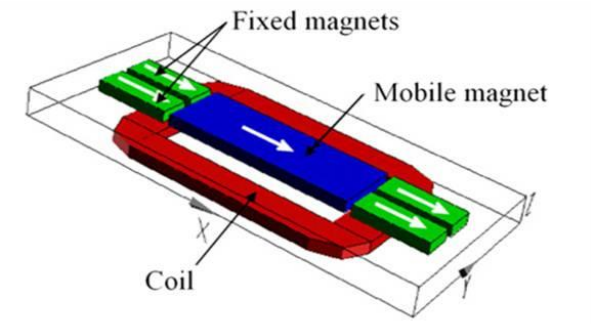

Figure I- 30: Electrical switch based on electromagnetic actuator [DIEP 2004]

I.3.2 Actuators array applications

Apart from the single actuation applications of digital actuators, the assemblies of digital actuators are also widely studied. Compared with the single actuation, the digital actuators can be used as array or assemblies to reach more discrete positions and realize more complex tasks by combing several elementary actions. In this part, the common applications of actuators array are introduced as optical switch array, tactile display, displacement tables etc.

I.3.1 Optical switch arrays

One very frequently encountered application of DAA is the realization of optical switch arrays. Jia *et al*. [JIAC 2009] have developed a MEMS optical switch array composed of 64 elementary digital actuators (EDAs) in 8×8 matrix (Figure I- 31 (b)). Each elementary actuator has two stable positions and is composed of a torsion beam, a cantilever beam and a mirror placed at the extremity of the cantilever (Figure I- 31 (a)). The torsion beam can be switched by electrostatic force when a voltage is applied, and the state can be maintained by the applied voltage. An array composed of 8 × 8 elementary actuators has been developed and is able to switch 8 input signals between 8 outputs channels. The switching time is less than 6ms and the actuating voltage is about 65V.

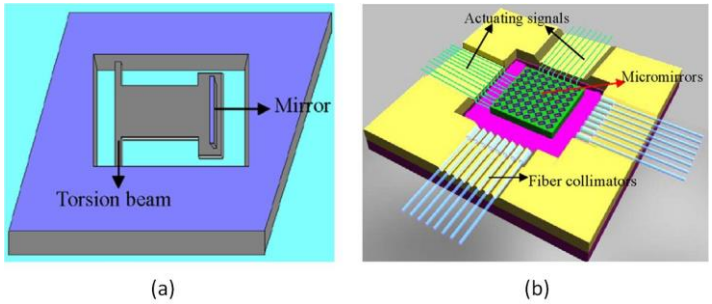

Figure I- 31: (a) elementary optical switch (b) optical switch array [JIAC 2009]

I.3.2 Tactile displays

DAAs are also widely used to realize tactile display devices for visually impaired people. Haga *et al*. [HAGA 2005] have developed a dynamic Braille display based on SMA actuators which have been introduced in previous part (Figure I- 32 (a)). When a current passes through one of the SMA coils, the compressed SMA extends, thus the pin will move up or down. The positions can be maintained by magnetic holding function. Based on this principle, a module composed of 16 pins has been fabricated. The displacement of the pin is 1 mm and the response time is less than 1s at a 300 mA driving current.

Matsunaga *et al*. [MATS 2013] have also developed a Braille tactile display based on the same principle as described above. This tactile display is composed of 100 pins arranged in a 10 × 10 matrix (Figure I- 32 (b)). The pin's stroke is 2 mm, the switch time of tactile information is 0.3 s and the pins are latched at 0.1 N by magnetic force.

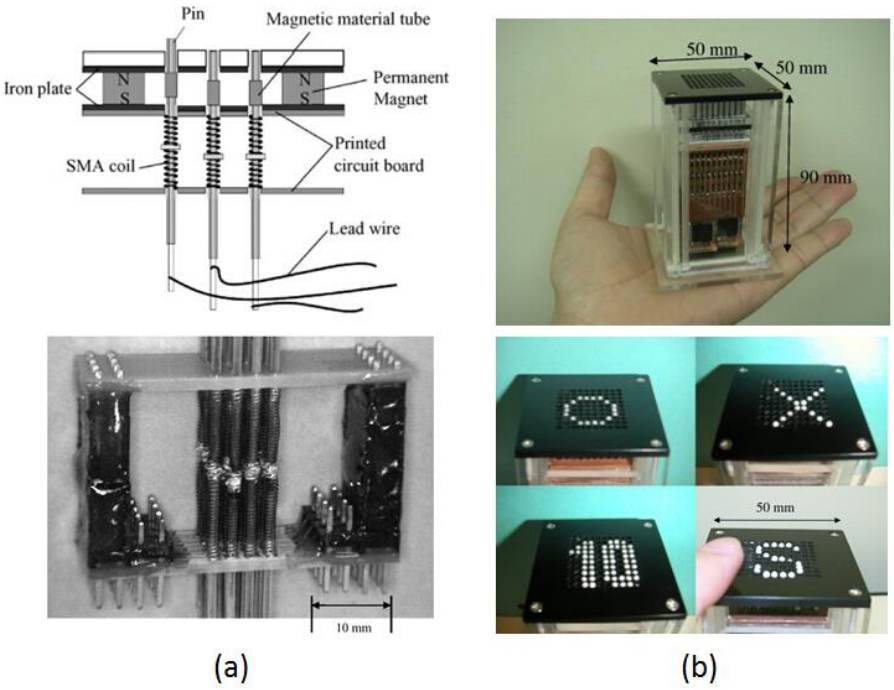

Figure I- 32: Braille tactile display (a) HAGA 2005 (b) MATS 2013

Benali-Khoudja *et al*. [BENA 2007] have developed a haptic tactile display based on 64 electromagnetic digital actuators arranged in an 8 × 8 matrix (Figure I- 33). Each elementary module is composed of a pin, a transmission cylinder, a magnet and a coil. The magnet is placed inside a cylindrical guide alternatively on the top or on the bottom of the cylinder, in order to lower the magnetic field interaction between the pins. Each pin is connected to the magnet or to the transmission cylinder at the top position. The transmission cylinder is surrounded by a coil. When a current passes through the coil, the pin will be pushed up.

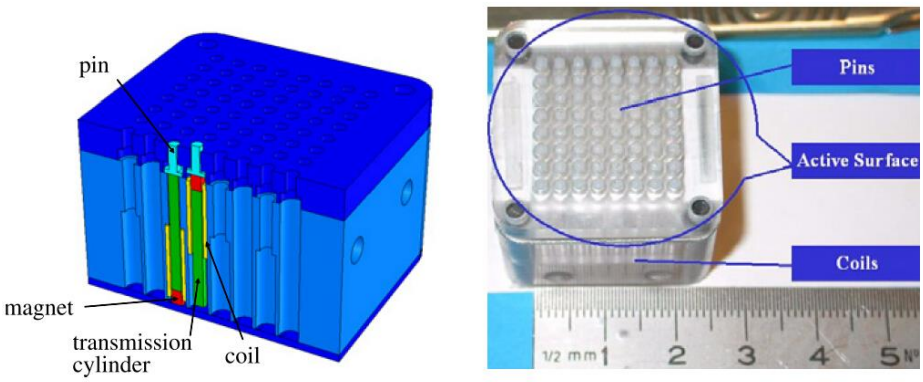

Figure I- 33: Tactile display based on electromagnetic actuator [BENA 2007]

Vitushinsky *et al*. [VITU 2009] have developed a tactile display based on bistable thin-film shape memory actuators. Each elementary actuator is composed of an active SMA layer (Ti-

Ni-Cu on the top and Ti-Ni-Hf at the bottom) and a passive metal carrier layer (Figure I- 34 (a)). Each pin is connected to the active SMA layer. When a voltage is applied, the elementary actuator can be switched between two stable positions and then drives the pin up or down. The holding function is realized with a compliant structure. An actuators array composed of 100 elementary actuators arranged in a 10×10 matrix has been fabricated (Figure I- 34 (b)). The dimensions of the prototype are 20-30 mm width and 30-35 mm length respectively.

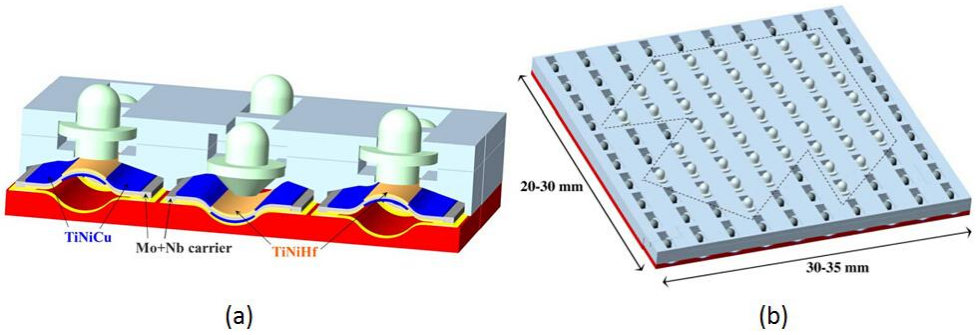

Figure I- 34: Tactile display based on bistable shape memory actuators [VITU 2009]

I.3.3 Digital robots

Abadie *et al.* [ABAD 2009] have developed a digital robot for endoscopy application based on SMA micro-actuator. The actuator is composed of two symmetrical elementary digital stages made by copper semi-rings. The two stages are connected by two NiTi blades. The diameter of copper ring is 4 mm, the length is 9 mm, and the thickness of NiTi blade is 200 µm (Figure I- 35 (a) and (b)). The switching is obtained thanks to the electrothermal principle. When a 0.6 A current is applied, an actuator rotation of 25° is obtained by the Joule effect. When the current is inverted, the actuator will rotate in the reverse direction. The actuator rotation angle can be maintained when the current is canceled. A multi stage endoscope head can be obtained by assembling elementary stages (Figure I- 35 (c)).

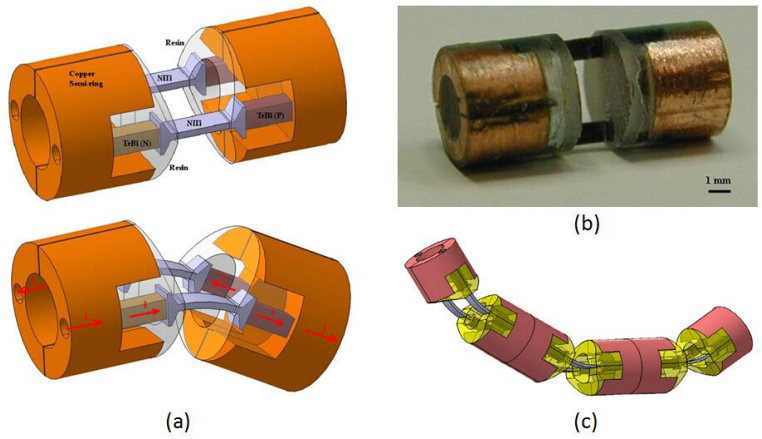

Figure I- 35: Endoscope head [ABAD 2007] (a) SMA actuator (b) prototype (c) multi stage endoscope head

Kim *et al*. [KIM 2010] have presented a bio-mimetic flytrap robot by assembling two bistable SMA actuators. The principle of the robot is illustrated in (Figure I- 36 (a)). The two leaves are made by two unsymmetrical CFRP composite as bistable structures. A SMA coil spring actuator is assembled on each leaf by a clamping bolt. The acrylic plate is added to clamp the leaf and to keep the leaf as flat as possible. A Y-shaped holder can hold the two leaves and incline their position to ensure a more tight closure (Figure I- 36 (b)). When the two actuators are heated or cooled at the same time, the robot will wing. It takes about 100 ms to accomplish one fly motion. The holding function is ensured by the bistable leafs, so the energy is only needed during the change of the shape, and the changed shape can be maintained without a continuous input energy.

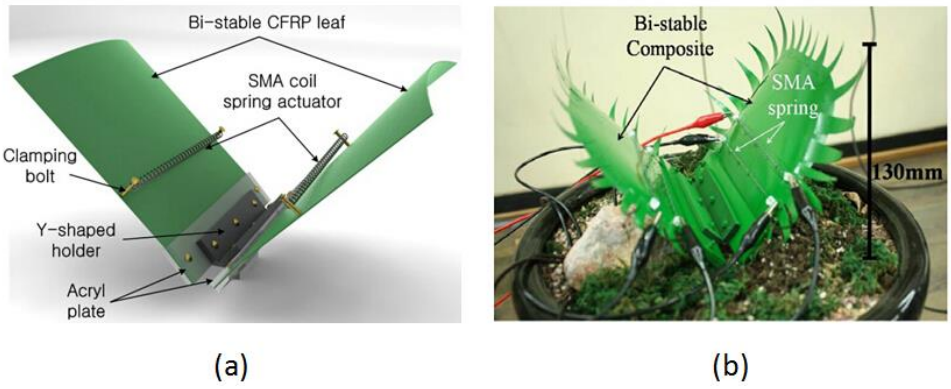

Figure I- 36: Flytrap robot (a) presentation of flytrap robot (b) prototype [KIM 2010]

I.3.4 Digital-to-analog converters

Digital actuators have also been used to realize digital-to-analog converter. Sarajlic *et al*. [SARA 2007] have developed a displacement MicroElectroMechanical Digital-to-Analog Converter (MEMDAC). A single binary unit of the MEMDAC corresponds to a digital actuator and is composed of a rigid segment and a suspended shuttle. The shuttle can move left or right to achieve two stable positions as the value "0" and "1". In Figure I- 37 (a), a 4-bits device composed of four elementary binary units is presented. The elementary digital modules can be switched thanks to the electrostatic principle by a pair of comb drive actuators (Figure I- 37 (b)). The holding function is obtained with a compliant structure. When the MEMDAC is driven by a binary input code, the digital motion of shuttles is converted into an analog output displacement. The digital actuator stroke is 5.8 µm. A 12-bit has also been manufactured.

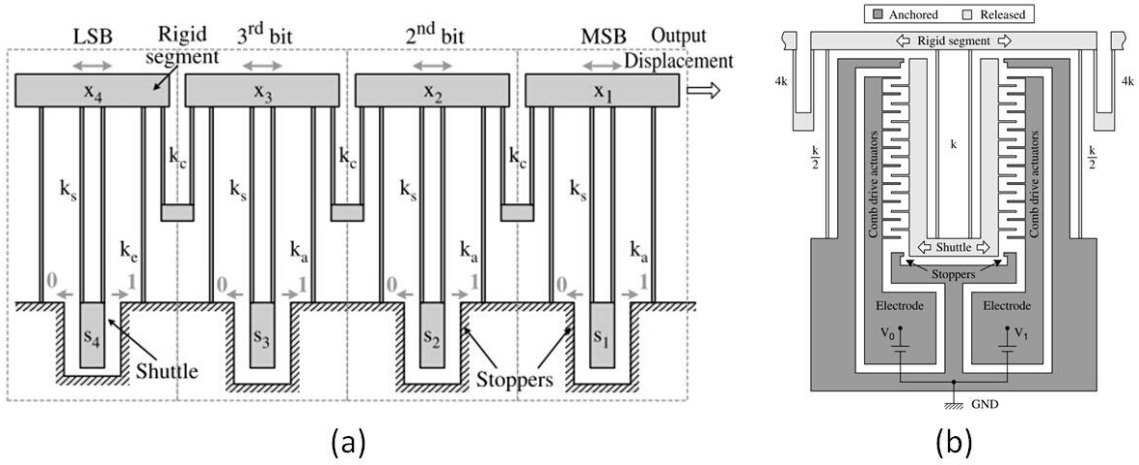

Figure I- 37 : A 4-bit MEMDAC (a) principle (b) comb-drive actuator [SARA 2007]

I.3.5 Displacement tables

Another application of DAA is as the realization of planar conveyance devices. Ataka *et al*. [ATAK 2009] have developed a 2D conveyance system based on ciliary actuator arrays. The conveyance device is composed of several elementary cells. Every cell is composed of four actuators of 500 µm in length and eight pads. The elementary actuator is made of a bimorph polyimide cantilever. The switching function of this actuator is based on the electro-thermal principle. The working principle of the conveyance is illustrated in Figure I- 38 (a)-(h). The actuator cantilevers bend down toward the substrate when a current is applied. The directions of the pads are also controlled by current. Firstly, the actuators and the pads contact the object placed above with all the pads. When the actuator is activated, the cantilevers bend down, the

right pads of each pair move down firstly, and then the left pads move down. Then the right pads move up and the left pads move up, a straight displacement is finished. The actuators return to initial positions. A device composed of 20 × 20 elementary cells has been manufactured, which is illustrated in Figure I- 38 (i). This device can realize straight conveyance, diagonal conveyance and rotation (Figure I- 38 (j)).

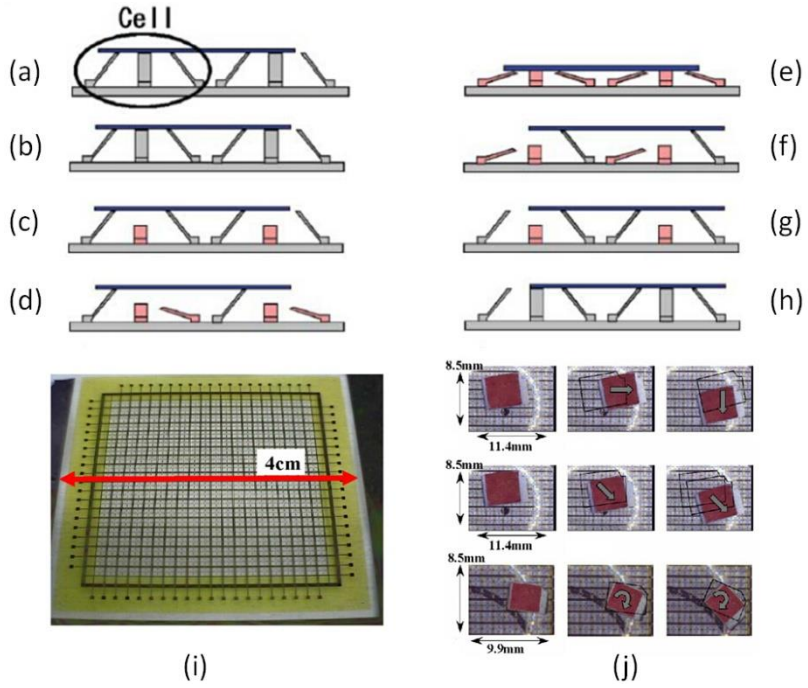

Figure I- 38: 2D conveyance device (a)-(h) principle (i) phototype (j) experimental motion [ATAK 2009]

Chapuis *et al*. [CHAP 2004] have developed a planar conveyance actuators array. The EDA is based on electrostatic actuation principle (Figure I- 39 (a)). The actuator is composed of a movable part with two pairs of suspended electrodes. The movable part is placed at the center position. When the right electrical circuit is connected, the movable part is attracted towards right by the electrode; the air jet will displace the object toward right direction. Based on this principle, an actuators array composed of 560 valves with a conveyance zone of 35 mm × 35 mm (Figure I- 39 (b)). This planar conveyance can realize the displacement in different directions by controlling the air jet.

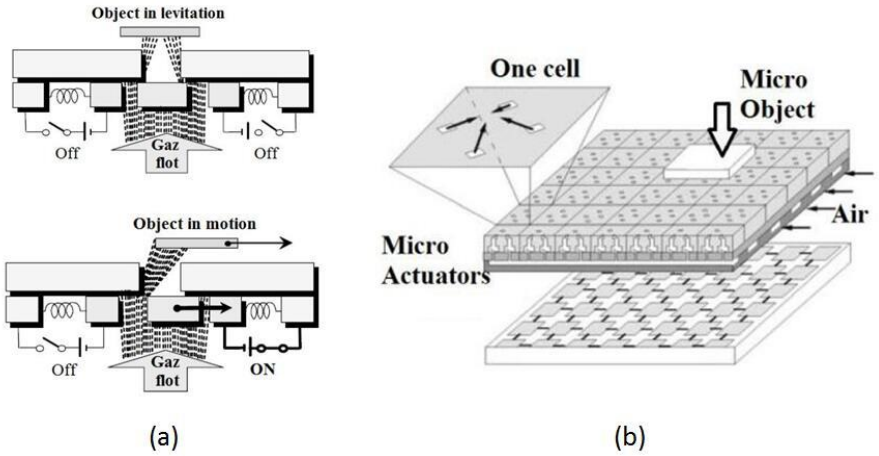

Figure I- 39: Displacement table (a) Two states of elementary cell (b) Assembly of modules [CHAP 2004]

Berlin *et al*. [BERL 2000] also have developed a device for planar conveyance by assembling 1152 digital elementary modules (Figure I- 40 (a)). The elementary module is based on electrostatic actuation (Figure I- 40 (b)). The electrostatic voltage between the flap electrode and the substrate electrode keeps the flap valve closed. When the voltage difference is removed, the supplied air blows the flap to be opened and the air jet moves the paper placed above.

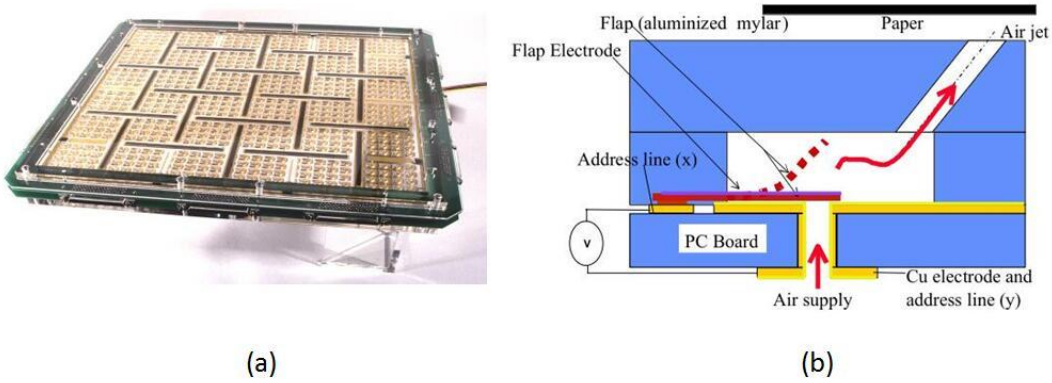

Figure I- 40: Displacement tables: (a) Prototype of experimental tables composed of 1152 elementary actuators (b) Principle of elementary actuator [BERL 2000]

In the Roberval Laboratory, Petit [PETI 2009] has developed a planar conveyance composed of 25 elementary actuators (Figure I- 41 (a)). Each EDA consists of four fixed PMs and one mobile permanent magnet (MPM) which can reach four discrete positions. Under the MPM, there are two orthogonal electrical wires. When a current passes through one of the electrical wires, the generated Lorentz force displaces the MPM. The holding of the mobile part in each discrete position is obtained by magnetic force generated by the fixed PMs. The stroke of the

mobile PM is 200 µm. A digital array composed of 25 EDAs arranged in 5 × 5 matrix has been designed and manufactured. The actuators array has been fabricated (Figure I- 41 (b)). This matrix has been used as a planar conveyance device with a flat glass plate in the thesis of P. Huyan [HUYA 2015].

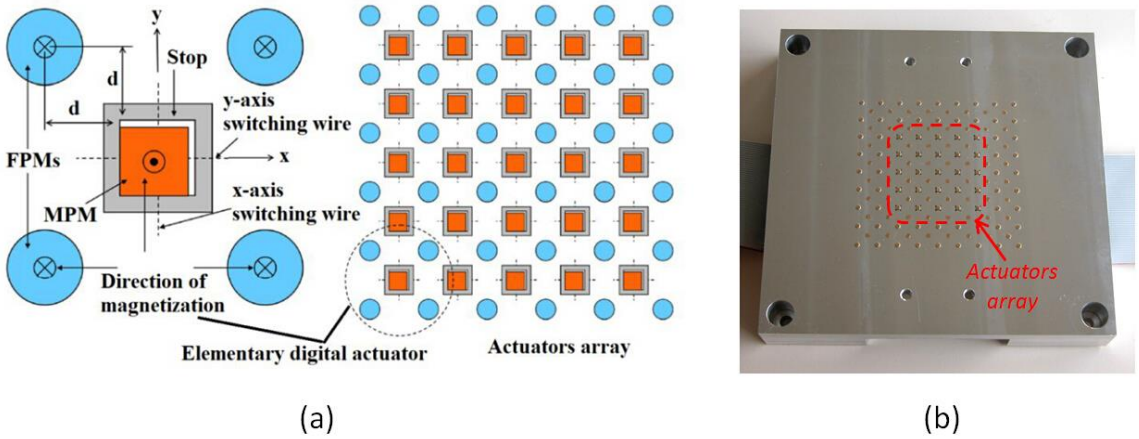

Figure I- 41: DAA (a) Principle (b) Prototype [PETI 2009]

I.4 Conclusion

In this first chapter, a state of art on digital actuation has been presented. Firstly, a definition of digital actuators has been proposed. Then, the two key functions of digital actuators (switching and holding) have been described. The solutions found in literature to realize these two functions have been detailed.

For the switching principle, four principles are used: electrothermal, electrostatic, electromagnetic and piezoelectric. The electrothermal switching principle uses the expansion of materials or phase change of some smart materials when a heating source is applied. This source is easily applied, but the drawback is that the response time is slow. The electrostatic actuators can provide contactless actuation, but the stroke of the actuators is limited, because the stroke is fixed during the fabrication. The electromagnetic principle is well adapted to the digital actuators as a switching method, because the magnetic properties of the mobile part can also be used for the holding function (magnetic holding). This kind of actuators has the advantage of high speed, low cost and the architecture is simple. The piezoelectric actuators have the advantages of instant response and high energy conversion. However, the displacement capacity is small.

To realize the holding function, four solutions are employed in literature: magnetic holding, locking structures, compliant structures and hinged mechanism. The magnetic principle uses the magnetic interaction force between magnetic materials which does not consume external energy to maintain the mobile part at stable positions. This method is easy to be realized and utilized. The holding method of locking structure needs extra architecture of the actuators to maintain the position. This method is simple due to the easy obtained of holding architecture but difficult to implement. The holding function realized by compliant structures and hinged mechanism are available but more difficult to be implemented. It increases the difficulty and complexity for the fabrication and the control.

Based on the switching function and holding function, applications of single actuation were firstly presented mainly for the discrete displacement and the mechanical switch. Then actuators array were presented to realize complex tasks, such as optical switch, tactile display, digital robots, digital to analog converter and table displacement. The presented digital actuators are compared in Table I- 2, comparing the Number of Stable Positions ("NSP"), the size ("Dimensions"), the stroke, the switching time, the energy consumption ("Energy") and the generated force or torque ("F or C output"). According to this table, most of the existed digital actuators have two stable positions and a millimeter scale in dimension. The range of the switching time is from several microseconds to a few seconds. The strokes vary from several micrometers to a few millimeters.

Based on the research of literatures and analysis of different actuators, a DAA composed of 25 EDAs have been design and experimented in our Roberval Laboratory of UTC [PETI 2009, HUYA 2015]. The EDA is based on the electromagnetic principle for switching method (especially Lorentz force). The magnetic holding force is also well suited to realize the holding function. It has four stable positions in two orthogonal displacement directions. This actuators array is used as a planar conveyance device with a flat plate placed above.

In this thesis, to continue the previous work in Roberval Laboratory, the actuators array is firstly studied with the flat plate. The plate displacement is simulated and compared with the experimental results obtained by P. Huyan. Due to the complex conditions of the friction force between the plate and the actuators, a new actuators array is proposed and designed to avoid the friction force with a structured plate. The principle of the new actuators array is similar to the previous actuators array designed by Petit. So the design, the fabrication and the experimentation of the new device will be presented in the following chapters.

Table I- 2: Comparison of the presented digital actuators

Ref.	NSP	Dimensions	Stroke	Switching time	Energy	F or C
Electrothermal actuators						
[SONG 2007]	2	≈50×50×50 mm^3	-	-	-	-
[GOLL 1996]	2	Ø5×1mm	-	-	-	-
[WIJN 2006]	2	0.8×2.2×2.3 mm^3	200 µm	-	-	-
[MAO 2010]	2	50 µm	-	-	-	-
[KHAZ 2010]	2	-	-	-	-	-
[ZAID 2011]	2	3.6×5.8×0.25 mm^3	-	-	-	-
[STAA 2011]	2	3.6×5.8×0.25 mm^3	74 µm	8 ms	-	12.4 mN
[CHEN 2005]	2	3mm×10mm	100 µm	5 ms	-	-
[CHAL 2013]	2	24 × 36 mm^2, 400µm	35 µm	-	-	-
[CRAL 2000]	2	200 × 20 $µm^2$	3 µm	-	50 mW	-
[COCH 2005]	2	3×50 nm^2	130 µm	40 ms	5280 mW	-
[LIU 2015]	2	22 × 19 × 0.4 mm^3	300 µm	2 s	-	300 mN
[HAGA 2005]	2	≈ Ø1.6×7mm	1 mm	1 s	-	-
[MATS 2013]	2	-	2 mm	0.3 s	-	-
[VITU 2009]	2	4×1×h mm^3	700 µm	100 ms	80 mW	2.2 mN
[ABAD 2007]	2	4×9 mm^2, 200 µm	25°	-	-	-
[KIM 2010]	2	240×80×160 mm^3	-	100 ms	-	-
[SARA 2007]	2	-	5.8 µm	-	-	-
[ATAK 2009]	2	500×100×6 $µm^3$	-	-	-	-
Electrostatic actuators						
[OBER 2006]	3	≈1 mm×1 mm	8.5 µm	400 µs	-	1.1 mN
[FREU 2004]	2	≈1.2 mm×1 mm	100 µm	-	-	50 µN
[HERD 2004]	2	-	65 µm	7 ms	-	-
[PLOT 2001]	3	≈100µm×100µm	-	10 µs	-	-
[CHAP 2004]	3	-	-	-	-	-
[BERL 2000]	2	-	-	-	-	-
Electromagnetic actuators						
[ZHAN 2007]	2	2mm×2.2mm	17 µm	20 µs	3 µJ	
[LUHA 2008]	2	3.4×6×h mm^3	10°	10 ms	-	1 µNm
[WUYI 2010]	2	150×150×0.32 mm^3	-	-	-	-
[LIAO 2010]	2	-	350 µm	10 ms	-	-
[AHNH 2014]	2	-	-	54.2 ms	-	-
[ROOD 2008]	2	-	25 mm	2 ms	-	200 kN
[WANG 2009]	2	≈4mm×1mm	90 µm	1 ms	-	-
[MENE 2006]	2	Ø5 mm× 6.7 mm	0.62	2.7 ms	20 mJ	
[BOHM 2000]	2	7×7×1 mm^3	200 µm	-	-	-
[DIEP 2004]	2	100×40×5 mm^3	-	30 µs	-	48 J
[BENA 2007]	2	≈ Ø10×3mm	200 µm	-	-	≈ 10mN
[PETI 2009]	4	100×100 nm^2	200 µm	-	-	
Piezoelectric actuators						
[CAZO 2008]	2	200×20 nm^2	-	-	-	-
[JIAC 2009]	2	180 µm×160 µm	-	6 ms	-	-

Chapter 2: Planar conveyance based on a digital actuators array and a flat plate

In this chapter, a planar conveyance device based on a Digital Actuators Array (DAA) and on a flat plate is presented. The principles of the Elementary Digital Actuator (EDA) and of the DAA are presented. An analytical model of the EDA is proposed to calculate the magnetic and electromagnetic forces exerted on the MPM. Then, a modeling of the DAA is described to calculate the plate displacement. The model is tested under various conditions, such as different driving current values or different friction coefficient values in order to observe their influence on the plate displacement. The influence of the number of controlled EDAs on the plate displacement is studied, and a control strategy is proposed to realize a certain plate displacement. At the end, simulated results are compared with the experimental results obtained by P. Huyan [HUYA 2015].

II.1 Elementary digital actuator

The EDA consists of a mobile part, which is a Mobile Permanent Magnet (MPM), and a fixed part. The fixed part regroups a square bracket, two orthogonal wires and four Fixed Permanent Magnets (FPMs). The MPM is placed in a square bracket and can reach the four corners which correspond to the four discrete positions of the EDA (Figure II- 1).The FPMs generate a magnetic force on the MPM to hold it in discrete positions without external energy supplying.

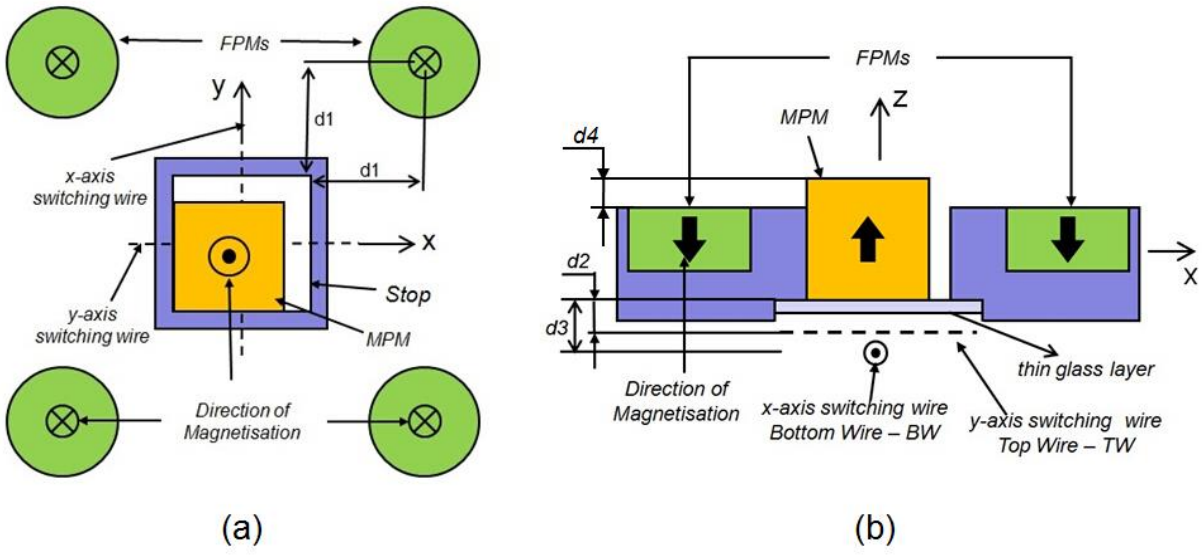

Figure II- 1: Schematic layout of the EDA (a) Top view (b) Side view

The properties of the MPM and the FPMs are given in Table II-1. The design of the EDA has been realized in another thesis [PETI 2009] considering the manufacturing constraints. The MPM corresponds to the maximum magnetization of all the existed magnets in order to obtain a high electromagnetic force. The MPM material and the mechanical support (square cavity) are NdFeB, and Aluminum, respectively. The distance between FPMs and square cavity and the distance between MPM and switching wires have been determined during the actuator design. The stroke of this elementary digital actuator, represented by the gap between the MPM and the square bracket, is 200 µm.

TABLE II- 1: EDA characteristics

Magnets properties			
Magnet type	Dimensions		Magnetization
MPM	2 mm × 2 mm × 2 mm		1.45 T
FPM	Ø2.26 mm × 1.25 mm		1.45 T
Mass of the MPM : 0.06g			
Distances			
d1	d2	d3	d4
3.85 mm	222 µm	458 µm	375 µm

A Printed Circuit Board (PCB) including two orthogonal electric wires is placed below the square bracket to generate the driving force. The wires are printed on a double-side PCB (one on each side) to avoid any electrical contact between the Top Wire (TW) and the Bottom Wire (BW) (Figure II- 2 (a)). Due to the PCB thickness, the distance between the bottom side of the MPM and the TW (d2) is smaller than the distance between the bottom side of the MPM and the BW (d3). The electromagnetic generated force is then lower using the BW than using the TW. The PCB has then been chosen as thin as possible (200 µm) (Figure II- 2) to minimize the electromagnetic force loss between the BW and the TW. Moreover, a thin glass layer (170 µm thickness) is placed between the MPM and the PCB to minimize the friction between the MPM and the fixed part, to provide a flat surface on which the MPM moves and to avoid electrical contact between the TW and the MPM.

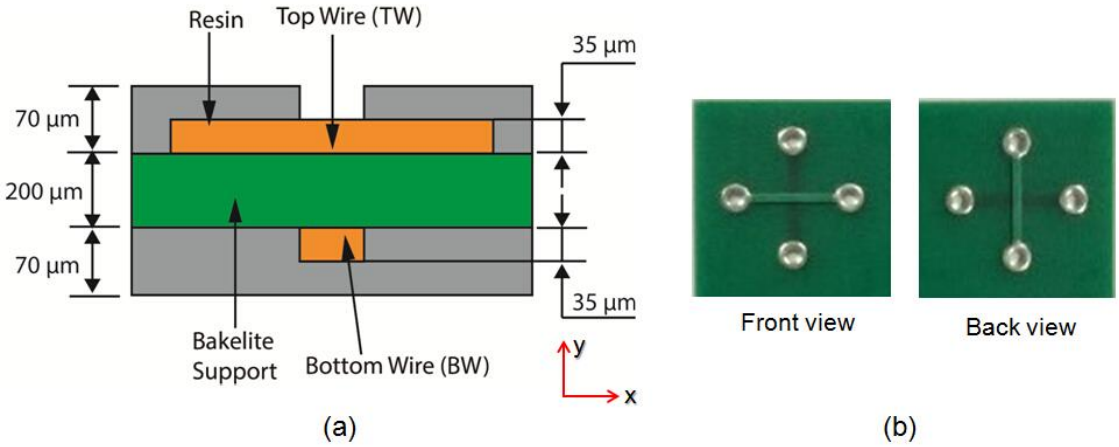

Figure II- 2: (a) Cross section of the PCB (b) Prototype of PCB

The principle of switching between the discrete positions is illustrated in Figure II- 3. From (a) to (c), the MPM is switched along +y-axis. At first, the MPM is located at (-x, -y) discrete position (Figure II- 3 (a)). The MPM is held in this position thanks to the magnetic holding force generated by the FPMs. When a driving current is injected through the x-axis wire in the +x direction, a Lorentz force is generated on the wire in the –y direction. Because the wire is fixed, the resulting force in the +y direction is applied on the MPM which switches along y-axis (Figure II- 3 (b)). The MPM reaches then the (-x, +y) discrete position (Figure II- 2 (c)). From (d) to (f), the MPM is switched back to the initial position with adding an electromagnetic holding force. So an inverse driving current along –x-axis wire is considered, the electromagnetic force exerted on the MPM is then also inverted (oriented along –y direction) and the MPM switches along –y-axis. In this case, another current through the x-axis wire is added to generate an electromagnetic force on the MPM along –x direction. The lateral contact force between the MPM and the left edge of the cavity is then increased (Figure II- 3 (e)). This current is called “holding current”. It can be added to ensure the lateral contact and reduces straightness error or external disturbances effect during the MPM switch. At last, the MPM comes back to the initial discrete position (Figure II- 2 (f)).

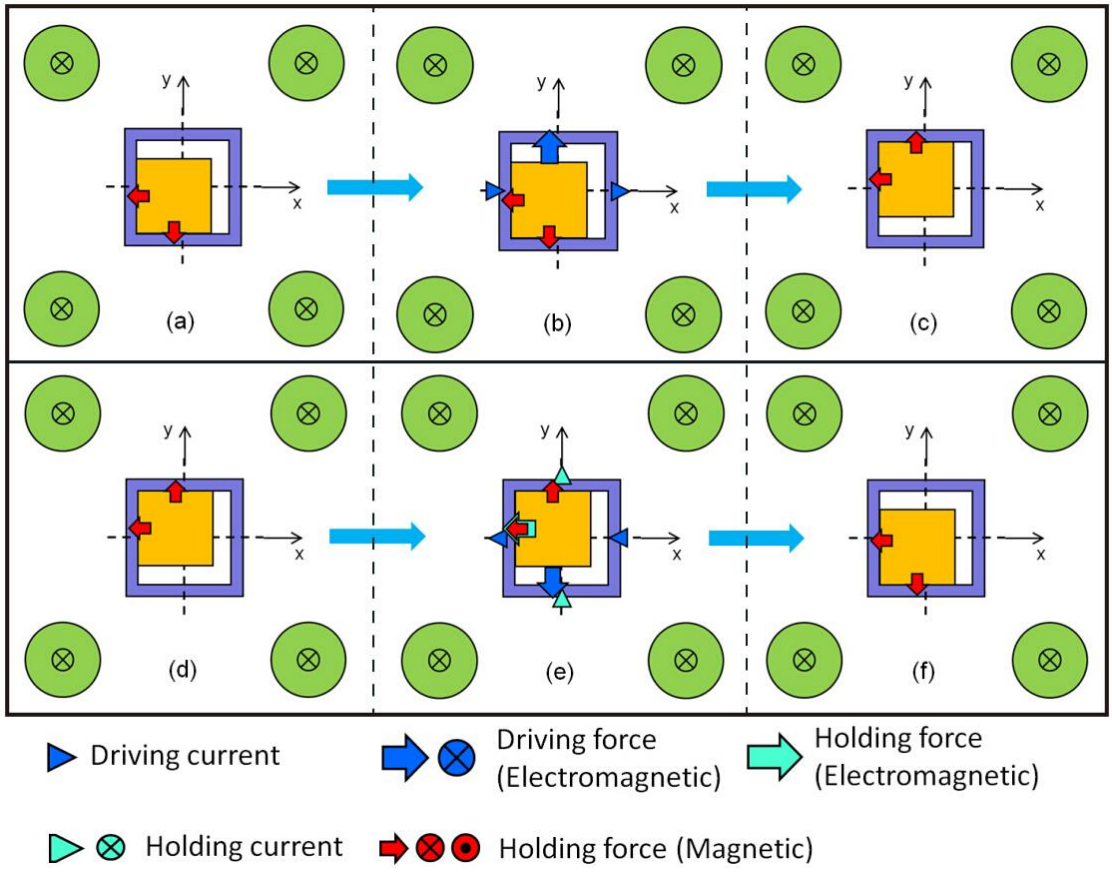

Figure II- 3: Principle of switching between discrete positions

II.2 Digital actuators array

II.2.2 Principle of DAA

In this section, a DAA composed of 25 EDAs arranged in 5 × 5 matrix architecture is presented (Figure II- 4). To reduce the size of the DAA, the FPMs are shared between two adjacent EDAs. During the DAA design, the magnetic and electromagnetic interactions between the EDAs have been considered. The EDA behaviors are different for the EDAs placed at the center of the DAA compared to the EDA placed at the boundaries. The EDAs placed at the center have a balanced magnetization, while the magnetic interactions on EDAs placed at the boundaries are different between the MPMs. In order to ensure a homogenous behavior, Additional Fixed Permanent Magnets (AFPMs) have then been added around the DAA (Figure II- 4). Three rows of AFPMs have been added (AFPM1, AFPM2 and AFPM3). The distances between FPMs and AFPM1 is d_{a1}, between AFPM1 and AFPM2 is d_{a2}, between AFPM2 and AFPM3 is d_{a3}. The AFPMs magnetization have been chosen as the same as FPMs to ensure a balanced interactive

magnetic force with the same distance between AFPMs. AFPM1 and AFPM3 correspond to MPMs, so they are chosen the same thickness as that of MPMs. The characteristics of the additional magnets and the distances between them are given in

TABLE II- 2. The overall dimension of the active area of the DAA is 42×42 mm^2.

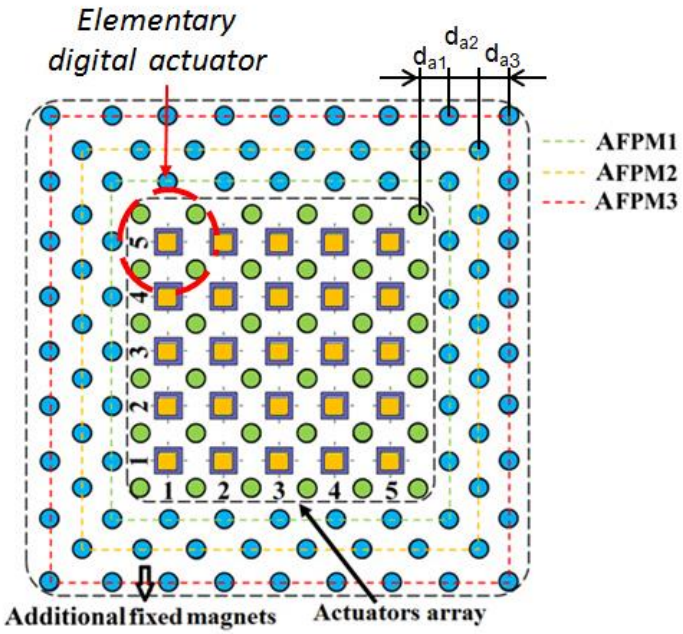

Figure II- 4: Model of DAA [HUYA 2015]

TABLE II- 2 : AFPM properties

Additional Fixed Permanent magnets properties		
Magnets	Dimensions	Magnetization
APFM1	Ø2.26mm×2mm	1.45T
APFM2	Ø2.26mm×1.25mm	1.45T
APFM3	Ø2.26mm×2mm	1.45T
Distance between AFPMs		
d_{a1}	d_{a2}	d_{a3}
4.95mm	4.95mm	4.95mm

II.2.2 Principle of planar conveyance device

An application of the presented DAA as a planar conveyance device is proposed. In this application, a flat plate is placed above the DAA. The plate is displaced thanks to the stick-slip principle between the MPMs and the flat plate. In Figure II- 5, a side view of the plate displacement sequence is shown. The sequence is composed of six steps. Initially, all the MPMs are placed at the same discrete position (left discrete position in Figure II- 5 (a)). Secondly, all

the MPMs are switched towards +x direction at the same time (Figure II- 5 (b)), the plate moves in the same direction thanks to the friction between the plate and the MPMs. Thirdly, the MPMs of the first column are switched one by one towards –x direction to reach their initial position (Figure II- 5 (c)). During this step, each MPMs slides relatively to the plate because the generated force is not high enough to move the plate. This one will then stay at its current position. In the next steps (Figure II- 5 (d)-(g)), the other MPMs are switched one by one to the initial position without plate displacement. Finally, when all the MPMs are back to the initial positions (Figure II- 5 (h)), a second displacement sequence can be realized. Long plate displacements can be realized by repeating this displacement sequence. The plate is a thin glass sheet with 50 × 50 × 0.13 mm^3 dimension and 0.96 g mass (m_p).

Due to the matrix structure, the plate displacement can be realized in several directions. Theoretically, in addition to plate displacement along x-axis or y-axis separately obtained by switching all the MPMs along one direction (x or y) (Figure II- 6 (a) and (b)), the plate can be displaced along diagonal direction when the MPMs are switched simultaneously along x and y axes (Figure II- 6 (c)). Moreover when the first two lines of MPMs are switched along x-axis, while the last two lines of MPMs are switched along – x-axis at the same time, a rotation of the plate can also be generated (Figure II- 6 (d)).

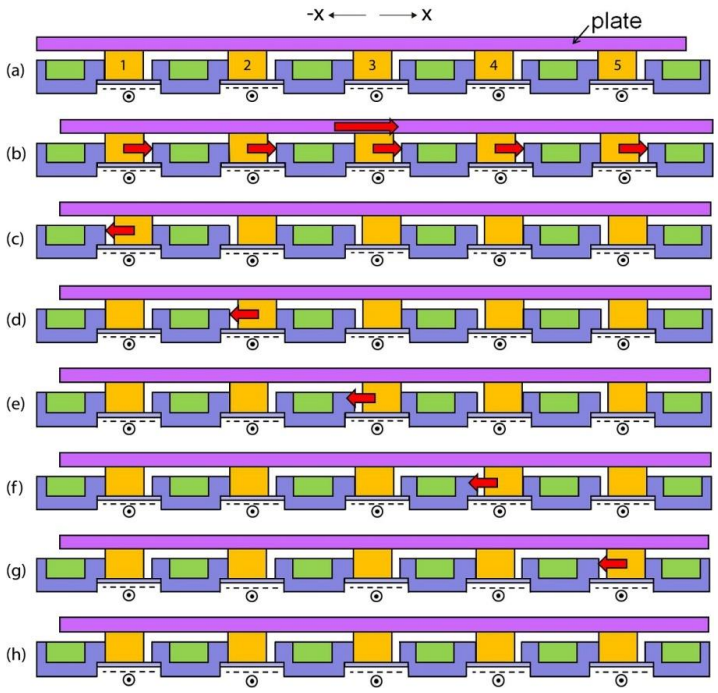

Figure II- 5: Side view of displacement sequence

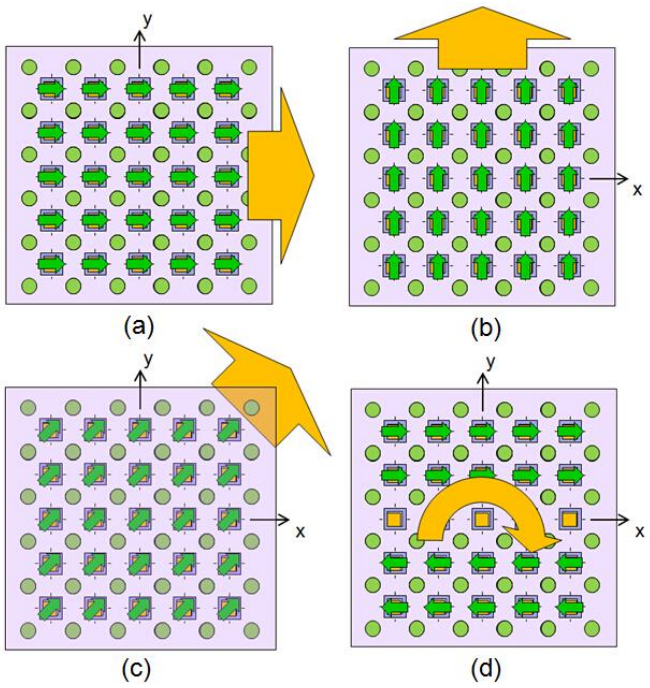

Figure II- 6: Plate displacement (a) displacement along x-axis (b) displacement along y-axis (c) diagonal displacement (d) plate rotation

II.3 Plate displacement modeling

In this section, a model is proposed to compute the flat plate displacement. The model is developed to characterize the planar conveyance application by considering the contribution of the EDAs. To compute the plate displacement, the MPM displacement has to be firstly determined. Then a magnetic flux density model is introduced to calculate the magnetic force and the electromagnetic force exerted on each MPM. Then, the acceleration, the velocity and the displacement of MPM can be computed. The friction between the MPM and the plate can then be considered in order to obtain the plate displacement.

II.3.1 Magnetic and electromagnetic force calculation

In this part, a static model of the EDA is presented to compute the magnetic and electromagnetic forces exerted on the MPM.

II.3.1.1 Magnetic flux density

In order to calculate the magnetic and electromagnetic forces on the MPM, a magnetic flux density model has been developed. This analytical flux density model is based on the charge model. Several assumptions have been supposed to develop this model. Firstly, the PM geometries are supposed to be perfectly rectangular and in free space. Secondly, the PM magnetizations are considered as uniform and oriented along z-axis. In this model, each PM is reduced to a distribution of equivalent magnetic charge [FURL 2001]. The expressions of the magnetic flux density are realized considering the PM presented in Figure II- 7. The origin of the coordinate system (0, 0, 0) is located at the center of the PM. The north and south poles of the PM are located on the surfaces +z and –z, respectively. The PM dimensions are ($x_2 - x_1$), ($y_2 - y_1$), ($z_2 - z_1$) along the x, y and z axis, respectively. The three components of the external magnetic flux density (B_x, B_y and B_z) generated by the PM at any point (x, y, z) located outside of the PM are given by equations (II.1).

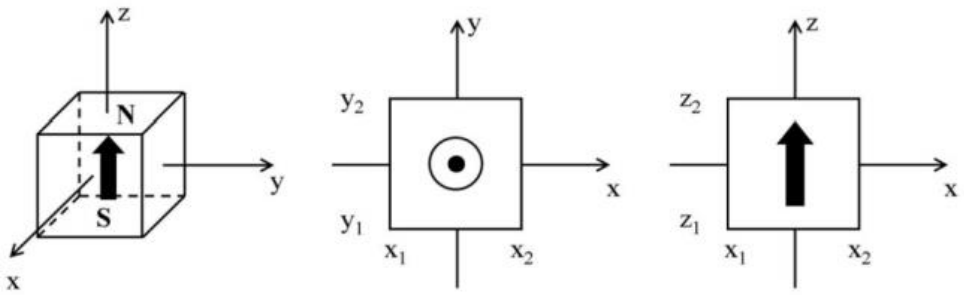

Figure II- 7: Model of magnetic flux density [FURL 2001]

$$
\begin{aligned}
B_x(x,y,z) &= \frac{\mu_0 M}{4\pi}\sum_{k=1}^{2}\sum_{m=1}^{2}(-1)^{k+m}\ln(F(x,y,\mathrm{z},\mathrm{x}_m,y_1,y_2,z_k)) \\
B_y(x,y,z) &= \frac{\mu_0 M}{4\pi}\sum_{k=1}^{2}\sum_{m=1}^{2}(-1)^{k+m}\ln(\mathrm{H}(x,y,\mathrm{z},\mathrm{x}_m,y_1,y_2,z_k)) \\
B_z(x,y,z) &= \frac{\mu_0 M}{4\pi}\sum_{k=1}^{2}\sum_{n=1}^{2}\sum_{m=1}^{2}(-1)^{k+n+m}\times \\
&\tan^{-1}\left(\frac{(x-x_n)(y-y_m)}{(z-z_k)}g(x,y,z;x_n,y_m,z_k)\right)
\end{aligned}
\qquad \text{(II.1)}
$$

Where,

B_x, B_y, B_z : Magnetic flux density components along x, y, z axis (T),

μ_0 : Magnetic permeability of air ($4\pi \times 10^{-7}$) (H/m),

M : Magnetization of the permanent magnet ($A.m^{-1}$),

(x, y, z) : Coordinates of computing point (m).

II.3.1.2 Magnetic force

Based on the magnetic flux density model, the magnetic force between two PMs can be calculated. To illustrate the calculation, the two PMs (Magnet 1 and Magnet 2) represented in Figure II- 8 are considered. The expression of the magnetic force generated by Magnet 1 on Magnet 2 is given in equation (II.2) [FURL 2001]. The σ_m represents the surface charge density of two surfaces located on the poles of Magnet 2. The B_{ext} vector is the magnetic flux density generated by Magnet 1 around Magnet 2 which is given by equation (II.1).

$$F_M = \iint_S \sigma_m B_{ext} ds \tag{II.2}$$

Where,

F_M : Magnetic force (N),

σ_m : Surface flux density ($A.m^{-1}$),

B_{ext} : Magnetic flux density (T) generated by Magnet 1

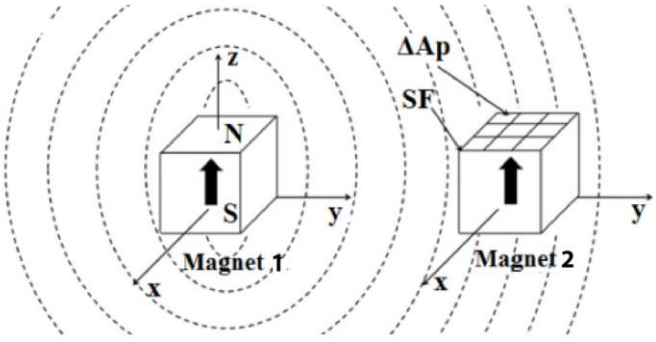

Figure II- 8: Magnets with coordinates for magnetic force calculation

However, in most cases, the equation (II.2) cannot be used for analytical calculation as explained in [FURL 2001]. Then, the magnetic force is calculated by discretizing the pole

surfaces of Magnet 2 into sub-surfaces ΔA_p (Figure II- 8). Then the magnetic flux density (B_{ext}) is calculated for each ΔA_p surface and the magnetic force is obtained with equation (II.3).

$$F_M = \sum_p \sigma_m(x_p) B_{ext}(x_p) \Delta A_p \tag{II.3}$$

II.3.1.3 Electromagnetic force

In this part, the calculation of the electromagnetic force (Lorentz force) is described. The expression of this force as function of the driving current is given in equation (II.4).

$$F_{EM} = I \int_{wire} dI \times B_{ext} \tag{II.4}$$

Where:

I : Driving current through electric wires under MPM (A)

B_{ext} : Magnetic flux density generated by the MPM around the considered wire (T).

II.3.2 Friction force calculation

II.3.2.1 Friction on MPM

As introduced in previous part, an application of the DAA as a planar conveyance device has been proposed. In this application, the DAA is used to move a flat plate placed above. An EDA is illustrated in Figure II- 9 to show the friction forces considered in the proposed displacement model. Three friction forces are considered in the modeling. F_1 is the friction force between the MPM and the glass layer placed below it; F_2 is the friction force between the MPM and the lateral stop of the square cavity; F_3 is the friction force between the MPM and the conveyed flat plate placed above it. The friction is calculated by averaging the plate on the 25 actuators.

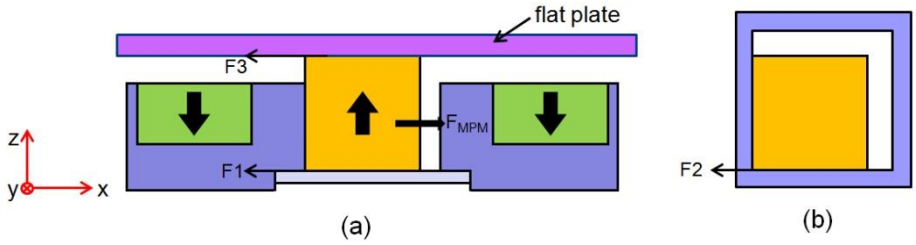

Figure II- 9: Analysis of friction forces exerted on MPM (a) Top view (b) Side view

The expressions of these friction forces are given in equation (II.5). To compute these friction forces, two friction coefficients are considered. The first one is the friction coefficient between the MPM and the glass is 0.41 (μ_1) and the other one is the lateral friction coefficient between the MPM and aluminum is 0.3 (μ_2); these values have been experimentally determined in former thesis [PETI 2009].

$$\begin{aligned} F_1 &= \left(m_m \times g - (F_{Mz} + F_{EMz}) + \frac{g}{Nb} \times m_p \right) \times \mu_1 \\ F_2 &= (\mathrm{F}_{My} + \mathrm{F}_{EMy}) \times \mu_2 \\ F_3 &= \frac{g}{Nb} \times \mu_1 \times m_p \end{aligned} \qquad \text{(II.5)}$$

Where:

g : Gravity acceleration (9.81 m/s^2).

m_m : Mass of MPM (kg)

m_p : Mass of the plate (kg)

Nb : Number of the controlled magnets

F_{My}, F_{Mz} : Magnetic force along y and z axis respectively (N)

F_{EMy}, F_{EMz} : Electromagnetic force along y and z axis respectively (N)

Finally, the total force exerted on the MPM (F_{MPM}) is computed with equation (II.6).

$$F_{MPM} = (\mathrm{F}_{Mx} + \mathrm{F}_{EMx}) - F_1 - F_2 - F_3 \qquad \text{(II.6)}$$

II.3.2.2 Friction on plate

The total force generated on the plate is due to the friction between the plate and the MPMs. To compute this friction force, two cases are considered. Firstly, at the beginning, if the friction force between the plate and the MPM is a static friction, the acceleration and the displacement of the plate equals to that of the MPM. Secondly, the friction between the plate and the MPM is kinetic friction. In this case, the friction of the plate is calculated in two conditions. During the switch of the MPMs, the MPM displacement is smaller than the stroke, the friction exerted on the plate is positive to make the plate move upward (equation (II.7)).

$$F_{p1} = n \times F_3 \tag{II.7}$$

Where n is the number of switched MPMs.

However when the MPMs arrive at the border of the cavity, the MPMs stop roughly, the plate continues sliding. In this condition, the force exerted on the plate has the same expression but with a negative sign (equation (II.8)). The plate continues moving until its velocity is null.

$$F_{p2} = -n \times F_3 \tag{II.8}$$

II.3.3 Displacement calculation

When all the forces ($\vec{F}$) exerted on the MPMs or on the plate are obtained, their acceleration ($\vec{a}$), velocity ($\vec{v}$) and displacement ($\vec{d}$) can be determined according to equation (II.9).

$$\sum \vec{F} = m\vec{a} = m\frac{d\vec{v}}{dt} = m\frac{d^2\vec{d}}{dt^2} \tag{II.9}$$

II.3.4 Flowchart of the plate displacement modeling

The displacement modeling has been implemented in MATLAB software. The flowchart of the modeling is shown in Figure II- 10.

In this model it is assumed that all the EDAs are identical and have the same influence on the plate displacement. Firstly, the parameters are set, including the driving current, step time, friction coefficients, MPM stroke and the initial settings of the DAA, including the number of EDAs and their initial positions. Secondly, the magnetic force (F_M) and electromagnetic force (F_{EM}) are calculated based on the magnetic flux density model. Thirdly, by comparing the MPM displacement (d_{MPM}) with the MPM stroke (stroke), the friction force between the MPM and the plate (F mp) is then determined. Therefore, the kinetic factors (acceleration, velocity and displacement of MPM and the plate) are computed by considering the magnetic, electromagnetic and friction forces, the new MPMs positions will then be returned to recalculate the electromagnetic force. Finally, the simulation stops when the plate velocity is null.

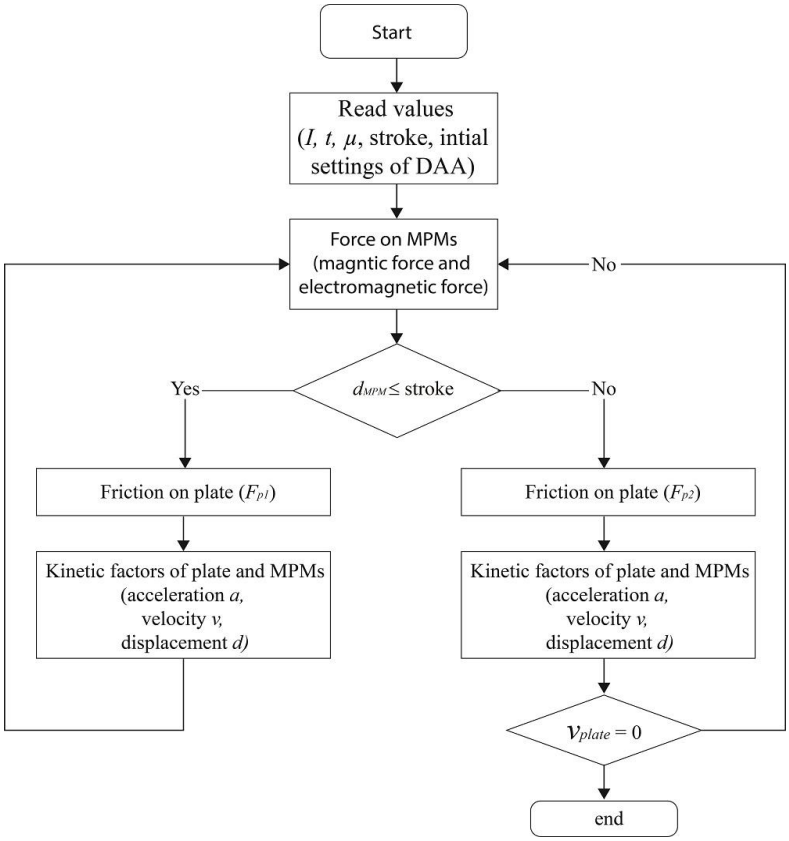

Figure II- 10: Flowchart of the displacement simulation

II.4 Simulation results

In this section, simulation results are presented. The MPM and plate displacements are computed for the two displacement axes and for different controlling current values. Some studies have been carried as the influence of the friction coefficient values on the plate displacement, the minimum number of controlled actuators to move the plate and the best control strategy to realize a 1 mm plate displacement. Then, simulated results are compared with experimental results obtained in the previous thesis [HUYA 2015].

II.4.1 Influence of the driving current value

In this part, the influence of the driving current value on the MPM and plate displacements is studied. The displacements have been determined for different driving current values as shown in Figure II- 11. In Figure II- 11(a) and (b), the minimum driving current able to move the plate has been used: 1.7A for x-axis and 1.8A for y-axis, respectively. With 1.7A, the MPM switching time along the x-axis is 7.8 ms which is the highest among the three values along x-axis. With

this current, the displacements of MPM and the plate are close at the beginning of the switch (< 2 ms), because the force generated on the MPM is small. The MPM acceleration is small then there is adhesion between the plate and the MPMs. After 2 ms, a sliding of the plate relative to the MPMs is visible. During the MPM displacement (between 2 ms and 8 ms), the plate velocity increases. When the MPM arrives in discrete position, the MPM will stop moving. The force exerted on the plate becomes negative then, the plate velocity decreases. The plate continues to move until its velocity becomes null. When the MPM stops, the plate continues to move, so the plate displacement (247.22 µm) is higher than the MPM stroke. For y-axis with a 1.8A driving current, the switching time is 13 ms and a 536.22 µm plate displacement is obtained. In this configuration, there is adhesion between the plate and the MPM throughout all the MPM displacement.

For the driving current 3A (Figure II- 11(c)), the MPM switching time is 3.9 ms and 4.7 ms for x and y, respectively. The switching time is higher for a switch along y-axis than x-axis because the distance between the bottom side of the MPM and the wire is higher for y (d_2) than for x (d_3) (see Figure II- 1(b)). By applying the same driving current value, the electromagnetic force is then lower along x-axis than along y-axis. So the acceleration and the sliding effect are reduced for y-axis compared to x-axis. The friction between MPM and the plate is less, while the switching time is longer and more important; the plate displacement is then higher when the MPM switches along y-axis than along x-axis which can be observed in Figure II- 11(d). In this case, the plate displacement obtained is 60.24 µm and 88.47 µm for x and y, respectively. The Figure II-12 (a) and (b) represent the MPM and plate velocity as function of time for the considered configuration. It can be observed that the MPM velocity increases throughout the switch because the electromagnetic force is applied throughout the switch. The plate velocity increases during the switch of the MPM and decreases when the MPM has reached the discrete position. With a 7A driving current, the switching time is 2.2 ms and 2.4 ms for x and y axis, respectively. In this condition, the plate displacement is 18.42 µm and 23.75 µm for x and y axis, respectively. With this driving current value, the MPM acceleration is high then the sliding between the MPM and the plate also.

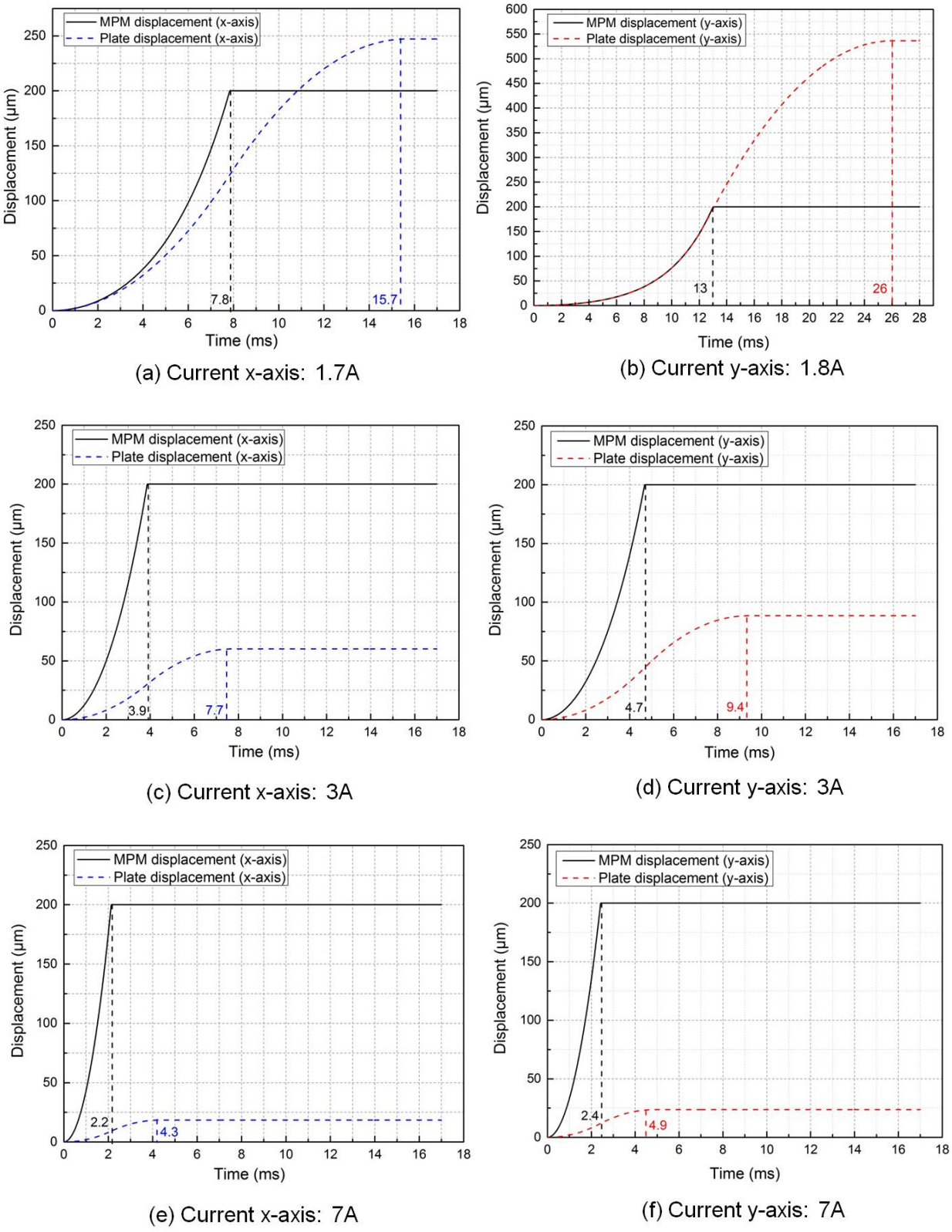

Figure II- 11: Plate displacement with different currents

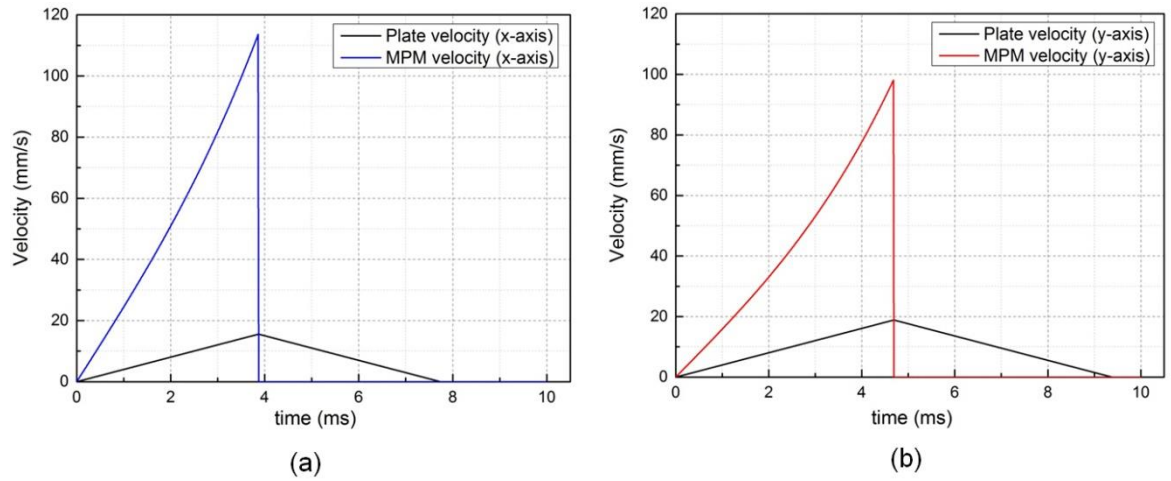

Figure II- 12: Velocity of MPM and plate along x and y axes

The plate displacements along x and y axes as function of the driving current value are illustrated in Figure II- 13. The plate displacement decreases with the increase of driving current value. With a low driving current value, the electromagnetic force exerted on the MPM is lower, the sliding effect between the MPMs and the plate is low and the obtained plate displacement is high. As a planar conveyance application, if large displacements are needed, low driving current should then be used to minimize the number of steps needed. However, to obtain a small displacement of the conveyed object, a high driving current should be used.

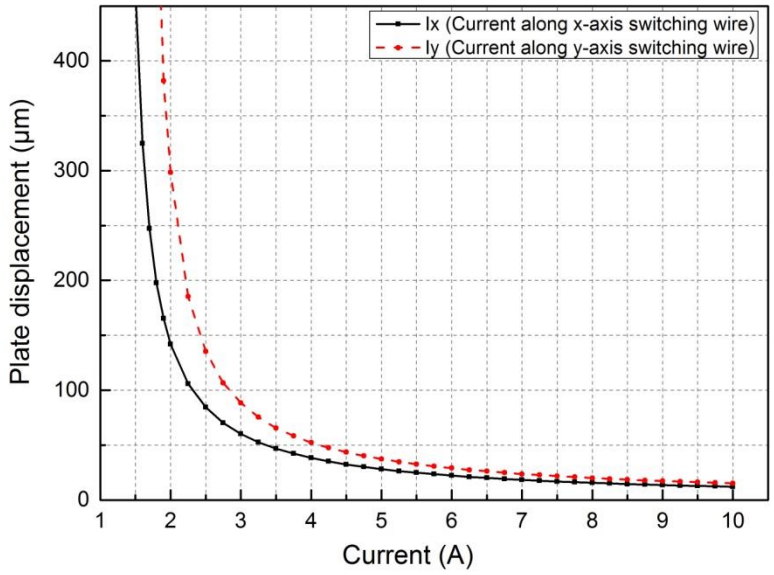

Figure II- 13: Plate displacement in x and y direction

II.4.3 Influence of friction coefficient variability

In this section, the influences of friction coefficient values (between the plate and the MPMs) and of the friction (between the MPMs and square cavities) are studied. The friction coefficients values have been determined in a previous thesis [PETI 2009] using an inclined plane technique. The obtained values are $\mu_1 = 0.41$ for contacts between gold and glass and $\mu_2 = 0.30$ for contacts between gold and aluminum. These two friction coefficients are considered in the calculation of the displacement of MPM and the plate. In the thesis of P. Huyan [HUYA 2015], the influence of friction nonhomogeneity has been observed during the experiment. The observed effect is a non-simultaneous switching of the different MPMs for low driving current values.

To evaluate the influence of the friction coefficient variation on the plate displacement, ±10% variability on the friction coefficient values have been considered. So, μ_1 varies between 0.369 to 0.451, μ_2 between 0.270 to 0.330. To observe the largest influence in extreme conditions, the two coefficients are considered the same on all the MPM. The influence of the friction coefficient on the plate displacement is presented in Figure II- 14. From this figure, it is shown that when the two friction coefficients are at the lowest values ($\mu_1 = 0.369$ and $\mu_2 = 0.27$), the plate displacement is the smallest and vice versa, when μ_1 and μ_2 are at the highest values, the plate displacement is the largest. It is also obvious that, the plate displacement varies more with the variation of μ_1 than of μ_2, the friction coefficient between MPM and the glass (μ_1) is indeed more important than that between MPM and the Aluminum part (μ_2) (equation (II.6) – equation (II.8)).

From the Figure II- 14, it is shown that the influence of the friction coefficients on the plate displacement is more important for low than for high driving currents. When the friction coefficient increases, the total force exerted on the MPM reduces (equation (II.6)), then the plate acceleration is smaller, the sliding effect is then larger. This phenomenon is clearly visible for low driving current values. The plate displacement difference between the two extreme cases is 58.52 µm with a 2A driving current value and only 2.57 µm with a 7A driving current value.

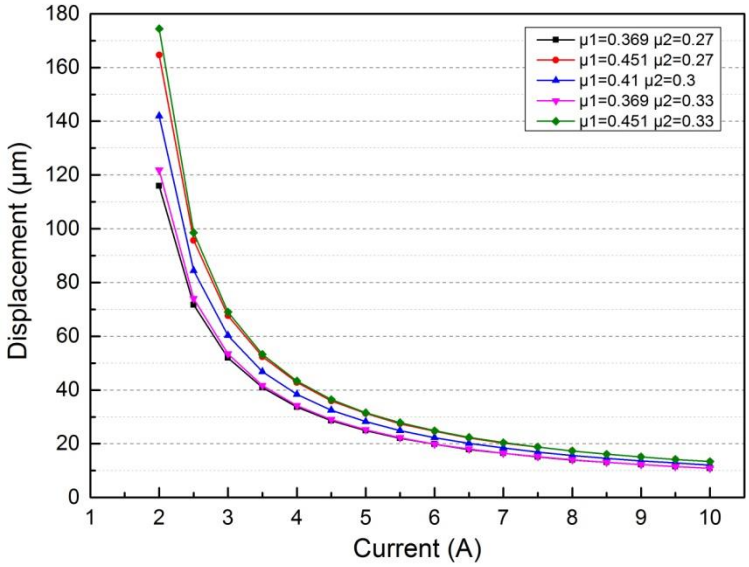

Figure II- 14: Influence of friction coefficient

II.4.4 Plate displacement as function of number of controlled EDAs

In the modeling, it is assumed that the DAA is composed of 25 identical EDAs. In the displacement sequence described in the planar conveyance principle (Figure II- 5), at the first step, all the MPMs are switched simultaneously to move the plate. After this step, the MPMs are switched alternatively to return to their initial position, and then a new displacement sequence can be realized. In this sequence, all the EDAs contribute to the plate movement. This section is dedicated to the study of the minimum number of MPMs needed to move the plate. To realize this simulation, the number of switched MPMs is varied and the plate displacement is calculated for each configuration. The plate displacement along x and y axes as function of the number of controlled actuators for two driving current values (3A and 7A) is shown in Figure II- 15. From this figure, it is visible that when the number of controlled MPMs is lower than half of the total MPMs number, the plate does not move. In this condition (number of controlled actuators lower than 13), the friction force between the actuated MPMs and the plate (equation (II.7)) is indeed lower than the friction force between the inactivated MPMs and the plate (equation (II.8)). When the number of controlled MPMs is higher than half of DAA, the plate displacement increases as function of the number of controlled MPMs (Figure II- 15). The minimum plate displacement is then obtained when only 13 MPMs are controlled. With 3A driving current value, the minimum plate displacement is 1.25 μm and 1.84 μm along x and y

axes, respectively. The same behavior is obtained with 7A but the plate displacement is lower as observed in the previous study.

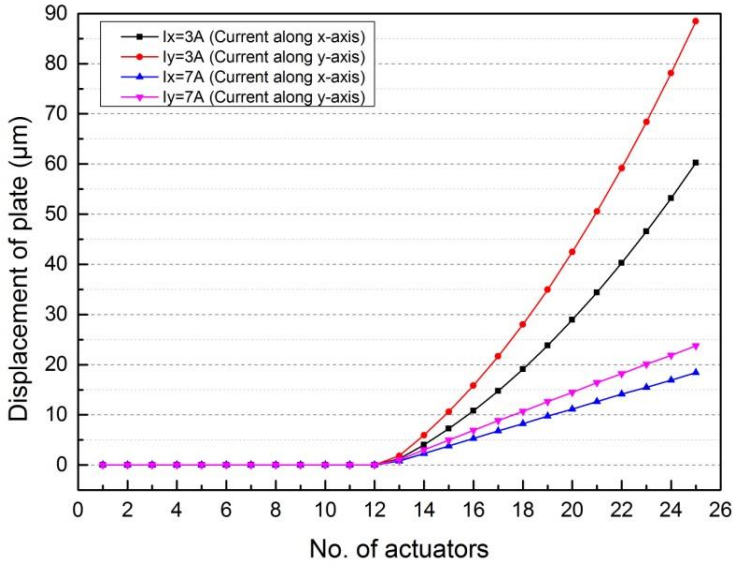

Figure II- 15: Plate displacement with number of controlled actuators

II.4.5 Control strategy for 1 mm plate displacement

In this part, a control strategy is proposed to realize a 1000 ±1 µm plate displacement with different driving current values. The objective is to realize this plate displacement in the shortest time.

The driving current value has an influence on the MPM switching time and on the plate displacement (Figure II- 13). With a low driving current, the plate displacement and MPM switching time are high and inversely with high driving current. A high driving current can realize a small plate displacement to reach a precise position, but the total time to finalize the displacement is much longer than the small currents (Figure II- 11).

For each driving current value, several plate displacements are simulated (considering the driving current value called main driving current value) in order to move the plate on a distance close to 1000 µm. Then, complementary plate displacements are realized by changing the driving current value in order to reach a 1000 ±1 µm plate displacement.

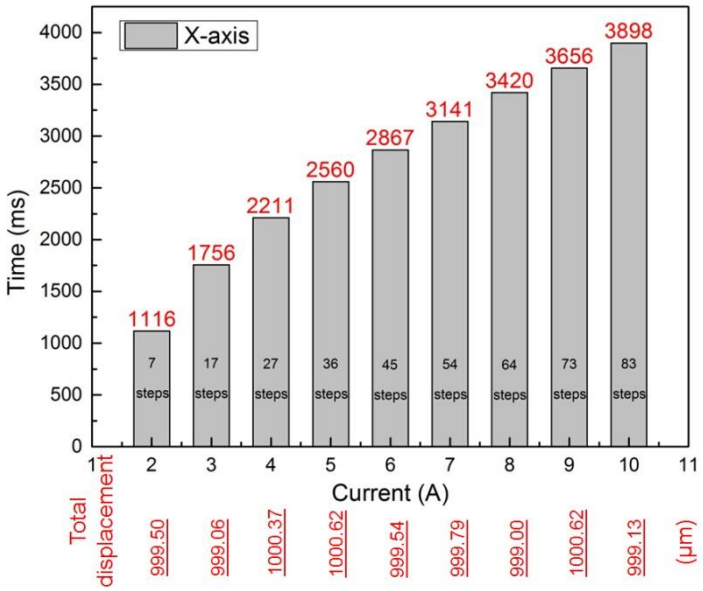

Figure II- 16: Time to reach 1mm displacement with different currents

In Figure II- 16, the time needed to realize 1 mm plate displacement and the number of displacement steps are illustrated as function of the main driving current value between 2 to 10A. The time necessary to realize the displacement is between 1116 ms and 3898 ms. The obtained plate displacements are in the desired range (minimum: 999.06 µm – maximum: 1000.62 µm). To reach the displacement objective (1000±1 µm), the driving current value of the last steps has been adapted. More details on the driving current values are given in Figure II- 17. For example with 3A driving current, 17 steps have been realized and the total time is 1756 ms. In this configuration, the 16 first steps have been executed with 3A to reach 963.82 µm (time needed 1676 ms). Then, the remaining displacement (36.18 µm) has been obtained using 4.25 A (time needed 80 ms). The total plate displacement is then 999.06 µm (total time needed 1756 ms). In this study, the minimum driving current variation considered for the added step is 0.25 A. For 2A and 4A, two complementary currents have then been used to reach the displacement objective. The step of driving currents used here are 0.25A to limit the number of experiments. Two complementary currents have been used, because there is no single driving current which can compensate the rest displacement to reach 1000±1 µm.

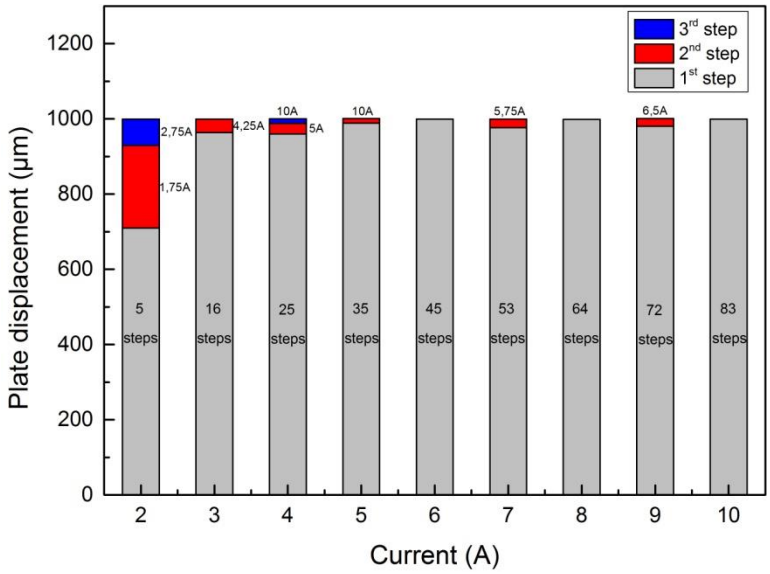

Figure II- 17: Steps to realize 1000±1 µm plate displacement with different main driving currents

Another way to reach 1 mm displacement is to control only a part of the 25 MPMs. As observed in section II.4.4, the minimum number of controlled MPMs should be larger than the half number of the DAA and is 13. In Figure II- 18, thirteen configurations are compared with different number of controlled MPMs between 13 and 25. In this case, the driving current is fixed at 3A. With 13 controlled MPMs, 342 steps are necessary to realize a 1 mm displacement. The time needed for these steps is 38 s. As in the previous proposed strategy with different current values, several main steps, then additional steps are realized to reach the displacement objective. With 19 controlled MPMs, a 1 mm plate displacement is then with 29 main steps, one step with 18 controlled MPMs and one step with 13 controlled MPMs. In this case, the time needed is 3.4 s According to the study, the total time to realize 1 mm displacement decreases with the increase of the initial number of actuated actuators.

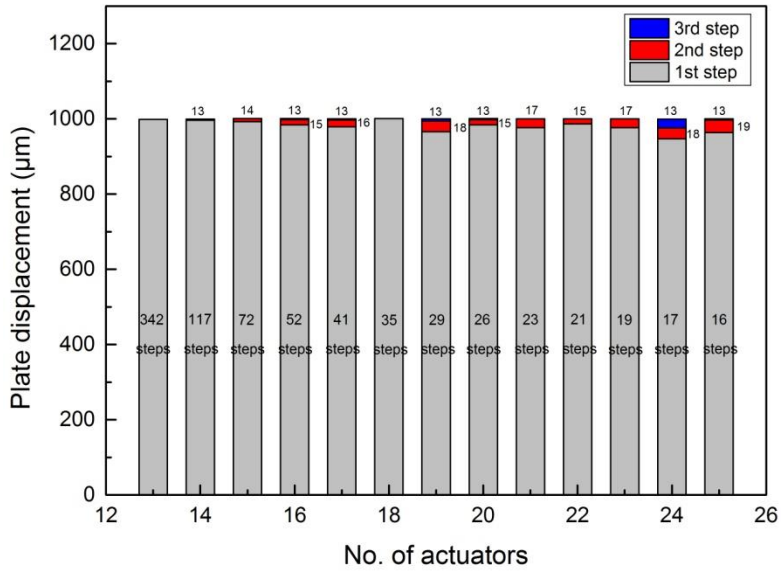

Figure II- 18: Steps to realize 1000±1 µm plate displacement with different number of controlled MPMs

Another proposed criterion, to compare the proposed strategies, is the energy consumption needed to realize the objective displacement. In previous part, the driving current values and the switching time are known, so the consumed energy can then be calculated using equations (II.10) and (II.11). The resistance of the electrical wire has been experimentally measured and is 0.4Ω.

$$E = UIt \tag{II.10}$$

$$U = RI \tag{II.11}$$

According to these equations, the energy consumed for the two controlled strategies proposed are represented in Figure II- 19. The Figure II- 19 (a) and (b) represents the energy consumption considering different driving current values and different number of controlled MPMs, respectively. When the main driving current is low (Figure II- 19 a), the consumed energy is minimized. The energy consumption is 1.9 J with 2 A main driving current value, while it is 155.9 J with 10 A. This is due to the high number of steps needed to reach the displacement objective with a high driving current value. Considering the number of controlled MPMs (Figure II- 19 b), the energy consumed is minimized for a larger number of initial actuated MPMs. The energy consumption is 136.9 J when 13 MPMs are controlled and 6.8 J when 25 MPMs are controlled. As in Figure II-19 a, a high number of steps induces a high energy

consumption. From this figure, it is then shown that, to save time and energy, a low main driving current with the most of active actuators is the best choice.

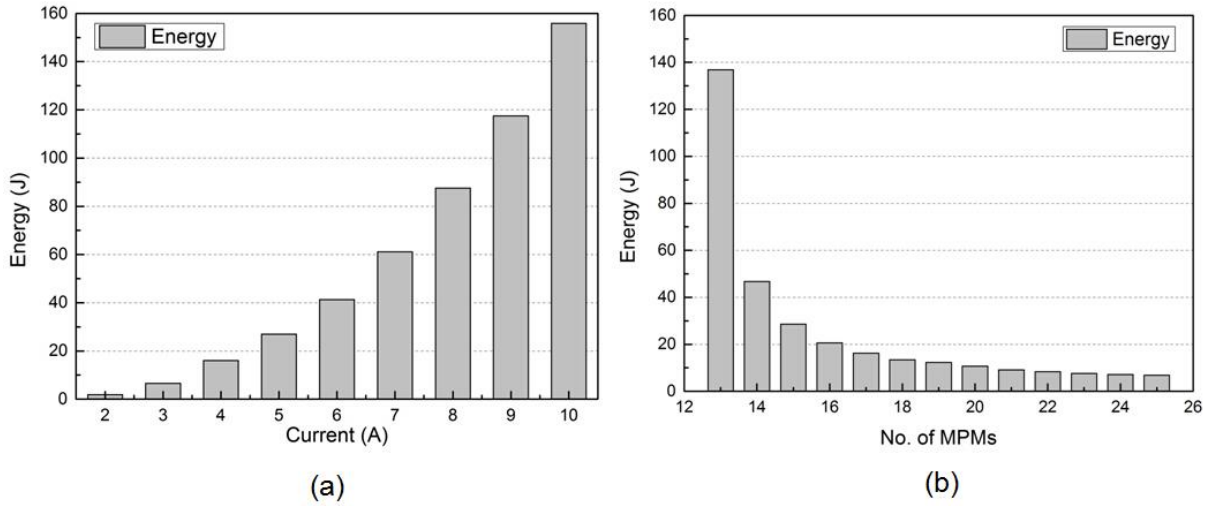

Figure II- 19: (a) Energy consumption with driving currents (b) Energy consumption with number of MPMs

II.5 Comparison between simulated and experimental results

A prototype of a DAA has been developed and experimentally tested as a planar conveyance device by P. Huyan [HUYA 2015]. However, due to experimental limitations, especially the number of available power supplies, only 8 EDAs of the DAA have been used to move the plate. In order to compare simulation and experimental results, the previous proposed model has then been adapted to consider only 8 EDAs. In this section, the experimental setup is firstly presented, then comparisons between the simulated and experimental results are shown.

II.5.1 Experimental setup

To measure the plate displacement, a camera has been positioned above the DAA and a sticker, with a white square on a black background, is placed at the center of the glass plate. The plate dimensions and mass are 50 mm × 50 mm × 0.13 µm and 0.93g, respectively. This non-contact measurement technique has been used in order to avoid disturbing the planar motion of the plate by a contact with a displacement sensor (Figure II- 20). The camera resolution is 10.42 µm/pixel. The camera takes pictures of the white square position when the DAA is controlled.

An image processing program, developed with MATLAB software, is used to compute the plate displacement from these images.

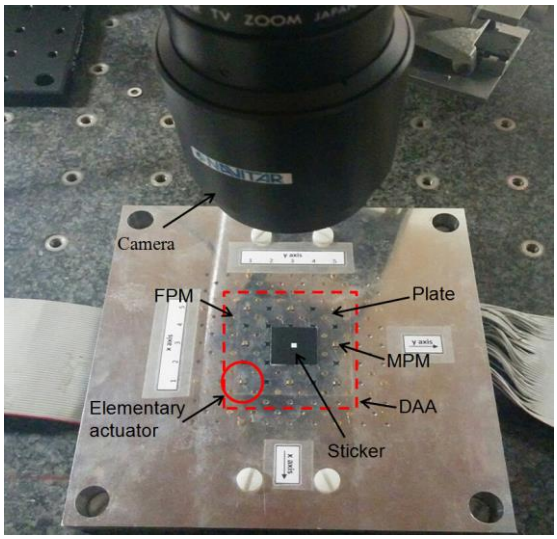

Figure II- 20: Prototype of experimentation

To control the MPMs displacement, a control system has been used. This system is composed of a computer, a National Instrument (NI) PCI data acquisition board and voltage to current converters (V-A converters). The control system is illustrated in Figure II- 21. The computer is equipped with LabView software which is used to generate voltage signals thanks to the PCI board. These voltage signals are then converted to current signals by voltage to current converters. These current signals are finally sent to the 8 EDAs.

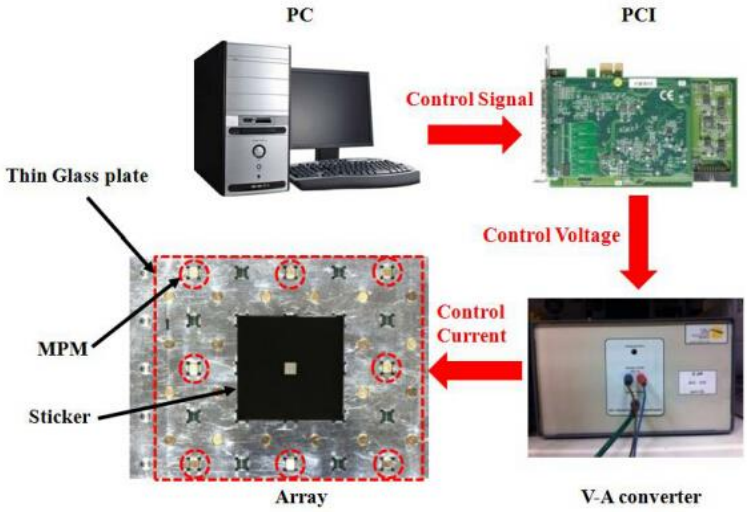

Figure II- 21: Control system of the DAA

II.5.2 Comparison between simulated and experimental results

The experiment has been done along x and y axis. Along each axis, 20 steps of the plate have been realized in two opposite directions (Figure II- 22). Then, the average displacement step value has been computed considering 20 steps in +x/y direction and 20 steps in –x/y direction. The comparison between experimental and simulated results is presented in Figure II- 23 (a) and (b) for plate displacements along x-axis and y-axis, respectively. The plate displacement has been measured with different driving current values from 2.5 A to 7 A for both axes. Because the camera resolution is 10.42 µm, the resolution of the displacement measure is within ±5.21 µm for each measuring point.

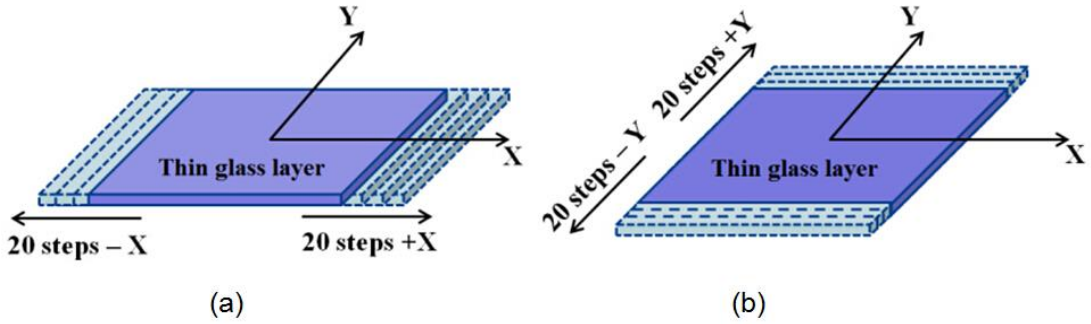

Figure II- 22: Experimental situation: (a) displacement along x-axis direction (b) displacement along y-axis direction

In Figure II-23, it can be observed that when the driving current value increases, the displacement step value increases for current between 2.5 A and 5A (x-axis) or 5.5A (y-axis). Then, the plate displacement decreases for currents between 5.5A to 7A [HUYA 2015]. For x-axis, the average plate displacement increases from 17.18 µm (2.5A) to 32.32 µm (5.5A) and then decreases to reach 16.61 ± 5.21 µm (7A) (Figure II-21(a)). The same behavior has been observed for y-axis (Figure II-21(b)).

In simulation, the plate displacement always decreases when the driving current increases (Figure II- 23) because the increase of the MPM acceleration generates a high sliding between the plate and the MPMs so that the plate displacement step is small. This effect is visible for driving currents between 5.5 A to 7 A in both simulated and experimental results. In this range of driving currents, there is a good correlation between the results.

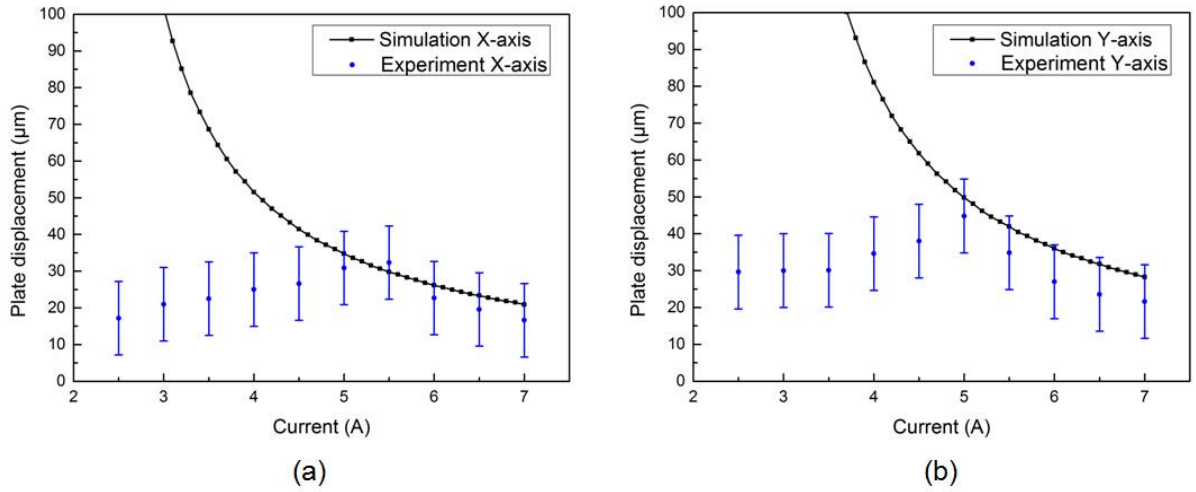

Figure II- 23: Simulated and experimental results: (a) comparison along x-axis direction (b) comparison along y-axis direction

For low driving current values, between 2.5A to 5A, the experimental results do not follow the same trend as the simulated results. Theoretically, the plate displacement increases when the driving current decreases but experimentally a decrease of the plate displacement has been observed. During experiment, the switch of the MPMs has been observed and it has been found that, for driving current lower than 5A, all the MPMs do not switch simultaneously. There is a loss of the collaborative effect to generate the plate motion then a reduction of its displacement. This effect has not been considered in the model that explains the difference observed between the results. With higher driving current values (from 5.5 A), the switch of all MPMs is obtained simultaneously. This is why the correlation between the experimental and theoretical results is good for driving current between 5.5A to 7A.

Several reasons can explain this non-simultaneous switching phenomenon. In the model used for the simulation, the cavities and all the PMs are considered as perfect and identical. Moreover, the friction conditions are considered identical for all EDAs. For the experimental prototype, manufacturing errors (dimensional and geometrical errors) are present and induce inhomogeneous holding forces for the different EDAs of the DAA. Besides, the friction conditions are not perfect and generate inhomogeneous adhesion force between the plate and the MPMs and between the MPMs and the square cavities. Variation of the friction conditions has been studied in the previous section and it is been shown this parameter affects significantly the plate displacement for low driving current values (Figure II- 14).

II.6 Conclusion

In this chapter, the principle and the properties of the EDA with four discrete positions have been firstly presented. Then a DAA composed of 25 EDAs arranged in 5 × 5 matrix is described. An application of this DAA as a planar conveyance device is then proposed.

In this chapter, a model of the planar conveyance device based on the DAA has been firstly proposed to determine the MPMs and plate displacements. The model has then been tested with several conditions. Firstly, the MPM and plate displacement along x and y axes have been compared. It has been observed that, for a given driving current value, the plate displacement along y-axis is larger than that of x-axis and that the plate displacement decreases with the increasing of driving current value. This effect is due to the sliding phenomenon between the MPM and the plate. When the driving current is small, the acceleration of MPM and the plate are then small and the sliding effect between the plate and the MPM is then more important. The influence of the number of controlled MPMs on the plate displacement has also been studied and it has been determined that to move the plate, the number of controlled MPMs should be larger than half number of the DAA. If a smaller plate displacement is required, only a part of the EDAs can be used. Moreover, the influence of friction variation has been considered. When the friction coefficients are all at the smallest values, the force generated on the plate is then small, so the plate displacement is also the smallest. Finally, two control strategies have been proposed to realize a plate displacement of 1000 ± 1 µm using different driving current values or using a limited number of controlled MPMs. Low driving current value can generate large plate displacements, and then can save time and energy consumption, so it's better to use a lower current to realize this displacement. However, extra steps are then necessary to compensate the remaining distance at the end of the displacement. High driving current values generate small plate displacement which can obtain precise displacement but that requires more time to realize the desired displacement.

After simulation of the DAA composed of 25 elementary actuators, the model has been modified to consider only 8 EDAs in order to compare the simulated results with the experiments presented in P. HUYAN thesis [HUYAN 2015]. For driving current values lower than 5A, a difference between simulated and experimental results is observed because with low driving current values, non-simultaneous switching of all the MPM has been experimentally observed. This effect is due to manufacturing errors of the experimental prototype and inhomogeneous friction conditions. For driving current higher than 5.5A, the switch of the

MPM is obtained simultaneously then the collaborative effect is ensured. In the range of driving current between 5.5A and 7A, a good coherence between simulated and experimental results has then been observed.

Chapter 3: Design of planar conveyance device with structured plate

In chapter 2, the DAA was applied as a planar conveyance device with a flat plate. Experimental results and simulated results have shown that the flat plate displacement is affected by several factors. The study has shown that the plate movements are linked to the simultaneous switching of the MPMs. The friction inhomogeneities between the MPMs and the fixed part and between the MPMs and the plate induce different behaviors which deprives the collaborative operation of the actuators array. Particularly, the variation of the friction coefficient between the plate and the MPM affects the simultaneous switch of MPMs then the plate displacement. In order to limit this drawback, a new planar conveyance device is proposed with a structured plate in this chapter.

III.1 Principle of conveyance device based on a structured plate

III.1.1 Principle of the conveyance strategy

In this section, the principle of the new 2D conveyance device is described. The principle of the EDA is unchanged and is composed of a MPM able to reach four discrete positions, four FPMs for the MPM holding and electric wires placed below the cavity for the MPM switching. A side view of the device is shown in Figure III- 1 where a structured plate is placed on the top side of the DAA. The structured plate is composed of studs on its bottom side. A small structured plate is also fixed on the top side of each MPM. When the MPMs switch, the structured plate will then be pushed in the same direction.

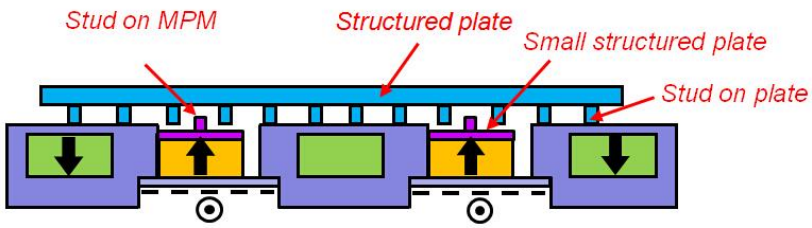

Figure III- 1: Side view of the 2D conveyance device with structured plate

To move the plate, a displacement sequence of the MPMs of the DAA is necessary. The different steps of this displacement sequence are detailed in Figure III- 2. The figures are the front view of the DAA composed of four EDAs. The blue squares represent the structured plate and the four purple squares represent the small studs on MPMs. The black squares represent the square cavities with four discrete positions of the studs on the MPMs.

At the initial step, all the MPMs are placed at the inner corner of the square cavities in order to be placed at the center of the four studs on the structured plate to simplify the displacement (Figure III- 3 (a)). Secondly, the two right studs “3” and “4” move upward (+y-axis) and downward (-y-axis), respectively without pushing the studs on the structured plate (Figure III- 5 (b)). Thirdly, the two right studs “3” and “4” switch to the right (x-axis) then push the structured plate in this direction (Figure III- 5 (c)). At the same time, the two left studs “1” and “2” move to the left (+y-axis) without touching the structured plate. After the first displacement, the plate moves towards right. Fourthly, the two left studs “1” and “2” and the two right studs “3” and “4” move upward (+y-axis) and downward (-y-axis) respectively without moving the plate (Figure III- 5 (d)). At this step, there is no plate displacement. Fifthly, the two left studs “1” and “2” are switch towards right to push the plate moving in x direction and the two right studs “3” and “4” are switched leftward (-x-axis) to be back to the original positions (Figure III- 5 (e)). At last, the two left studs “1” and “2” return to the original positions (Figure III- 5 (f)) and a total step sequence is realized. During this one step displacement sequence, the plate displacement is realized by two sub-steps (steps c and e).

The presented displacement sequence realizes a plate displacement along the +x-axis. From the initial position, the first step starts with a switch of the two left studs along x-axis. If a plate displacement along –x-axis is wanted, the two left studs have to be switched along –x-axis at the first step (Figure III- 3 (a) and (b)), then the plate will be moved along –x-axis. Still considering the initial position, a plate displacement along +y-axis can be obtained by switching the two top studs along +y-axis at the first step (Figure III- 3 (c) and (d)). Similarly, a plate displacement along –y-axis can be realized by switching the bottom studs along the –y-axis at the first step (Figure III- 3 (e) and (f)).

Figure III- 2: One displacement sequence along x-axis

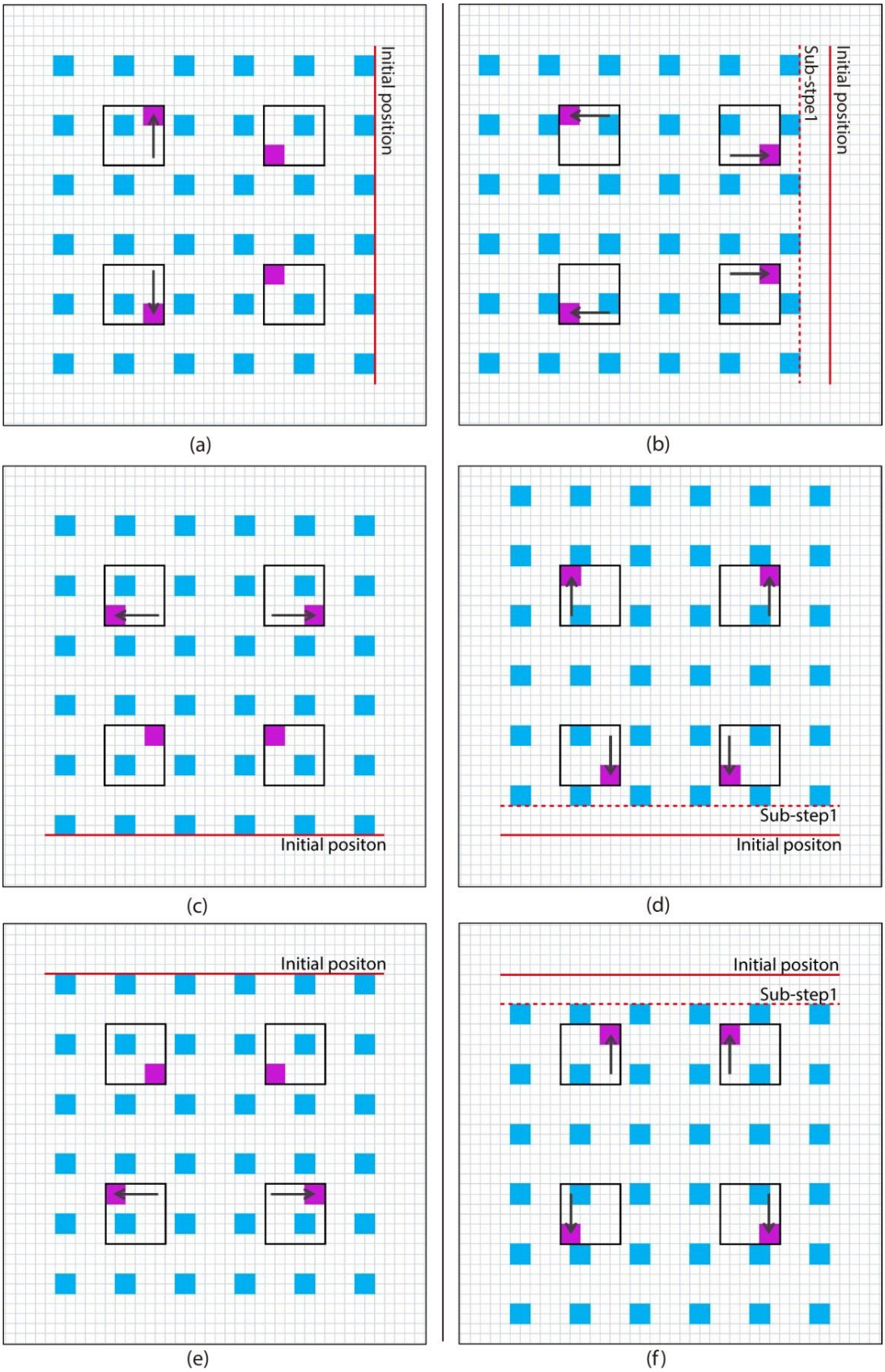

Figure III- 3: The 1st sub-step in different directions: (a) and (b): -x-axis (c) and (d): y-axis (e) and (f): –y-axis

III.1.2 Modeling and calculation of the geometrical parameters

A geometrical model of the proposed principle has been developed and used for the design of the structured plate and the studs fixed on the top side of the MPMs. The geometrical parameters considered in the study are detailed in Figure III- 4. In this figure, the structured plate is not placed in contact with the mechanical part of the DAA in order to facilitate the understanding. The distance between two studs on the structured plate is defined as "a", the width of the stud is "b", the stroke of the actuator is "c", the width of the stud on the magnet is "d" and the distance between two MPMs is "e". The objective of the proposed study is to find a set of these parameters which ensures the functioning of the conveyance device. The relation between these geometrical parameters is given in equation (III.1), where n is a positive natural number.

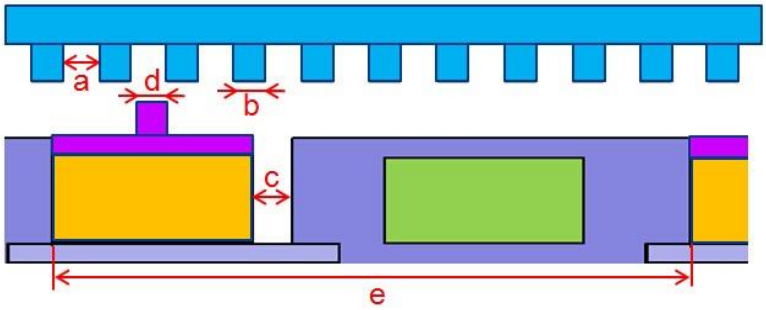

Figure III- 4: Parameters of digital actuators array

$$e = n(a+b)+b+(c-d) \tag{III.1}$$

According to the conveyance strategy presented before, the distance between two studs on the plate is selected to be equal to the stoke value, so the value of "a" is the same as "c". To simplify the model and the manufacturing, the same value has also been considered for "b" and "d". In the previous work in Roberval laboratory, a DAA with a 0.2 mm stroke has been realized. For stroke less than 1 mm, manufacturing problems can appear. Moreover, stroke higher than 4 mm is not adapted for conveyance application. So in this thesis, the stroke values are limited between 1 mm and 4 mm according to existing MPMs to reduce the scope of the study and the number of considered configurations. According to the conditions given above, several sets of the parameters values are given in Table III- 1. In this table, a new parameter called "e_0" is given in equation (III.2) before obtaining "e", "e_0" is the minimum distance between two MPMs, which is calculated considering n equals to 1.

$$e_0 = (a+b)+b+(c+d) \quad \text{(III.2)}$$

Table III- 1: List of the values of the parameters (mm)

No. of configuration	c (mm)	a (mm)	d (mm)	b (mm)	e_0 (mm)
1	1	1	0.5	0.5	2.5
2	2	2	0.5	0.5	4.5
3	2	2	1	1	5
4	2	2	1.5	1.5	5.5
5	3	3	0.5	0.5	6.5
6	3	3	1	1	7
7	3	3	1.5	1.5	7.5
8	3	3	2	2	8
9	3	3	2.5	2.5	8.5
10	4	4	0.5	0.5	8.5
11	4	4	1	1	9
12	4	4	1.5	1.5	9.5
13	4	4	2	2	10
14	4	4	2.5	2.5	10.5
15	4	4	3	3	11
16	4	4	3.5	5.5	11.5

The objective of this thesis is to validate the principle of a conveyance device based on a DAA and a structured plate. The value set No. 13 with a MPM stroke of 4 mm and a stud width of 2 mm has been chosen in order to maximize the studs' dimensions, and then to reduce the manufacturing constraints of the structured plate. More compact DAA can be designed by choosing smaller stroke when manufacturing can be improved.

III.2 Principle and design of the actuators array

In this section, the principle of the EDA is firstly introduced, and then the DAA composed of four EDA is designed and applied as a planar conveyance device.

III.2.1 Design of the elementary actuator

III.2.1.1 Principle of the elementary actuator

The principle of the EDA is identical as the one introduced in Chapter 2. The main characteristics difference lies in its stroke. Compared to the previous design, the MPM stroke is 20 times more important (0.2 mm vs. 4 mm). To ensure the MPM switch along each

displacement axis, five electrical wires are used instead of only one electrical wire (Figure III-5). A double-side PCB with five wires printed on each side is used. The distance between two parallel wires is 0.75 mm. The five electric wires are serially connected to ensure a high enough electromagnetic force to switch the MPM. The PCB is shown in Figure III- 6.

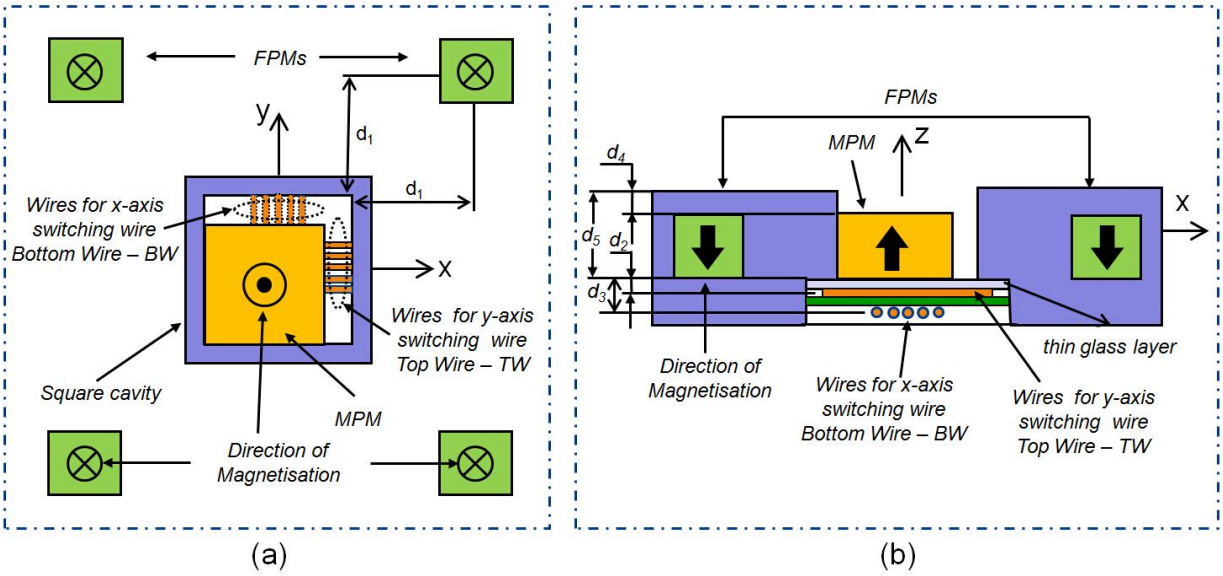

Figure III- 5: Principle of elementary actuator (a) Top view (b) Side view

The distance between the FPM and the square cavity (d_1) has been chosen in order to ensure that the magnetic holding force is higher than the adhesion force when the MPM is placed near each discrete position. The distance between the bottom side of the MPM and the top wires is d_2 and between the bottom side of the MPM and the bottom wires is d_3. In the previous model, the plate is displaced thanks to the friction between the flat plate and the MPMs, so the height of the MPM was higher than the mechanical support. In this new device, the thickness of the MPM has to be less than the thickness of the mechanical support to place a small structured plate on each MPM. The distance between the top side of the MPM and the mechanical support is d_4 (Figure III- 5 (b)). The thickness of the mechanical support d_5 is 3mm, the thickness of the MPM is 2mm, the value of d_4 is 1mm. The characteristics of the EDA are given in Table III- 2. The electric wires along x-axis are placed as top wires.

The MPM used for this new EDA is bigger than the one used in the previous version of the DAA in order to be adapted to the new stroke (4 mm). The FPMs for this new DAA are chosen as square magnets with 1.45 T to ensure a strong enough magnetic force. The friction coefficient remains the same between MPM and the thin glass under it (0.41). The friction coefficient

between MPM and the mechanical support made of PMMA is 0.27 and has been measured using an inclined plane technique.

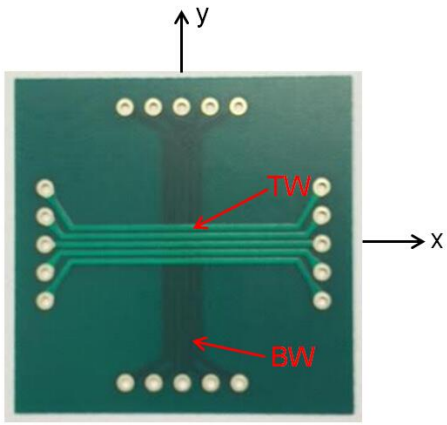

Figure III- 6: PCB with five electric wires on each side

Table III- 2: EDA properties

PMs properties		
PM type	Dimensions	Magnetization
MPM	10 × 10 × 2 mm^3	1.35T
FPM	2 × 2 × 2 mm^3	1.45T
Materials		
Permanent magnets	NdFeB	
Mechanical structure	PMMA	
Mass of MPM: 1.5g		
Adhesion coefficients		
Gold/Glass layer	0.41	
Gold/ABS	0.27	
Distances		
Stroke	4 mm × 4 mm	
d_1	3.5 mm	
d_2	222 µm	
d_3	458 µm	
d_4	1 mm	
d_5	3 mm	

III.2.1.2 Magnetic and electromagnetic force calculation

To design the EDA, the magnetic and electromagnetic forces exerted on the MPM have been calculated. A semi-analytical model has been developed with MATHEMATICA software using the RADIA package. RADIA is semi-analytical electromagnetic computing software based on the MATHEMATICA environment. This computing solution has been selected, because it is a rapid calculation technique and a visualization of the modeled objects can be easily obtained.

Unlike the methods based on finite elements calculation, RADIA is based on a method of limit integration, which does not necessitate the mesh of the magnets. So the integrations of the field can be calculated directly by using analytical equations [RADI 1997]. All the objects (i.e. PMs) of the model are created and divided into sub-objects in the software, and then the general problem is solved. In this section, RADIA has been used to design and size the EDA then to calculate the magnetic and electromagnetic forces exerted on the MPM.

The electromagnetic force exerted by each electrical wire on the MPM as function of its position between the two discrete positions is presented in Figure III- 7 (a). In this figure, a 1A driving current is used and the electromagnetic force along y-axis, using the TW, is only represented. The electromagnetic force varies according to MPM position between the discrete positions. The electromagnetic force is symmetrical only for the central electric wire (wire 3). The total electromagnetic force, defined as the sum of the electromagnetic force generated by the five wires, is plotted in Figure III- 7 (b) for the two displacement axes.

It can be observed that the total electromagnetic force is symmetrical along the center of the cavity. The electromagnetic force is the smallest at the center of the square cavity, while the force is the largest in discrete positions. The electromagnetic force generated on the MPM in a discrete position is 8.85 mN for 1A for the TW, and 8.36 mN for the BW. The difference of the electromagnetic force between TW and BW is 5.5% due to the gap between the two distances d_2 and d_3.

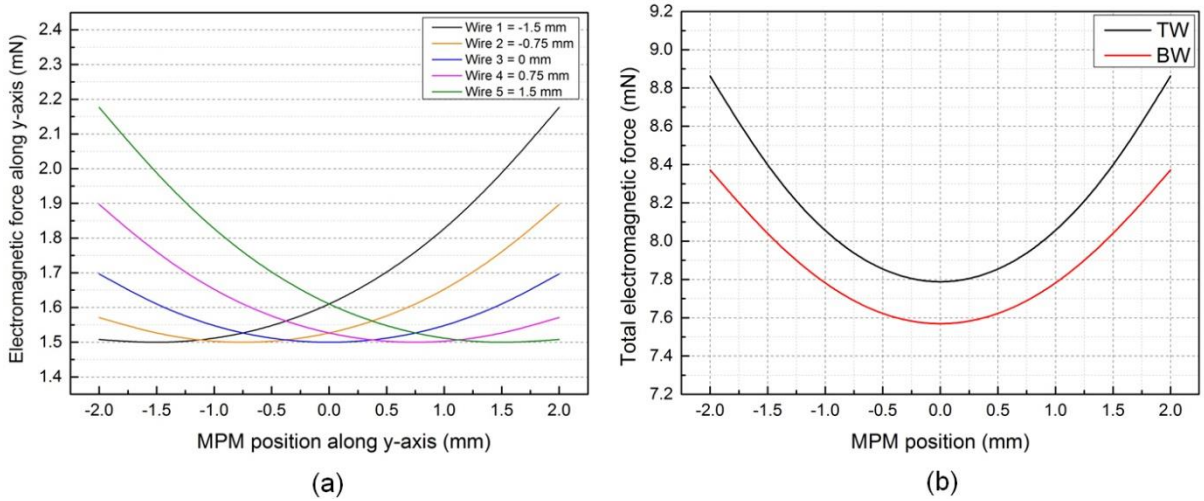

Figure III- 7: (a) Electromagnetic force generated by each electric wire with 1A at different positions (b) Total electromagnetic force with 1A for top wires and bottom wires

The magnetic force exerted on the MPM is presented in Figure III- 8 (a). This force is linear as function of the MPM position and is null when the MPM is located at the center of the cavity. In this position, the magnetic interactions between the MPM and the four FPMs are indeed equilibrated. The magnetic holding force value is the highest when the MPM is in the discrete positions. In this position, the force exerted on the MPM is 16.85 mN.

The total force, considering the magnetic and electromagnetic forces, is represented in Figure III- 8 (b) as function of the MPM position and for different driving current values. When a driving current is applied, the curve of the initial force (magnetic force) is vertically shifted. The shifting value corresponds to the added electromagnetic force. Due to the evaluation of electromagnetic force shown in Figure III- 7 (b), the total force of a driving current is not linear shifted. Three driving current values are compared (1A, 3A and 5A), and shown in Figure III- 8 (b).

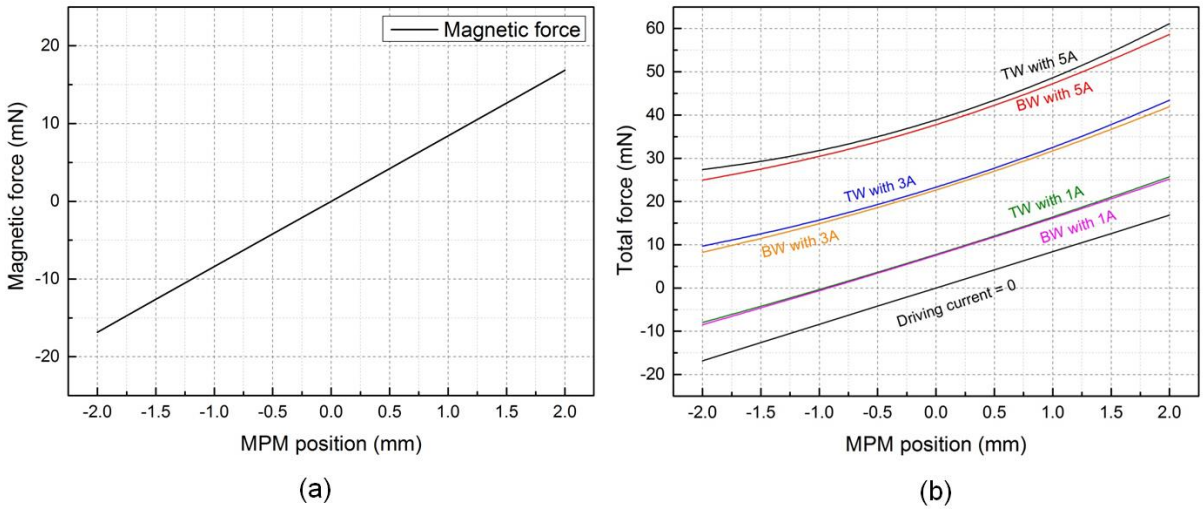

Figure III- 8: (a) Magnetic force generated on MPM at different positions (b) Total force generated on MPM at different positions

III.2.1.3 Determination of self-returning zone and minimum driving currents

In this section, the Self-Returning Zone (SRZ) of the EDA is described. The SRZ has been defined in previous thesis [PETI 2009] and is an important parameter to characterize the digital behavior of the presented EDA. It helps to evaluate the holding function of the EDA which defines the maximum distance from which one the MPM can return to a discrete position without extra energy consumption. The SRZ is used to characterize the robustness of the EDA to maintain the stable positions. An illustration of the SRZ is provided in Figure III- 9.

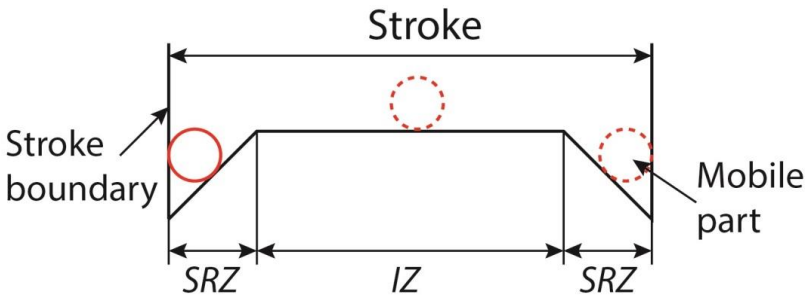

Figure III- 9: Self-returning zone of elementary actuator

The two stroke boundaries represent the two discrete positions. In the SRZ zone, the magnetic holding force is higher than the adhesion force. If the displacement of the mobile part from a discrete position is less than the length of SRZ, the mobile part will return to its discrete position. Otherwise, if it stops in the Intermediate Zone (IZ), it will not return to a discrete position. In IZ, the magnetic force is less than adhesion force.

To define the SRZ length, all the forces exerted on the MPM have to be considered. During the switch, there are the magnetic holding force exerted by the FPMs, the electromagnetic force exerted by the two sets of electrical wires and the adhesion forces due to the contact between the MPM and the fixed part. Two adhesion forces are defined in the actuator: horizontal adhesion force and lateral adhesion force. The horizontal adhesion force ($F_{horizontal}$) is the adhesion force due to the contact between the MPM (gold coated) and the thin glass layer. It is generated due to the MPM gravity and the corresponding adhesion coefficient μ_1 is 0.41. The lateral adhesion force ($F_{lateral}$) is due to the contact between the MPM and the lateral stop of the square cavity. The mechanical support is made of PMMA, the adhesion coefficient between the MPM and the cavity μ_3 is 0.27. The calculations of all these forces are presented in equation (III.3)

The relationship between the force and the position is shown in Figure III- 10. The holding force is equal to the adhesion force when the MPM is located in position A and B which define the length of the SRZ for each discrete position. The expression of SRZ length is given in equation (III.4), where both the holding force and adhesion force have been defined in previous part.

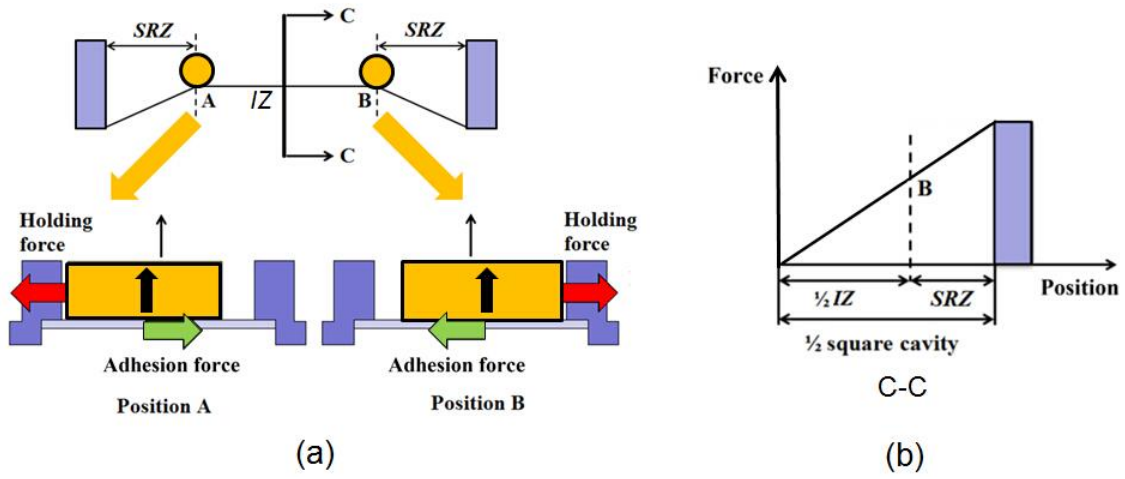

Figure III- 10: Calculation of SRZ length: (a) Analysis of two stable positions (b) Relationship between the force and the position [HUYA 2015]

$$\begin{aligned} F_{adhesion} &= F_{horizontal} + F_{lateral} \\ F_{horizontal} &= \mu_1 \times m_m \times g \\ F_{lateral} &= \mu_3 \times F_{holding} \end{aligned} \tag{III.3}$$

Where,

m_m : Mass of MPM (kg),

g : Gravity acceleration (9.81 m/s^2).

$F_{holding}$: Magnetic holding force (N)

$$SRZ = \frac{L}{2} \times \left(1 - \frac{F_{adhesion}}{F_{holding}} \right) \tag{III.4}$$

Where,

L : Stroke of the MPM (m)

For the actuator, the MPM mass is 1.5 g and the chosen MPM stroke is 4 mm. With these parameters, the value of the SRZ has been calculated with different magnetic holding force. The variation of the SRZ as function of the holding force value is illustrated in Figure III- 11.

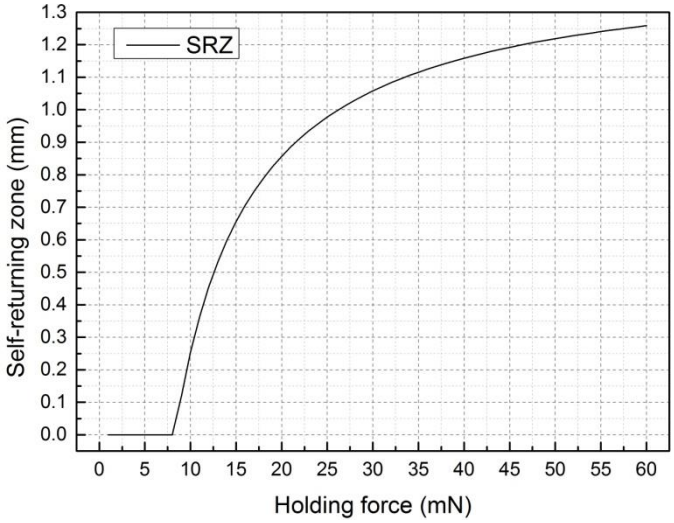

Figure III- 11: SRZ as function of the holding force

When the magnetic holding force is lower than 8 mN, the SRZ length is null. In this case, the adhesion force is always higher than the holding force. For holding force higher than 8 mN, the SRZ length increases when the magnetic holding force rises.

To determine the SRZ value, the holding force value has to be selected. However, this holding force value is directly linked to the driving current value needed to switch the MPM. The minimum driving current needed to switch the MPM has then been calculated. Due to the distance between the TW and the BW of the PCB (Figure III- 12), the minimum driving currents for the two displacement axes are different. With 1A driving current, the electromagnetic force generated is 8.85 mN and 8.36 mN for the TW and BW, respectively (Figure III- 7 (b)). So the expressions of the minimum currents for both wires are given in equation (III.5).

$$\begin{aligned} I_{TW} &= (F_{holding} + F_{horizontal} + F_{lateral}) / 8.85 \\ I_{BW} &= (F_{holding} + F_{horizontal} + F_{lateral}) / 8.36 \end{aligned} \tag{III.5}$$

According to these equations, the minimum driving currents for TW and BW as function of the holding force is presented in Figure III- 12. When the holding force increases, the minimum driving current to switch the MPM also increases. Because the SRZ length is larger with a higher holding force, so a larger SRZ requires a higher driving current. It is important to consider these two factors for the design of the EDA.

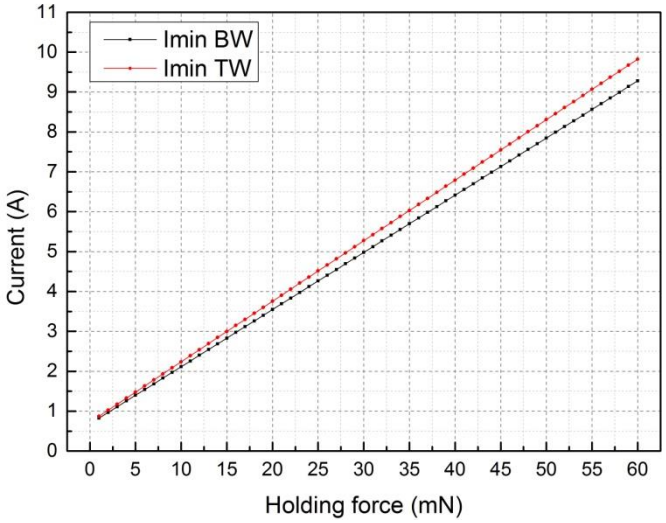

Figure III- 12: Minimum driving current value as function of the holding force for TW and BW

The minimum holding force value is 8 mN, to minimize the driving current and then to minimize the energy consumption, the holding force is chosen as 9mN. With this value, the minimum current to switch the MPM is 1.97A for TW and 2.09A for BW. In this case, the value of SRZ adjacent to each discrete position is 120 µm.

III.2.2 Design of the DAA

In this section, the design of the DAA is presented. The effect of added balancing magnets is highlighted and the theoretical characteristics of the DAA as minimum driving current and SRZ length are determined.

III.2.2.1 Architecture of the DAA

The DAA is composed of four EDAs arranged in 2 × 2 matrix configuration as shown in Figure III- 13. In order to ensure an identical behavior for all EDA, eight Added Fixed Permanent Magnets (AFPMs) are added around the four EDAs. The AFPMs balance the magnetic interaction force between each MPM. To simplify the DAA design, the PMs for the AFPMs have been chosen as identical to the PMs used for the FPMs (2 mm × 2 mm × 2 mm, 1.45T). The proposed architecture of the DAA ensures a symmetrical array along the two displacement axes. To finalize the design of the DAA, the distance between two elementary actuators (d_0), and the distance between FPM and AFPM (d_f) should be calculated. According to the holding force, the two values are chosen: d_0 is 15 mm and d_f is 5.2 mm.

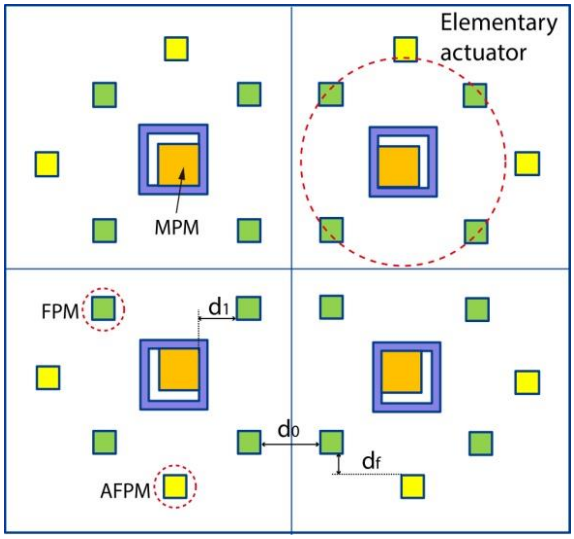

Figure III- 13: Digital actuators array

III.2.2.2 Determination of the DAA parameters

In the displacement sequences presented in Figure III- 2, there are four positions for MPMs. The corresponding positions are illustrated in Figure III- 14. The magnetic forces exerted on the four MPMs are computed separately for these four positions. The values and the directions of the magnetic holding force exerted on each MPM by the FPMs are presented in Figure III- 14. The left column is the DAA without AFPMs, while the right column is with AFPMs. These two configurations are compared in order to show the position influence of the AFPMs on the DAA homogeneity.

Without AFPMs, the minimum and maximum magnetic holding forces are 4.9 mN for position 1 and 17.9 mN for position 2. When the DAA is surrounded by AFPMs, the minimum and maximum magnetic holding forces are 8.6 mN for position 4 and 10.3 mN for position 3, respectively. The total average magnetic holding force of the four positions and the variation of the magnetic holding force are given in TABLE III- 3. The variation of magnetic holding force is 5.2 mN of the DAA without AFPMs, which is much larger than that of the DAA with AFPMs (0.4 mN).

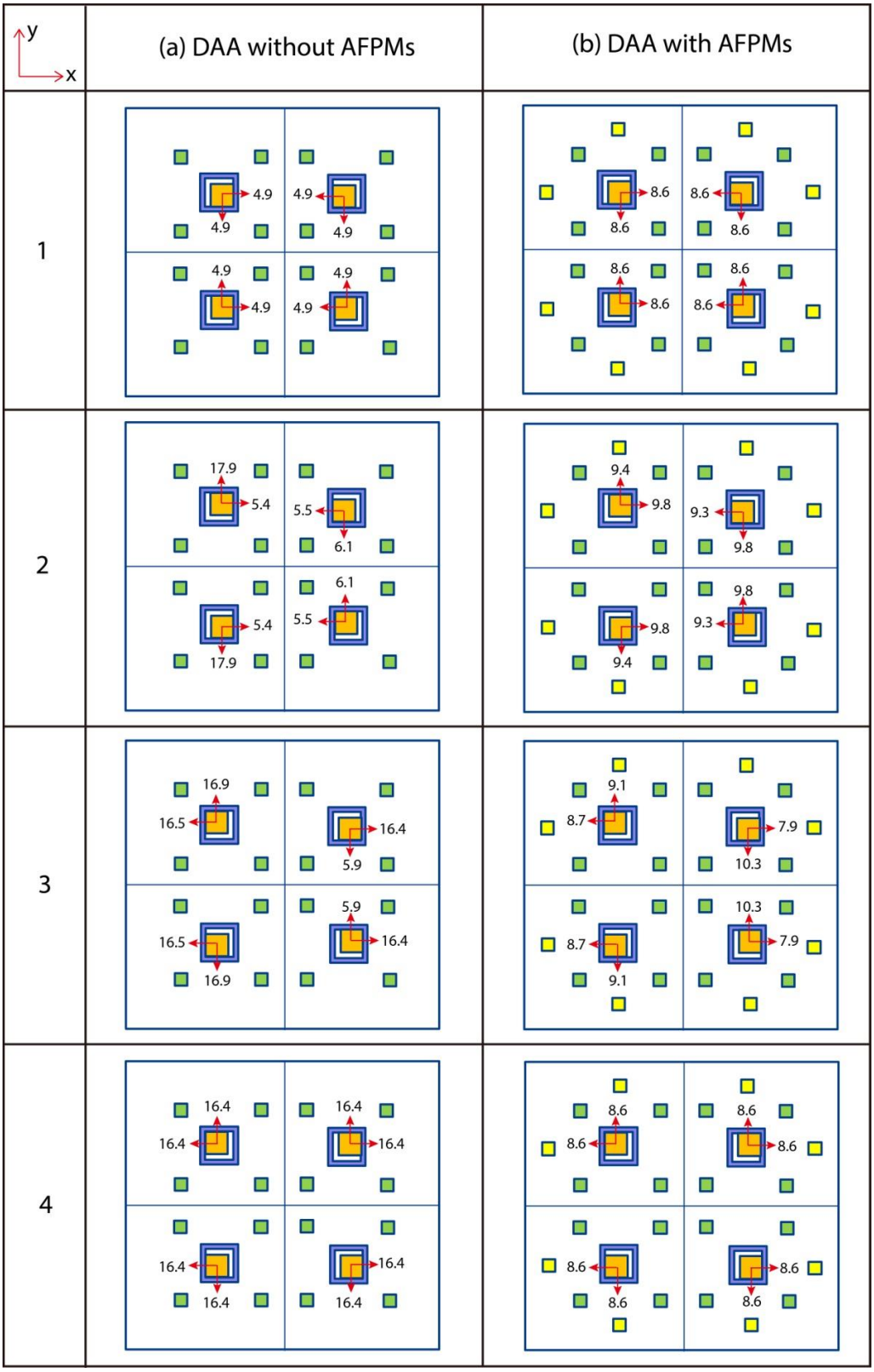

Figure III- 14: Comparison between of the two configurations in four positions

TABLE III- 3: Average and variation of the magnetic holding force

Type of DAA	Average magnetic holding force of four positions	Variation of magnetic holding force of four positions
DAA without AFPMs	10.9 mN	5.2 mN
DAA with AFPMs	9.0 mN	0.4 mN

According to the maximum magnetic holding force obtained for each positon with AFPMs illustrated in Figure III- 14, the minimum driving currents for TW and BW and the SRZ length can then be calculated. The values of the minimum driving current and SRZ length for each position corresponds to Figure III- 14 are detailed in TABLE III- 4.

TABLE III- 4: Characteristics of the DAA with APFMs

Position	Maximum Magnetic holding force	Minimum driving current of TW	Minimum driving current of BW	SRZ length
1	8.6 mN	1.92 A	2.03 A	60 µm
2	9.8 mN	2.09 A	2.21 A	230 µm
3	10.3 mN	2.16 A	2.29 A	290 µm
4	8.6 mN	1.92 A	2.03 A	60 µm

According to this table, to ensure the functioning of the DAA, the minimum driving current should be 2.16 A of TW and 2.29 A of BW. The SRZ length is 290 µm.

III.2.3 CAD model of the DAA

All the geometrical parameters of the DAA have been determined in the previous section. A 3D model of the DAA has then been realized with the Creo software. The 3D structure of the DAA is presented in Figure III- 15. The figure (a) shows a global view of the DAA, and then the four PCBs are presented in figure (b). In the proposed design, two mechanical supports are used. The first one is the upper support in which all the PMs are inserted. The second one supports the four PCBs and is placed below the DAA (Figure III- 15 (b) and (d)). The mobile structured plate moved by the EDAs has a "#" shape (Figure III- 15 (c)) to minimize its weight. The details of the DAA components are given in TABLE III- 5.

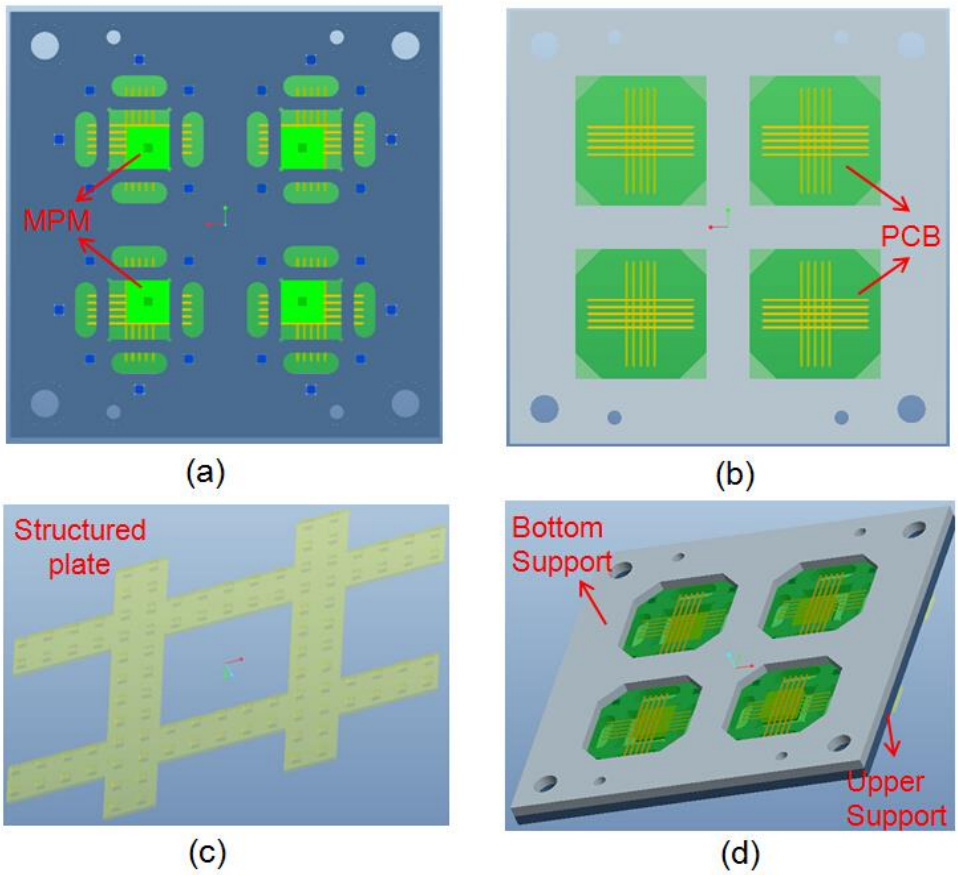

Figure III- 15: Global structure of 3D model (a) front view (b) four PCBs (c) structured plate (d) back view

TABLE III- 5: Properties of the components of the DAA

Pieces	Dimensions	Properties	Quantities
MPM	10×10×2 mm^3	B=1.35T	4
FPM	2×2×2 mm^3	B=1.45T	16
AFPM	2×2×2 mm^3	B=1.45T	8
Thin glass	15×15×0.17 mm^3	BK7	4
PCB	30×30×0.34 mm^3	-	4
Support	100×100 mm^2	PMMA	2
Plate	100×70 mm^2	VeroWhite-FullCure 830	1

For the 3D CAD design, the thickness of the studs placed on the top side of the MPMs and on the bottom side of the structured plate have to be determined. The thickness of the stud on the small plate is defined as "d_{sp}" (Figure III- 16 (a)). The thickness of the plate is defined as "d_{p1}" and the thickness of the studs on the plate as "d_{p2}" (Figure III- 16 (b)). The value of the d_{sp} is smaller than the value of d_{p2} according to the design of the planar conveyance device (Figure

III- 1). In this thesis, the geometrical values are given in TABLE III- 6. With all these values, the design of the planar conveyance is finalized.

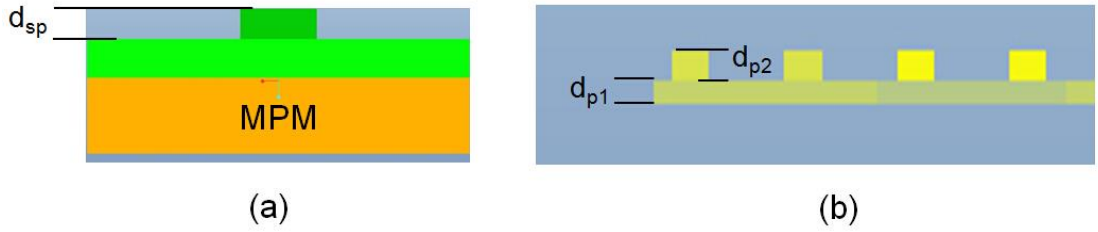

Figure III- 16: (a) Small structured plate on MPM (b) Structured plate

TABLE III- 6: Properties of two plates

Values of the thickness		
d_{sp}	d_{p1}	d_{p2}
0.8 mm	0.8 mm	1 mm

III.3 Conclusion

In this chapter, a new planar conveyance device composed of a structured plate and a DAA is presented and designed. The DAA is composed of four identical EDAs. The EDA principle and design have been firstly described. The conveyance strategy has then been introduced with the description of a displacement sequence to show the movement of the MPMs and the plate. A geometrical model is presented to analyze the parameters of the DAA.

To design the DAA, the properties (magnetic holding force, SRZ length and minimum driving current) of the EDA have been determined. The actuators array is composed of four EDAs. The magnetic holding forces generated by the FPMs on MPMs are calculated using the RADIA software. Two models of the DAA are compared in four configurations corresponding to the four positions of the MPMs displacement. One is without considering AFPMs and the other one is with considering AFPMs to show the positive influence of these added PMs. Then, the minimum driving currents and the corresponding SRZ values are calculated. At last, a 3D model of the DAA has been realized to show the structure of the planar conveyance.

Chapter 4: Experimental characterization of a planar conveyance device with structured plate

The design of the planar conveyance device composed of a DAA and a structured plate has been presented in Chapter 3. In this chapter, experimental tests of the device are presented. Different rapid prototyping methods (laser cutting and 3D printing) have been used to manufacture the prototype. Then the pieces have been assembled to form the prototype. The control system is presented and the characterization of the DAA is given. The experimental results are obtained in different conditions and compared with theoretical values.

IV.1 Realization of the DAA prototype

IV.1.1 DAA manufacturing

To realize the conveyance device, four components have to be manufactured (Figure III-17), including two mechanical supports (upper support and bottom support), four small structured pieces on the MPMs and the structured plate. In this section, the manufacturing methods used are introduced. One manufacturing method is laser cutting used to obtain the mechanical supports of the DAA. The other method is 3D printing used to realize the structured plates.

IV.1.1.1 Laser cutting

Two mechanical supports of the DAA were manufactured by a laser cutting machine (Trotec speedy 400) available at the Centre d'Innovation of UTC. A laser cutting machine works by focusing a high-power laser directly on the material to be cut. A computer is used to control the motions of the material and of the laser beam. The motion of the material is realized along z-axis and the laser is moved along x and y-axis. When the material is placed on the workbench, it can be moved up and down to ensure the laser working distance. When the laser is activated, the material is melted, burnt, vaporized away, or blown away by a jet of gas. Usually, this kind of machine is used as laser cutting to cut materials but it can also used for laser engraving. The deepness of engraving can also be controlled by the power and velocity. The laser cutting precision is ±0.05mm along x, y and z axes.

The material used here is PMMA, because it is a non magnetic material. According to the requirements of the components, the manufacturing processes are separated into two parts: laser cutting and laser engraving, which are illustrated in Figure IV- 1 for different components.

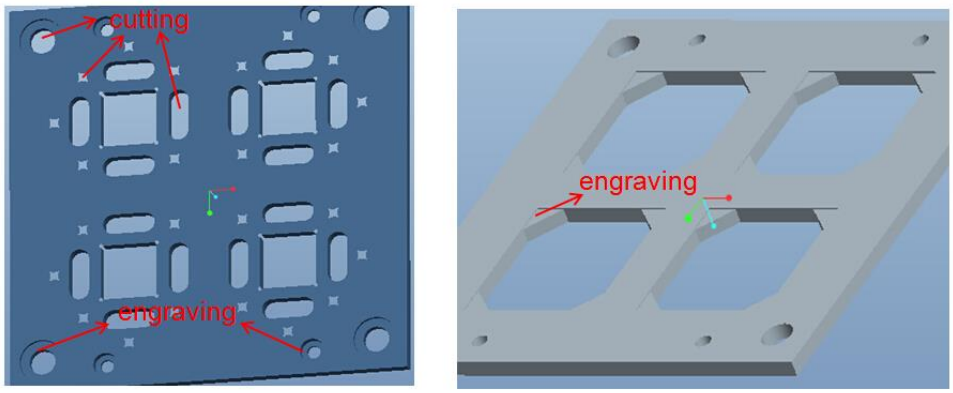

Figure IV- 1 : Manufacturing of different components

The engraving parts are used to place the screws and PCBs. The deepness of the engraving for screws is 0.8mm and 0.3 mm to place PCBs. The two machined mechanical supports are presented in Figure IV- 2.

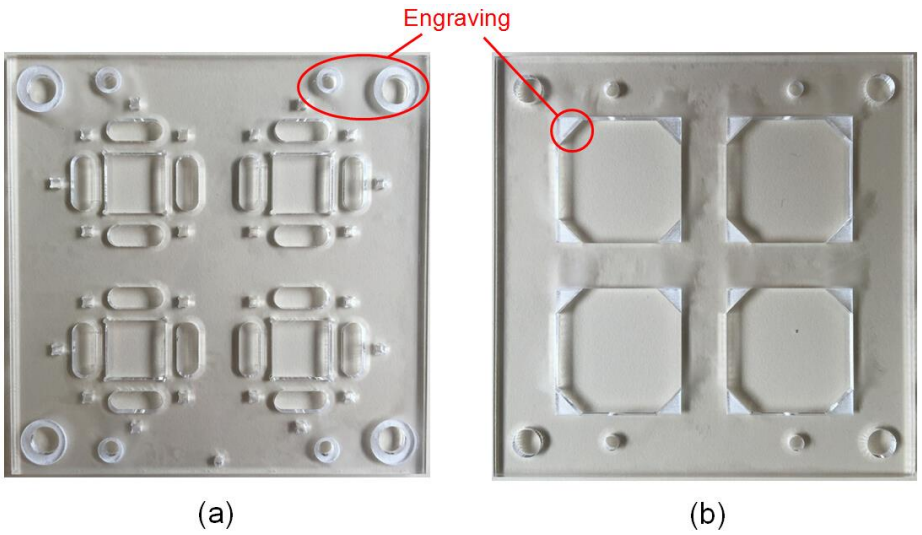

Figure IV- 2 : Prototype of two mechanical supports (a) Upper mechanical support (b) Bottom mechanical support

IV.1.1.2 3D printing

The geometries of the structured parts (structured plate and small pieces placed on the MPMs) are not adapted to laser cutting manufacturing process. The 3D printing manufacturing process has then been selected to obtain these parts. 3D printing is known as additive manufacturing process which is adapted to obtain three-dimensional objects thanks to the deposition of successive layers. The structured plates in this thesis are manufactured by the company STRATASYS Ltd. The material used is VeroWhite-FullCure® 830. The small pieces on the

MPMs and the structured plate are visible in Figure IV- 3 (a) and (b), respectively. The studs on the MPMs are colored in blue to see them more clearly during experimentation. The mass of the structured plate is 1.5 g.

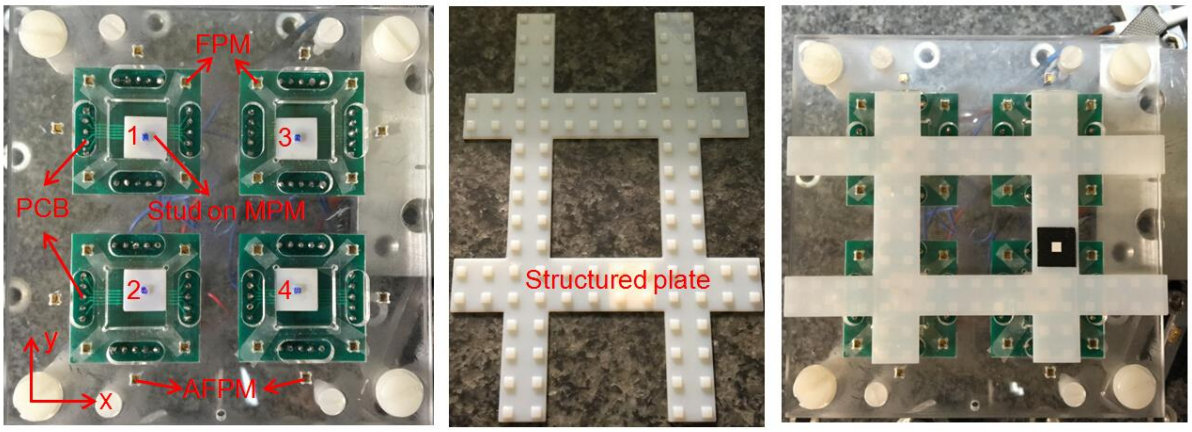

Figure IV- 3: (a) Four small structured plates on MPM (b) Structured plate (c) Structured plate placed on the DAA

IV.1.2 Characterization of prototype dimensions

All the components of the prototype have been manufactured using laser cutting machine or 3D printing as introduced previously. The real dimensions of the parts which have an influence on the device performances (stud dimensions on the structured plate ("a" and "b"), stud dimension on the MPM ("d") and stroke of the MPMs) (Figure IV- 4) have been measured using a caliper with a measurement precision of 0.01 mm. A comparison between the theoretical values and measured average values is presented in Table IV- 1. The errors are in the order of a few tens of microns, the maximum error is 60 µm. From this table, the errors due to manufacturing are observed. These manufacturing errors have been considered to determine the theoretical values of the plate displacement in the following section.

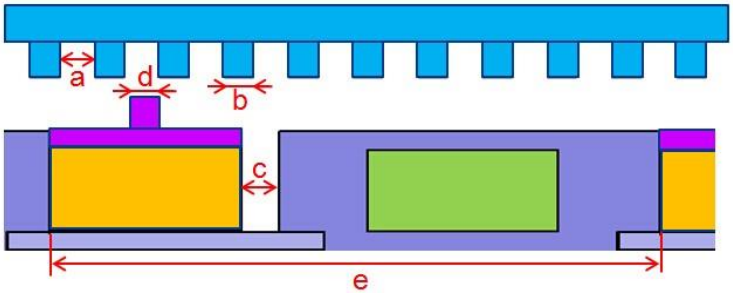

Figure IV- 4: Measured parameters of experimental setup

Table IV- 1: Comparison between experimental and theoretical values

Parameters	Theoretical value	Average experimental value
a	4.00 mm	3.94 mm
b	2.00 mm	2.06 mm
c	4.00 mm	4.02 mm
d	2.00 mm	2.06 mm
e	40.00 mm	40.00 mm

IV.1.3 Presentation of the experimental setup

IV.1.3.1 Control system

To control the MPMs displacement, a control system has been used (Figure IV- 5). It is composed of a computer equipped with a National Instrument data acquisition board (NI PCI-6733) and four voltages to current converters (V-A converters). The computer is equipped with LABVIEW software used to generate the control voltage signals [-10V; +10V] thanks to the data acquisition board. The Table IV- 2 gives the properties of the acquisition board.

Table IV- 2: Acquisition board properties

Board	Sampling frequency	Output Resolution	Utilization	Analog output
NI PCI-6733	1 MHz	16 bits	Output	8

Four analog outputs of the data acquisition board are used to generate four output voltages [-10V; +10V] which are converted into four power current signals thanks to the four V-A converters. Two types of V-A converters have been used during experimentation with different output current ranges: V-A1 and V-A2 with [-7A; +7A] and V-A3 and V-A4 with [-10A; +10A]. As a matter of fact, the generated electromagnetic force is different along the two axes due to the different distances between the bottom side of the MPM and the wires. With the same input current, the electromagnetic force generated using the TW is higher than using the BW. For the presented prototype, the TWs are used to switch along x-axis while the BWs are used to switch along y-axis. The V-A3 and V-A4 are then used to switch along y-axis while V-A1 and V-A2 are used to switch along x-axis in order to ensure the same switching time by adapting the current magnitude. With this choice, a higher driving current can indeed be generated to switch along y than along x-axis in order to compensate the electromagnetic force difference.

To measure the plate displacement without disturbing it, a contactless measurement technique has been used. A camera is placed above the DAA and a black sticker with a white square in the middle is pasted on the top side of the structured plate. The camera takes pictures of the structured plate during its displacement. A MATLAB image processing program detects the sticker position in each image and, thanks to a calibration using a target made by Thorlabs (Figure IV- 6), the plate displacement can be calculated. This calibration is composed of several grid arrays. The 500 µm grid is used in this experimentation. The dimension of each square of the grid is 500 µm. In a picture, the square dimension represents 13 pixels. So the resolution of the measurement in this chapter is 38.5 µm for one pixel.

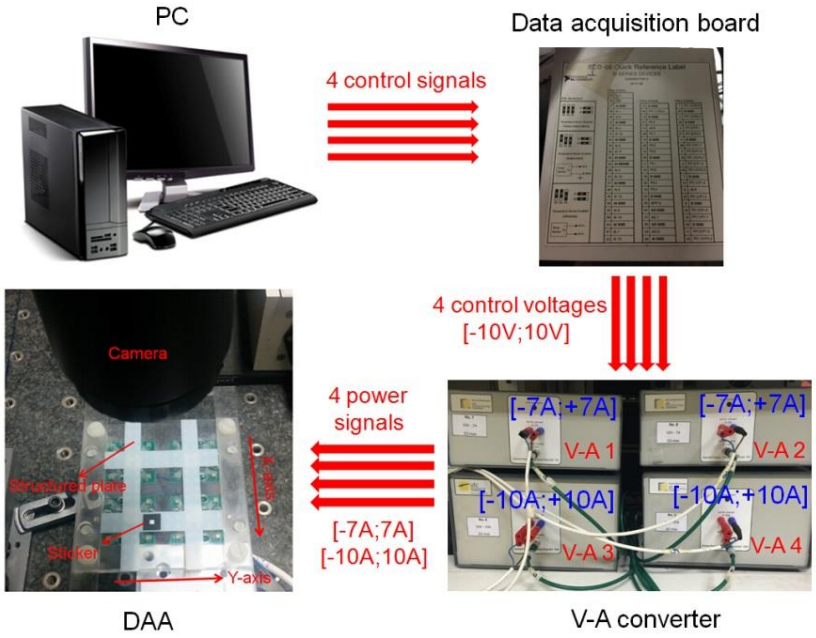

Figure IV- 5: Control system of DAA

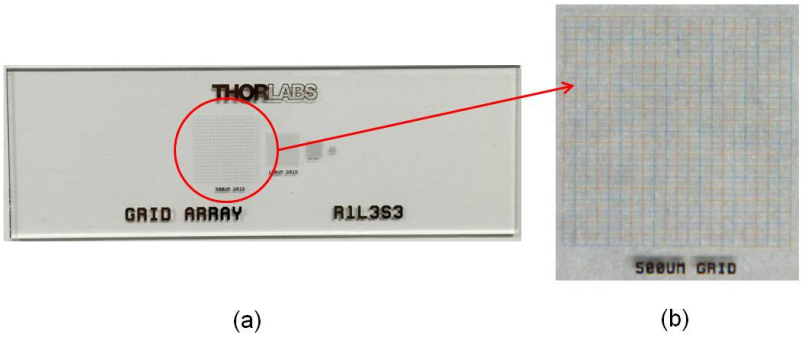

Figure IV- 6: (a) Calibration target (b) Zoom on the 500 µm grid

IV.1.3.2 Electrical connections

In the displacement sequence presented in the previous chapter, it is shown that, if the structured plate is moved along x-axis, [MPM "1" and MPM "2"] and [MPM "3" and MPM "4"] are switched together, respectively (Figure IV- 7).

Figure IV- 7: Steps of MPM displacement

Four identical PCBs have been used (one for each EDA) and placed below each square cavity. On each PCB, two sets of five electrical wires are used, one set for each displacement axes. To ensure a fully independent control of the four EDA, eight V-A converters are needed. However, due to experimental limitation in the number of V-A converters available, four V-A converters have been used with the electrical connections presented in Figure IV- 8.

To realize simultaneous displacement of MPM "1" and MPM "2" (resp. [MPM "3" and MPM "4"]), PCB1 and PCB2 (resp. [PCB3 and PCB4]) have to be connected together as illustrated in Figure IV- 8. Two pairs of PCBs are then connected to four V-A converters. For each pair of PCBs, one V-A converter is used to switch the two MPMs along x-axis or along y-axis. V-A1 controls the displacement of MPM "3" and "4" along y-axis and V-A2 controls the

displacement of MPM “1” and “2” along y-axis. Whereas, V-A3 controls the displacement of MPM “1” and “2” along x-axis and V-A2 controls the displacement of MPM “3” and “4” along x-axis.

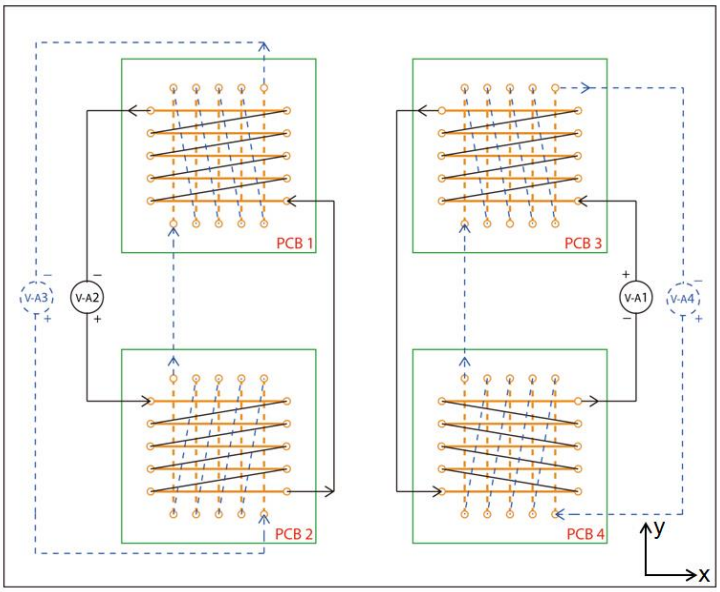

Figure IV- 8: Electrical connections between PCBs and V-A converters

Considering the electrical connections shown in Figure IV-9, the MPMs displacement directions are represented as function of the driving current direction in Figure IV- 9.

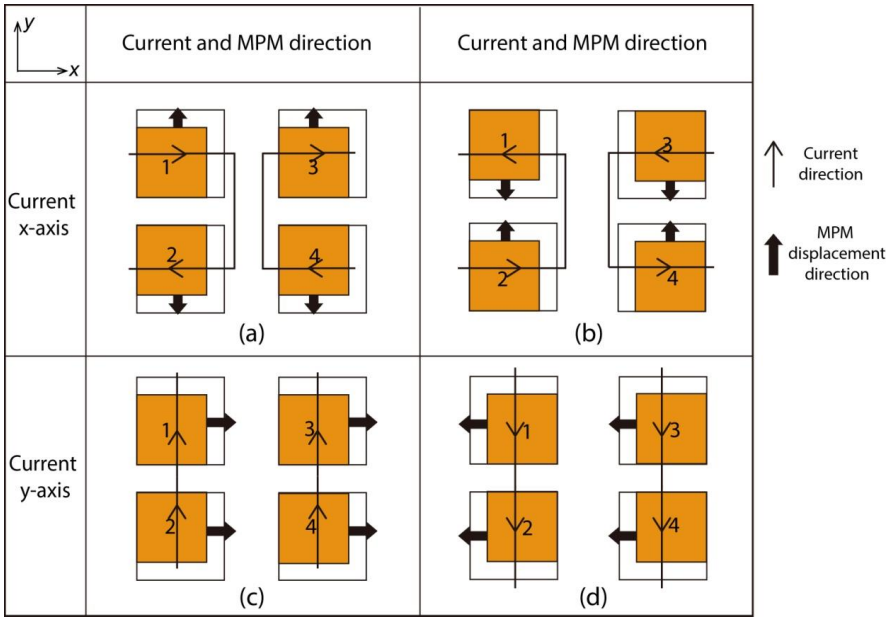

Figure IV- 9: Relations between driving currents and MPM displacement directions

IV.1.3.3 Control current signals

The current signals used to switch the MPMs between the discrete positions according to the displacement sequence (plate displacement along x-axis) are shown in Figure IV- 10.

The driving and holding currents for every MPM are represented considering the eight states of the displacement sequence (Figure III-2). The current "1x" represents the current needed to switch the MPM "1" along y-axis. A positive (resp. negative) current is used to switch a MPM along +x-axis or +y-axis (resp. –x-axis or –y-axis).

In the initial position, the four MPMs are placed in the discrete position close to the DAA centre. At step 1, MPM "3" and "4" are switched along +y-axis and –y-axis, respectively. According to Figure IV- 9 (a), the input current is positive in MPM "3" and negative in MPM "4", so a positive driving current is then injected through the wire "3x" and a negative driving current through the wire "4x". During this switch, holding force is generated along -x-axis. So a negative holding current is injected in the wires "3y" and "4y" to ensure the contact between the MPMs and the lateral stop (Figure IV- 9 (d)). At step 2, MPM "3" and MPM "4" are switched along +x-axis. Positive driving currents are then injected through the wires "3y" and "4y". During this step, the holding force on MPM "3" is along y-axis and along –y-axis on MPM "4". So a positive holding current is injected in the wire under "3x" and a negative current in the wire "4x". According to the relations between the input currents and MPM displacement, the control of can then be obtained of the following steps (Figure IV- 10).

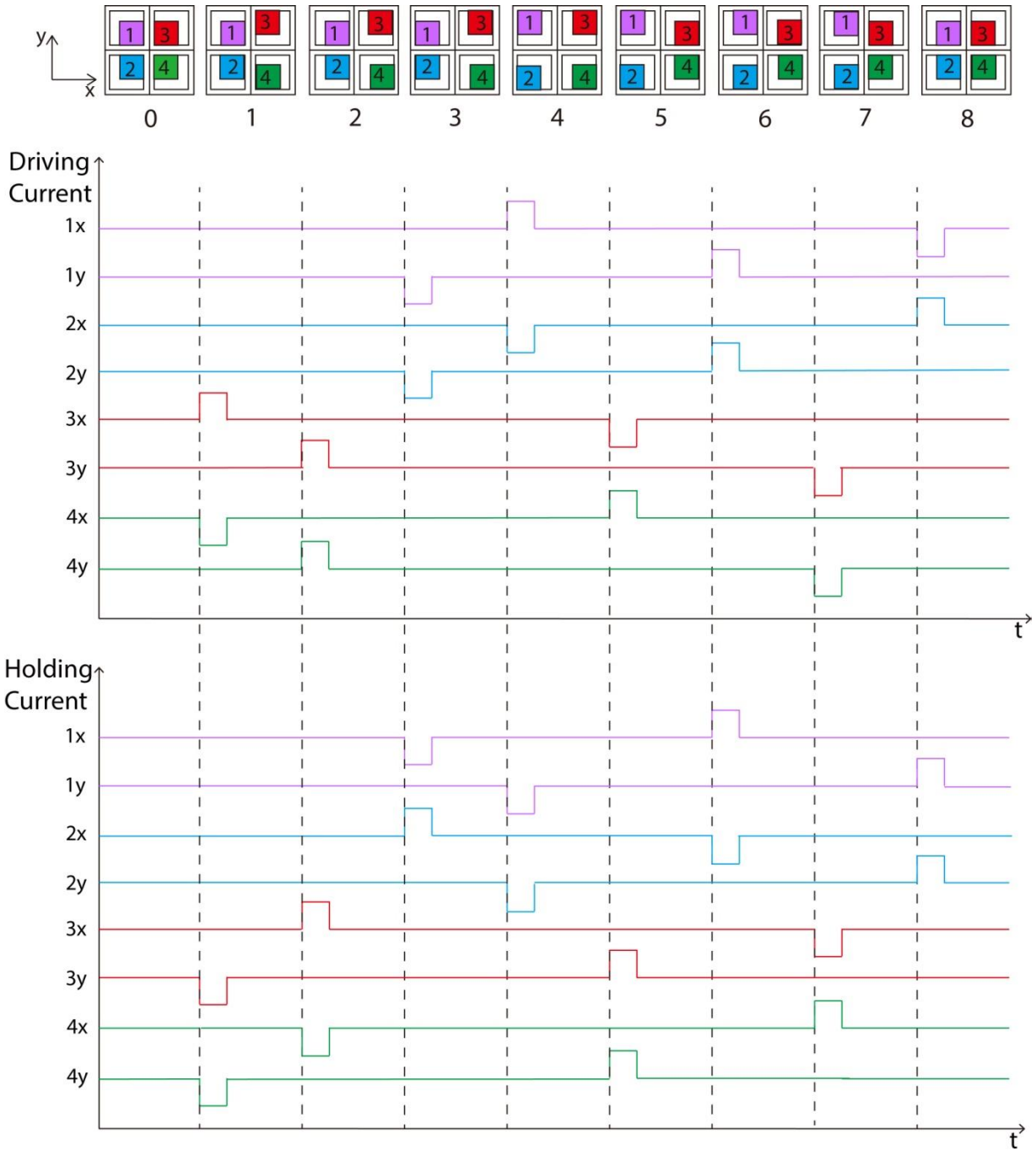

Figure IV- 10: Sequence of driving and holding currents

IV.2 Experimental results

IV.2.1 Characterization of the DAA

In the previous chapter, the theoretical minimum driving currents needed to switch each MPM have been calculated. These theoretical values are between 1.92A and 2.16 A for x-axis and between 2.03A and 2.29 A for y-axis (see Table III-4). The minimal driving current has also

been determined experimentally for the two displacement axes and for the four EDAs. To determine this value, the structured plate and the studs on the MPM have been removed. The details of the minimum driving current values are given in Table IV- 3. Ten measures have been realized for each MPM. To switch the MPM along x and y-axis, the average minimum driving currents are 1.80 A and 2.00 A, respectively. The variation of the currents is ± 0.1 A. The current along y-axis is larger than along x-axis due to the gap between BW and MPM (Figure III- 5). The differences between the experimental and theoretical values have several origins as the manufacturing errors of the fixed part, errors on the MPM dimensions and magnetizations and friction inhomogeneity. The minimum driving current to switch along x and y-axis varies between 1.80 ± 0.1 A to 2.05 ± 0.1 A and 2.00 ± 0.1 A to 2.15 ± 0.1 A, respectively. These variations have the same origins as the difference between the theoretical and experimental values.

Table IV- 3: Minimum experimental driving currents to switch each MPM

MPM	Current along x-axis	Current along y-axis
1	1.90 ± 0.1 A	2.10 ± 0.1 A
2	1.80 ± 0.1 A	2.00 ± 0.1 A
3	2.05 ± 0.1 A	2.15 ± 0.1 A
4	1.95 ± 0.1 A	2.10 ± 0.1 A

IV.2.2.1 Validation of the conveyance function

In the following paragraph, the conveyance function of the structured plate along x-axis has been tested. During experimentation, to avoid disturbances due to straightness errors along y-axis, a linear guide has been added on the top side of the DAA (Figure IV- 11 (a)).

Then, the control sequence is used to move the MPMs and the camera placed above the DAA takes pictures during the displacement. In Figure IV- 11 (b), several images of the sticker positions are presented to show the plate initial position and its position after one displacement sequences. It can then be observed that the proposed concept is suitable for conveyance application.

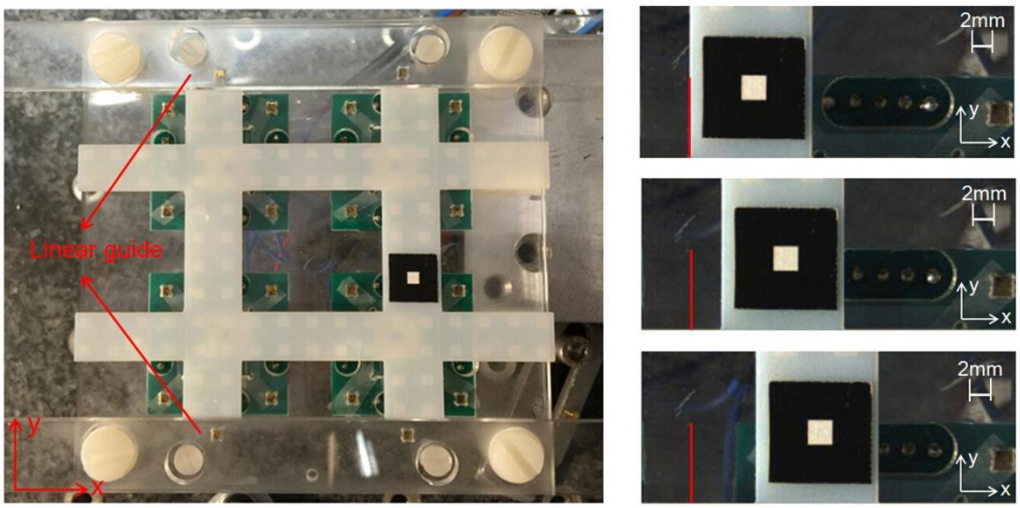

Figure IV- 11: (a) Experiment with linear guide (b) Plate displacement of one sequence

IV.2.2.2 Influence of the initial position on the plate displacement

To ensure the plate displacement according to the displacement sequence presented in Figure III-2, the structured plate has to be well initially positioned. A bad positioning of the plate will result in a poor engaging/disengaging of the studs or the impossibility to move the plate. With the architecture of the device, it is not easy to initially place the plate relatively to the DAA. A series of gauge blocks with different dimensions have then been manufactured in order to facilitate the initial plate positioning. To initially position the plate, a gauge block is placed in the cavity defined by the guide part and in contact with the edge of the DAA as illustrated in (Figure IV- 12).

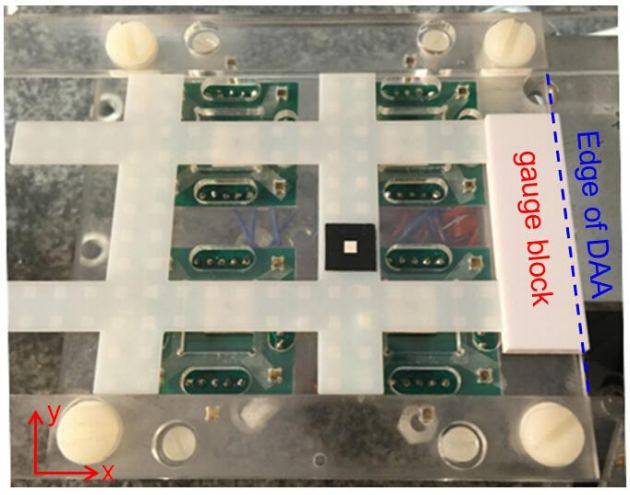

Figure IV- 12: Experiment with gauge block

The theoretical perfect dimension of the gauge block is 15 mm. Different gauge blocks from 14 mm to 16 mm with a step of 0.2 mm have been realized in order to quantify the influence of the initial position on the plate displacement. The Figure IV- 13 represents the theoretical influence of the gauge block dimension on the initial plate position for three gauge block dimensions: 14 mm (a), 15 mm (b) and 16 mm (c).

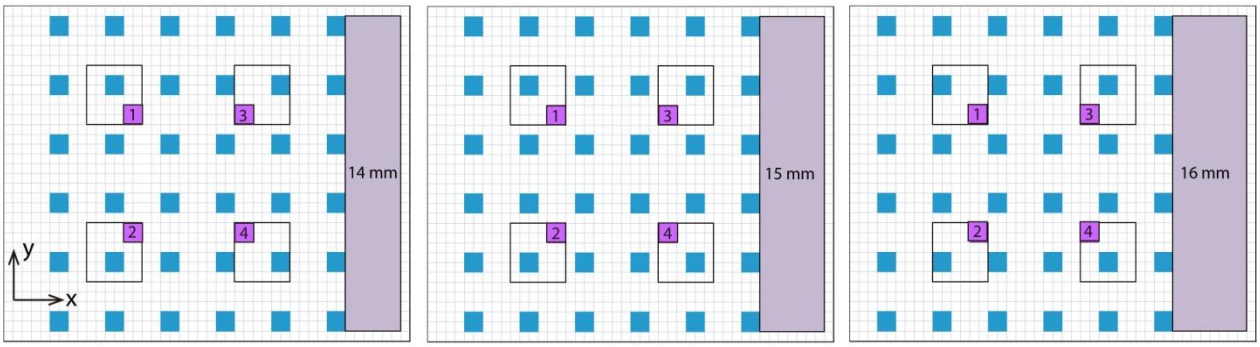

Figure IV- 13 : Initial plate positions with different gauge blocks (a) 14mm (b) 15 mm (c) 16mm

According to these three figures, it can be observed that the 14 mm and 16 mm gauge block dimensions correspond to the minimal and maximal dimensions, respectively. If the dimensions of the gauge block is lower than 14 mm or higher than 16 mm, the MPMs "3" and "4" cannot switch along +y and –y axes, respectively, as needed in the first step of the displacement sequence. It can also be observed that the plate displacement obtained will increase with the increase of the gauge block dimension after the first sequence. If the dimension of the gauge block is larger, the gap between the studs on MPM and the studs on the plate is smaller, and then the displacement value to be compensated by the first sub-step is smaller, so the displacement is larger. The plate displacement obtained for the first sub-step of the displacement sequence with different gauge blocks is illustrated in Figure IV- 14. It is shown that the plate displacement with 16 mm gauge block is 2 mm larger than the one obtained with 14 mm gauge block.

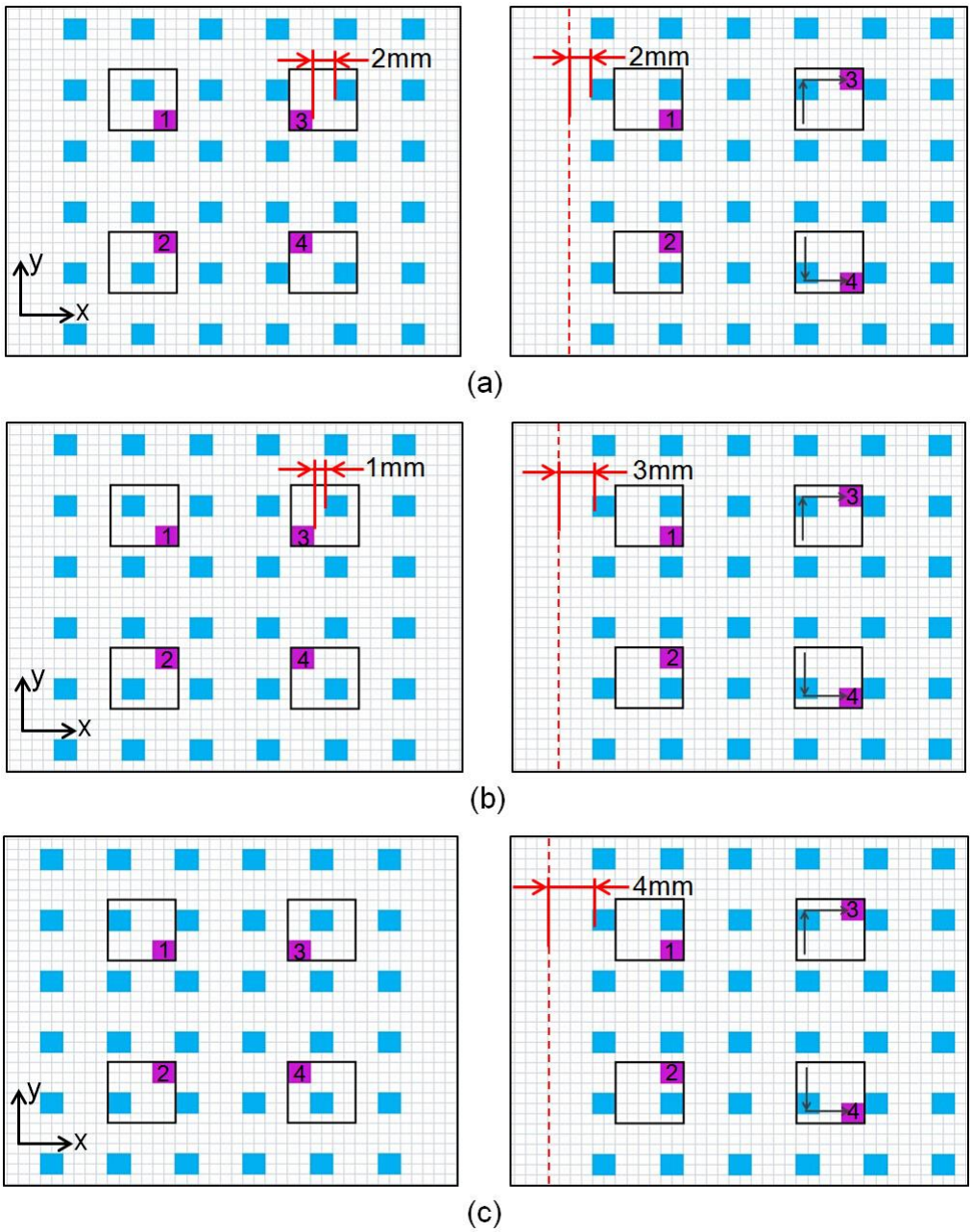

Figure IV- 14: Plate displacement of first half step with different gauge block: (a) 14 mm (b) 15mm (c) 16mm

An experimental test has been realized with these different gauge blocks and the plate displacement after one displacement sequence has been measured. During the experimental characterization of the DAA, a 3A driving current has been used to ensure that all MPMs switch properly. The theoretical and experimental results are compared and presented in Figure IV-15. The experimental measurement has been repeated five times for each gauge block dimension and the standard deviation (represented by the error bars in the figure), has been computed for each experimental point. The increase of the plate displacement as function of the

gauge dimensions illustrated in Figure IV- 14 is clearly visible. Moreover, it can be observed that the experimental results are close to the theoretical values.

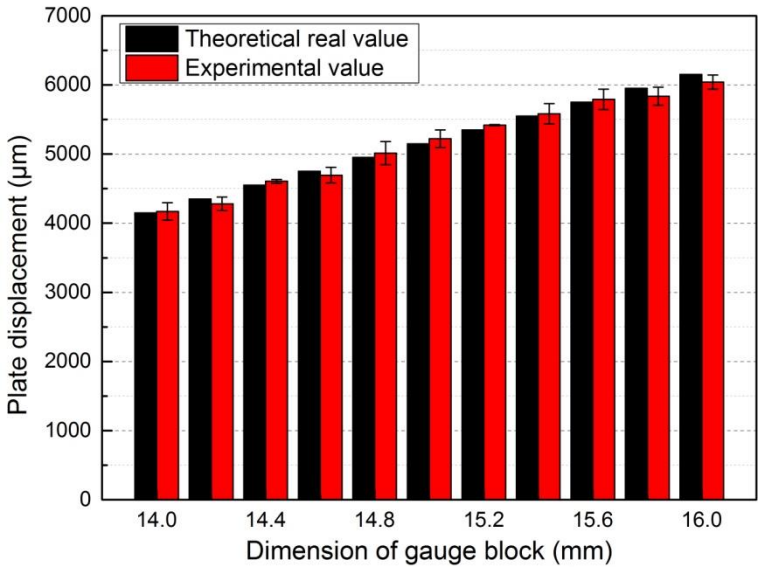

Figure IV- 15: Plate displacement of the first step with different gauge blocks

IV.2.2.3 Experiment for one direction plate displacement

In this section, five experimental displacement sequences have been realized along +x-axis. This displacement has been repeated five times. In this experiment, the 15 mm gauge block has been used to ensure the initial plate positioning. The input current is 3A with 150 ms impulse width. Comparisons between the experimental and theoretical plate position and plate displacement are presented in Figure IV- 16 (a) and Figure IV- 16 (b), respectively.

In Figure IV- 16 (a), it can be observed that the error between the experimental and theoretical positions increases when the number of displacement sequence rises. After the five sequences, the plate has experimentally moved over a distance of 30.36 mm while the theoretical value is 29.55 mm. In Figure IV- 16 (b), the experimental values correspond to the average of the five measurements and the error bars represent the standard variations. A repeatability error is visible between the different measurements and the maximal error represents 155.9 µm which is due to friction inhomogeneity and manufacturing errors of the prototype. The errors at each sequence lead to the accumulation of errors after several plate displacement sequences.

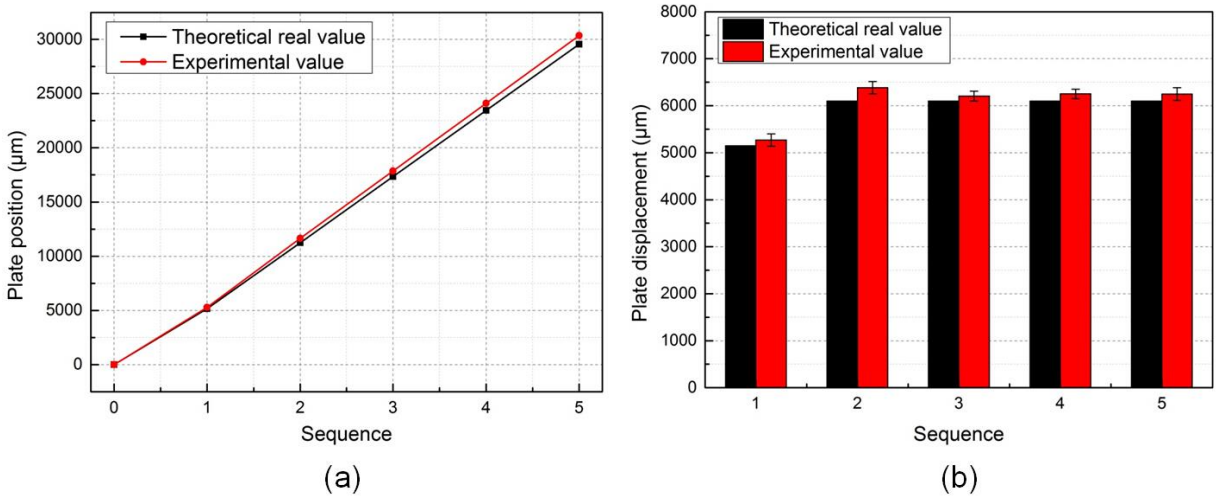

Figure IV- 16: Comparison between theoretical and experimental value for five steps displacement (a) Plate position (b) Plate displacement

Theoretically, the plate displacement at the first step (5150 µm) is lower than the ones obtained for the next steps (6150 µm). This difference is due to the initial gap between the studs on the structured plate and the studs on MPMs which is different for the first step than for the next ones. As illustrated in the displacement sequence shown in Figure III-2, the position reached after a sequence corresponds to the initial position of the next sequence. In Figure IV- 17, the initial position for the first step is compared with the initial position for the next step. The position in Figure IV- 17 (a) is the initial position obtained with a 15 mm gauge block. The initial position of the next sequence (Figure IV- 17 (b)) corresponds to the same as the position with a 16 mm gauge block. So the plate displacement of the next sequence is theoretically 1 mm larger than the first sequence. Experimentally, the same effect can be observed with a first displacement step of 5269.6 ±129.8 µm and an average plate displacement of 6272.9 ± 123.3 µm for the next ones. From Figure IV- 16, it can be observed that the experimental results are close to the theoretical ones.

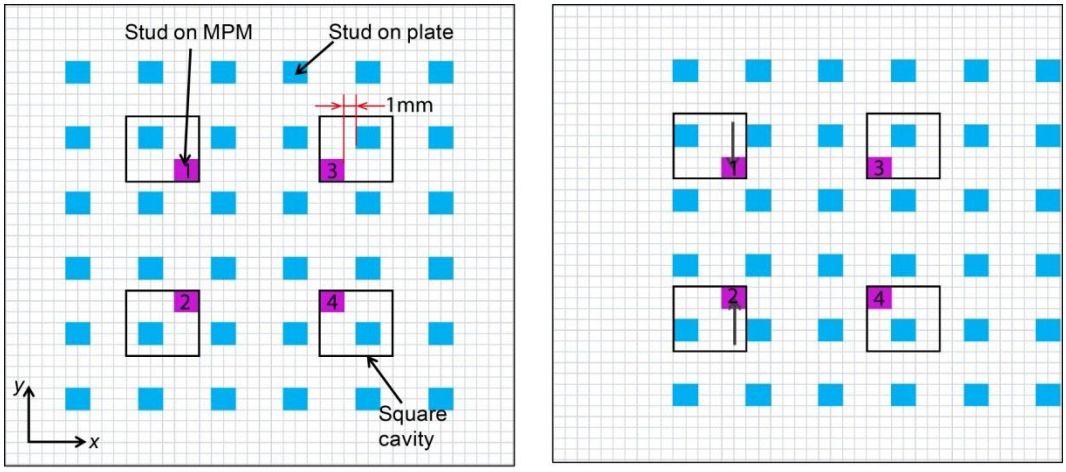

Figure IV- 17: (a) Initial position for the 1st sequence (b) Initial position for the 2nd sequence

IV.2.2.4 Experiment for a round trip displacement

In this section plate displacement along +x and –x have been realized. A displacement step along +x-axis has been firstly realized, then three steps along -x-axis, and finally two steps along +x-axis to return to the initial position. The controlling conditions (3A driving current with an impulse width of 150 ms) are identical as the ones used in the previous section. The plate position and the plate displacement for each sequence are illustrated in Figure IV- 18 (a) and (b), respectively.

It can be observed that the experimental results are close to the theoretical ones. The experimental results correspond to the average value and the errors bars represent the standard variation. From the theoretical values, it can be observed that when the plate displacement direction changes (from +x-axis to –x-axis), the plate displacement obtained just after the change is lower than the previous one. The initial position is placed with a 15 mm gauge block, the plate displacement is theoretically 5150 µm. After the first sequence along +x-axis, the position of the plate is the same as Figure IV- 17 (b), which is also the initial position of the second sequence of this round trip displacement. Then the displacement steps of the second sequence are illustrated in Figure IV- 19.

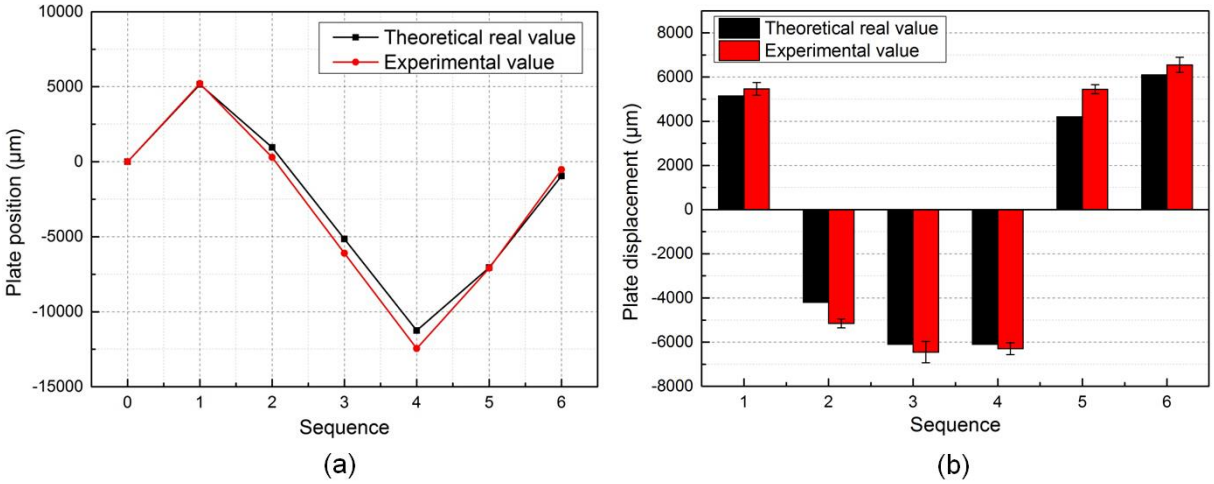

Figure IV- 18: Comparison between theoretical and experimental value of plate position for a round trip displacement

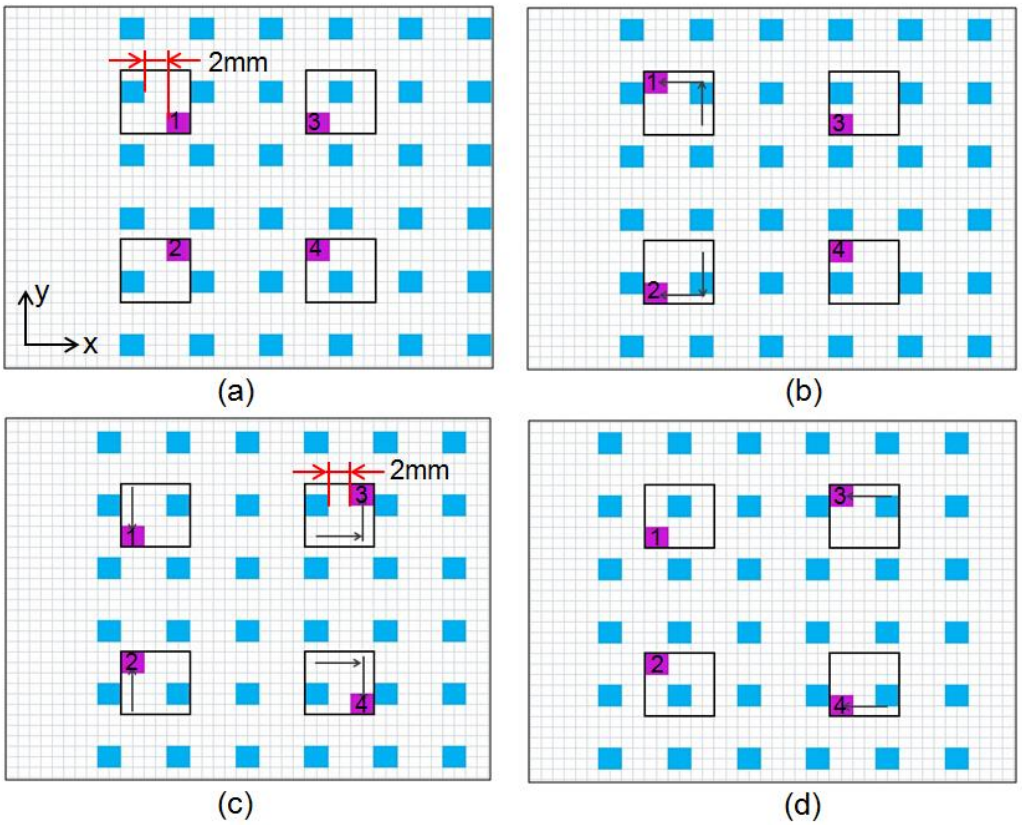

Figure IV- 19: Steps of the 2nd sequence along –x-axis (a) Initial position (b) The 1st sub-step (c) Initial of the 2nd sub-step (d) The 2nd sub-step

MPM "1" and "2" realize the first sub-step displacement (Figure IV- 19 (a)) and MPM "3" and "4" realize the second sub-step displacement (Figure IV- 19 (d)). So the total plate displacement of this second sequence is theoretically 4200 µm. After the second sequence, the plate

displacement is the same for the third and forth sequence as that along one direction movement, the theoretical plate displacement is 5150 µm for each sequence. At the fifth sequence, the plate displacement changes from –x-axis to +x-axis, the theoretical plate displacement is then 4200 µm. So the first sequence displacement after every change of direction is theoretical 4200 µm. In Figure IV- 18, the experimental values show the same tendency as theoretical values.

IV.2.2.5 Plate displacement with different driving current values

The experimental results presented in the previous sections have been obtained with a 3A driving current value. This value has been chosen in order to be higher than the minimal driving current needed to switch the MPMs. However during the realization of the measurements presented in the previous sections, it has been observed some sliding of the plate during the conveyance. In order to highlight engaging problem due to this sliding, the plate displacements with 3.5 A driving current values are compared with a 2.5 A driving current in Figure IV- 20.

The initial plate position has been obtained with the 15 mm gauge block and is visible in Figure IV- 20 (a). A displacement sequence is then realized. At the first step (Figure IV- 20 (b)), the MPMs "3" and "4" are moved up and down. The Figure IV- 20 (c) and (e) represent the second step with the two different driving current values. At this step, the MPMs "3" and "4" move toward x-axis, the MPMs stop moving when they reach the stop of the square bracket. With a 2.5A driving current, the plate is moved by the MPMs and stops moving at the same time as the MPMs (Figure IV- 20 (c)). In this configuration, the studs on the plate are still in contact with the studs on the MPMs after the displacement. With 3.5A driving current, it can be observed that the plate displacement is larger than with 2.5A (Figure IV- 20 (e)). This is due to a sliding of the plate after the MPMs have stopped. At the third step, the MPM "1" and "2" are moved toward +y and –y-axis, respectively. With 2.5A, it can be observed that the MPMs are well positioned and the studs on them can be engaged between the studs on the plate. With 3.5A driving current, the sliding distance observed at the previous step disturb the behaviour because the studs on the MPMs cannot be engaged between the studs on the plate (Figure IV- 20 (f)).

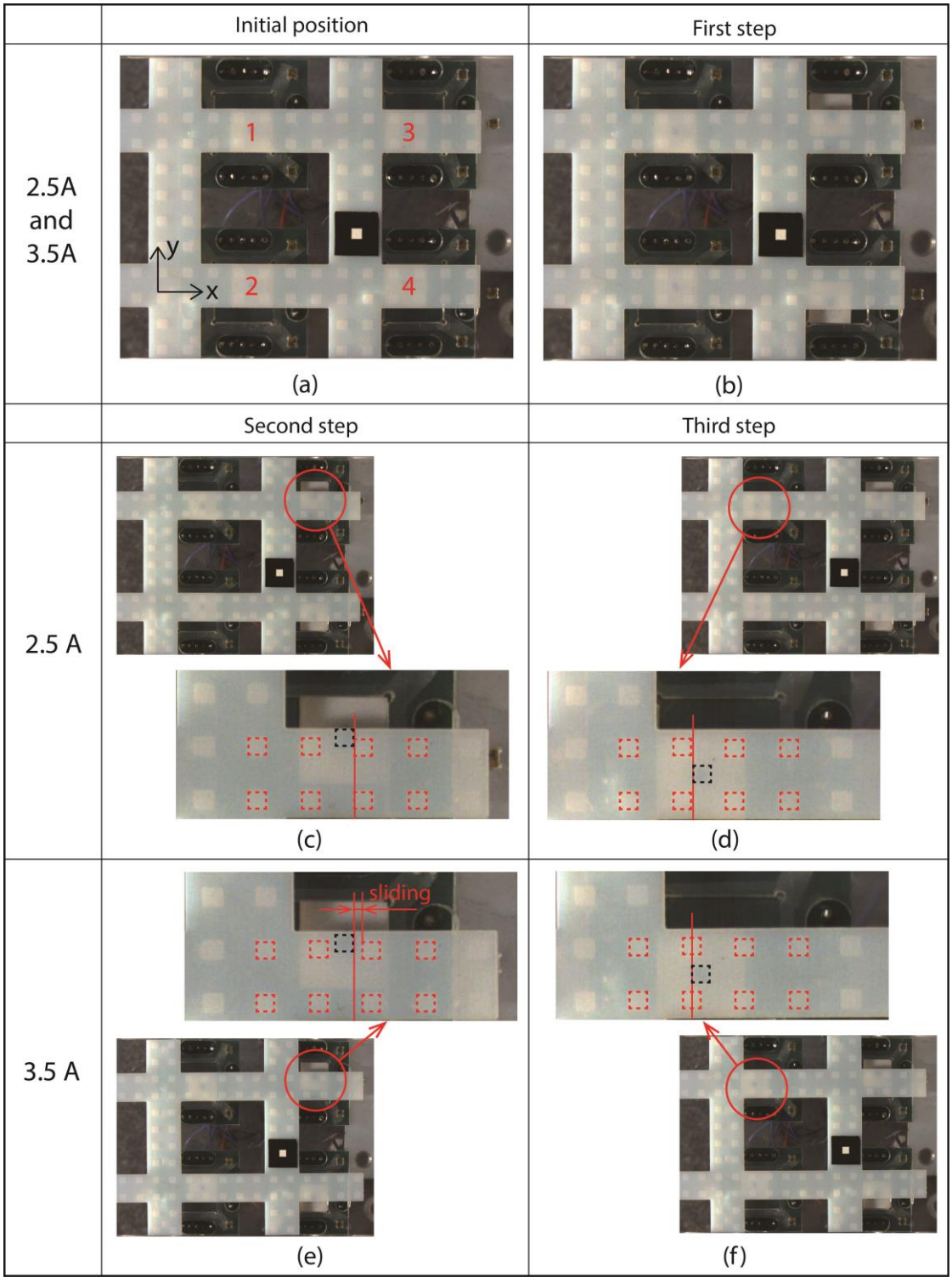

Figure IV- 20 Comparison of plate displacement with different driving currents: (a) Initial position (b) 1st step (c) 2nd step with 2.5A (d) 3rd step with 2.5A (e) 2nd step with 3.5A (f) 3rd step with 3.5A

The plate displacement and position are compared for different driving current values in Figure IV- 21 (a) and (b), respectively. The displacement and position values are given after the first

half step (“0.5” in horizontal axis) and after the second half step (“1.0” in horizontal axis). The total displacement obtained after the second half step for all the driving currents are close to the theoretical value. The maximum plate displacement is 5524 µm with 2.5A. The half plate displacement is larger with 3.5A (4500.3 ± 103.0 µm) than with 2.5A (3008.9 ± 82.6 µm) due to the sliding distance observed in the previous figure. With 2.5A, the plate displacement obtained after the first half step is close to the theoretical value. In Figure IV- 21 (b), it can be observed that the sliding distance after the first half step increases with the increase of the driving current value. Then, the second half plate displacement decreases due to the bad engaging of MPM “3” and “4”. The displacement of the second half sequence is 836.9 ± 88.1 µm, which is much less than that obtained with 2.5A (2515.5 ± 104.5 µm).

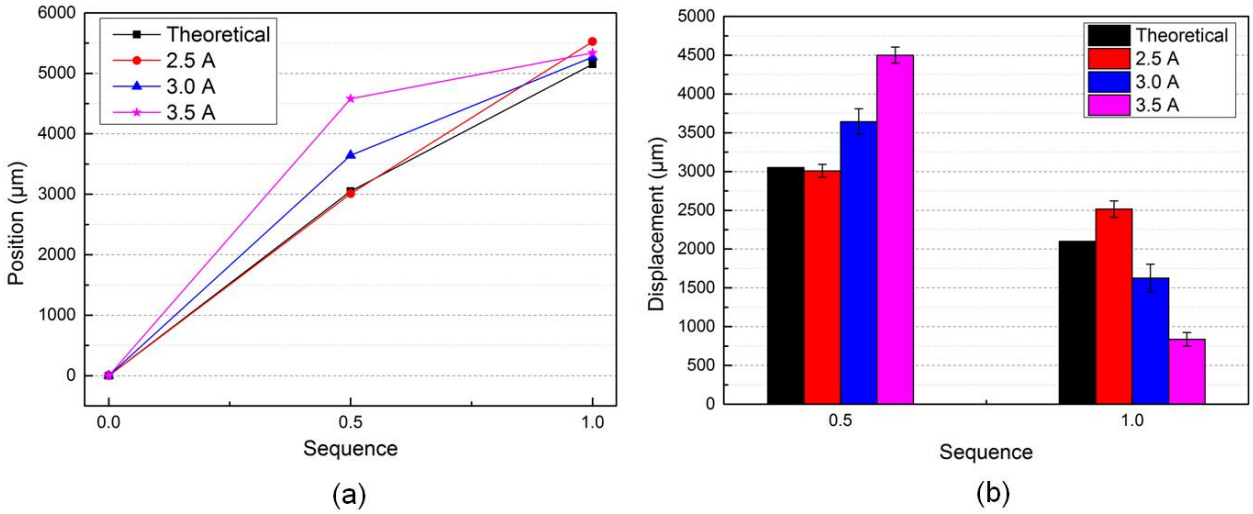

Figure IV- 21: Comparison of plate displacement with different currents: (a) Plate position (b) Plate displacement

To control this conveyance device, the driving current value is a very important parameter to generate the plate displacement. During the experiment, a 2.5A driving current value corresponds to be the minimum driving current to move the structured plate. However, due to the inhomogeneous working conditions of each EDA, it is difficult to switch all EDAs well and to generate the plate displacement without sliding. However, with a large driving current, the sliding of the plate can occur to affect the MPMs’ engagement. So the driving current should be high enough to ensure the MPMs switching but not too high to minimize the sliding of the structured plate.

IV.3 Conclusion

In this chapter, the experimental characterization of the planar conveyance application is presented. The manufacturing methods used for the prototype are firstly introduced. The prototype has then been manufactured using rapid prototyping techniques: laser cutting machine for the mechanical support and 3D printing for the structured plate and the studs on MPMs.

The experimental setup composed of the DAA, the control system and the V-A converters is then described. The electrical connections of the PCB are detailed. The MPM displacement directions are defined according to the current directions in the two sets of wires. The control signals of the DAA needed to obtain the planar conveyance function are presented.

Then, the prototype is presented and tested. In order to characterize the behavior of each EDA, the minimum driving current needed to switch each MPM (without structured plate) has been measured for the two displacement directions. The variation observed between the EDAs is due to the manufacturing errors of the prototype and to friction inhomogeneity. To ensure all EDAs to be switched well, a 3A driving current has been chosen. So, experimental characterizations of the planar conveyance application have been realized. Firstly, the ability to move a structured plate with the DAA is proved. However, the influence of the initial position has been observed. A series of gauge blocks have been manufactured and used to ensure the initial positioning of the structured plate relatively to the DAA. One direction plate displacement has been realized and the experimental results have been compared with theoretical ones. The experimental results are close to the theoretical results. The maximum difference of the plate displacement is less than 300 µm. After several steps, displacement errors are however visible compared to theoretical results. Then, a round-trip displacement is realized to observe the plate displacement by changing the displacement direction. The influence of the driving current value has been observed and plate displacement with 2.5A and 3.5A have been realized. The sliding effect is observed for a high driving current. The displacements of the first half sequence are compared with different driving currents. The displacement of 2.5A is close to theoretical value, while the displacement is much larger for a higher current. However, the inhomogeneity of the EDAs makes the displacement with a small driving current difficult.

Chapter 5: Conclusion and Perspectives

In this chapter, a comparison between the two conveyance principles studied in the thesis; based on a flat plate (Chapter 2) and on a structured plate (Chapters 3 and 4), is firstly presented. A conclusion of the work presented in the thesis is then done and perspectives are finally given for future researches.

V.1 Comparison between conveyors based on flat and structured plates

In this thesis, two conveyance principles based on a DAA have been studied. The first one is based on a flat plate and the second one on a structured plate. Four criteria have been chosen to compare these two principles and are given in Table V-1.

Table V- 1: Comparison of three conveyor considering four criteria (+ favorable; – unfavorable)

Criteria	Manufacturing constraints	Displacement capability	Sensitivity to friction	Possibility to realize variable plate displacements
Conveyor with flat plate	–	+ +	–	+
Conveyor with structured plate	– –	–	+	–

The first criterion corresponds to the manufacturing quality required for the device. With a flat plate, the influence of manufacturing errors will introduce variability in the EDAs performances (variation of stroke, switching time…). During the motion generation, the influence of these variations will be averaged between all the EDAs. The plate motion will be ensured, nevertheless with degraded performance. With a structured plate, the manufacturing constraints on the DAA will be more important because some geometrical properties will directly influence the device and could prevent the functioning due to the impossibility to engage the studs on the MPM with the structured plate. Moreover, the manufacture of the structured plate is obviously more complex than for the flat plate.

The second criterion corresponds to the displacement capability. The possible motions of the two principles are illustrated in Figure V- 1. The DAA with a flat plate can realize complex planar motions such as x, y and xy displacement and rotations. With a structured plate, only x and y motions are possible due to the studs on the MPMs and on the plate.

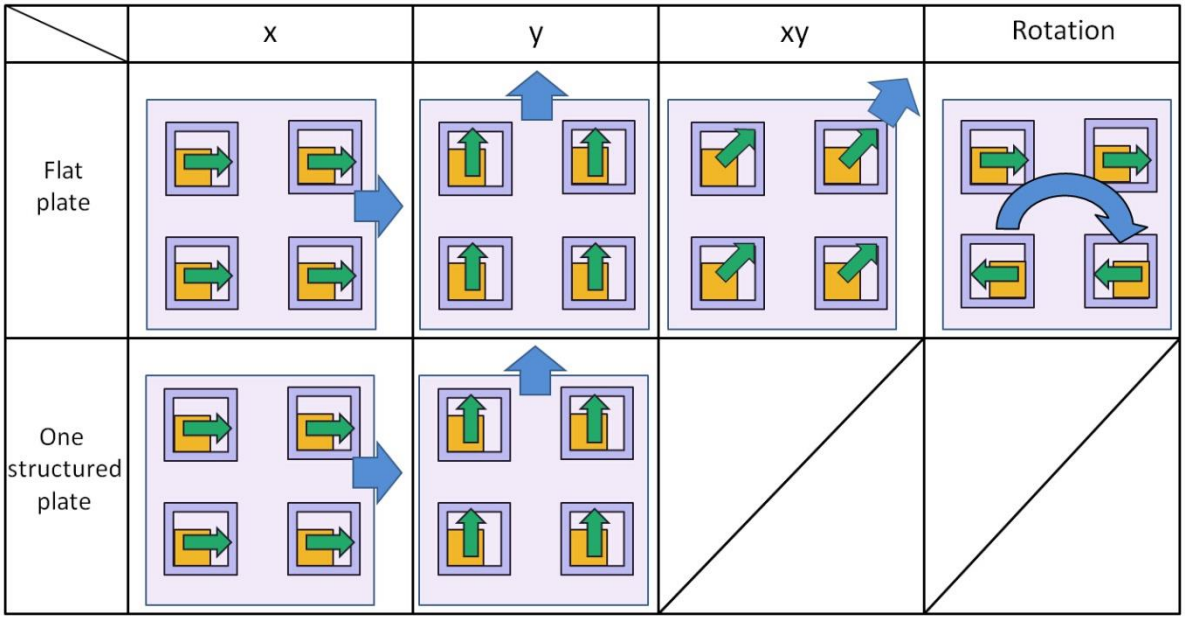

Figure V- 1: Comparison of motions with different plates

The third criterion corresponds to the sensitivity of the conveyance principle to friction. The conveyance application model based on a flat plate presented in Chapter 2, has shown that, when a high driving current is used, the plate displacement is small due to the large sliding effect. The experimental results have confirmed this phenomenon when the driving current is larger than 5A. For the DAA with a structured plate, a sliding of the plate has been experimentally observed for high driving current value however, the plate displacement is less sensitive to the friction coefficient, because the plate displacement is mainly generated by contact and not by adherence.

The fourth criterion characterizes the ability to the principle to realize variable plate displacements steps. With the flat plate principle, variable displacement steps can be easily obtained by changing the driving current value or the number of controlled actuators. With a structured plate, the displacement step is fixed by the geometries of the DAA (i.e. EDA stroke) and the structured plate. With a structured plate, the displacement step is then fixed at the manufacturing step and with a given prototype; it is not possible to realize variable steps.

V.2 Conclusion

In the first chapter of this thesis, a state of the art of digital actuation has been presented. A definition of digital actuation is given and the different solutions or physical principles used in literature to obtain the driving and holding functions are detailed. In this chapter, applications

of digital actuators have also been described and discussed. Based on the literature and the previous work of the Roberval laboratory, the electromagnetic principle actuation has been selected because this principle is well adapted to digital actuators. Magnetic holding force and electromagnetic driving force can indeed be easily obtained using the magnetic properties of PMs. The present thesis is a continuation of previous works in the Roberval laboratory. L. Petit [PETI 2009] has proposed and developed an elementary digital actuator based on a MPM which can reach four discrete positions. Based on this actuator, a DAA composed of 25 EDAs has then been designed and manufactured. P. Huyan [HUYA 2015] has characterized this DAA and validated a planar conveyance device based on it.

In the second chapter, a dynamic model of the conveyance application based on the DAA has been proposed. The principle of the EDA has been firstly introduced. Then, the principle of the DAA composed of 25 identical EDAs is presented. The planar conveyance application based on this DAA and on a flat plate placed on top of the DAA is described and the motion ability of this planar conveyance device has been illustrated. The objective of the proposed model is to calculate the MPM and plate displacements taking into account the magnetic, electromagnetic and friction effects. An analytical model has then been presented and implemented in the MATLAB software. The model has then been used to study the influence of several parameters on the plate displacement such as the driving current magnitude and the friction coefficients values. The minimum number of controlled actuators needed to displace the plate has been determined and a control strategy has been proposed. An example showing how to generate a 1 mm plate displacement is described. At last, the simulated results have been compared with the experimental results presented in the thesis of P. Huyan. For this comparison, the model has been adapted to consider the experimental conditions (only eight EDAs used). A good accordance has been observed between the simulated and experimental results for the two displacement axes and for different driving current values.

In the third chapter, a concept of a new planar conveyance device based on a DAA and a structured plate is proposed to minimize the effect of sliding between the MPM and the plate. The principle of this new conveyance device is firstly presented. A study on the relations between the geometrical parameters has been realized and a prototype has been designed. With the help of RADIA software, the magnetic force and electromagnetic forces have been computed and used to design the DAA. Using the model, the minimum driving current needed

to switch the MPM has then characterized. A CAD model of this new planar conveyance device has then been realized considering the chosen geometrical parameters.

The prototype is presented and tested in the fourth chapter. Two rapid prototyping techniques have been used to manufacture the different parts of the prototype. The support parts and the structured parts of the device have been manufactured by laser cutting machine and 3D printer, respectively. The dimensions of the manufactured parts have measured to compare them with theoretical values. Then, a control circuit is presented to explain the method used to switch the MPMs of the DAA. The four MPMs can be switched along x-axis and y-axis using four V-A converters. The plate displacement is measured with a camera placed above the device. During the experiment, the structured plate displacement is firstly validated. It is observed that the initial position of the structured plate has a high influence. Several series of experimentations are then done with different gauge blocks to ensure the initial position of the structured plate. Round trip displacements are also tested and the plate displacements and positions are compared with theoretical results. A good accordance has been observed between these results. However, the half plate displacement step is strongly affected by driving currents. When the driving current is large, a sliding of the plate is observed. The driving current have to be high enough to ensure all the actuators switch well, nevertheless, a too high current can generate a sliding of the structured plate leading to a jamming situation.

V.2 Perspectives

In this section, several perspectives of the presented work are proposed. These perspectives include motions with two structured plates, improvements of the mechanical parts of the device and of the control strategy used to ensure the conveyance.

V.2.1 Conveyance device with two structured plates

In order to realize more complex motions, two independent structured plates can be used as represented in Figure V- 2. In this case, the two structured plates can be moved in the same directions to realize motions along x and y axis. Rotations are also available when one plate is moved in a direction (for example +x) and the second one in the opposite direction (-x).

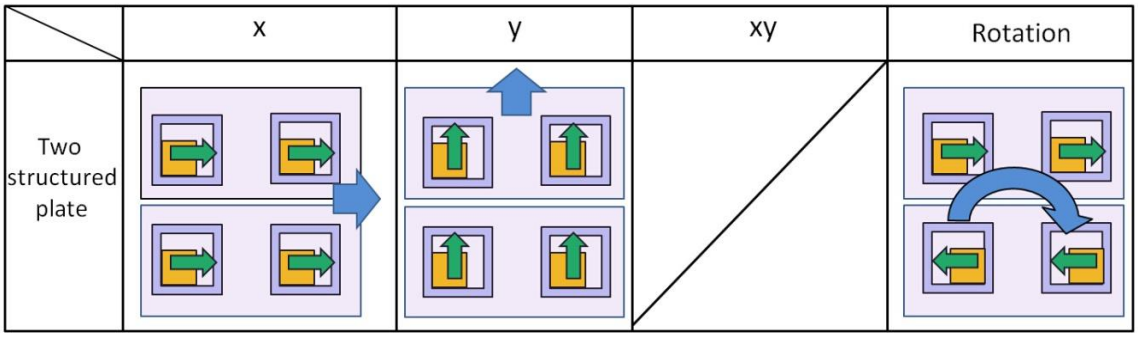

Figure V- 2: Available displacement with two structured plates

Based on this principle, the rotation of the gear is illustrated in Figure V- 3 (a) - (d). Two structured parts are placed above the DAA. In this example, an internal gear is fixed on the top side of the structured plate 2 and there is a rotational axe of the gear placed on the structured plate 1. In this figure, the EDAs below the structured plate 1 are not actuated, while the EDAs below the structured plate 2 are switched to generate a rotation of the gear.

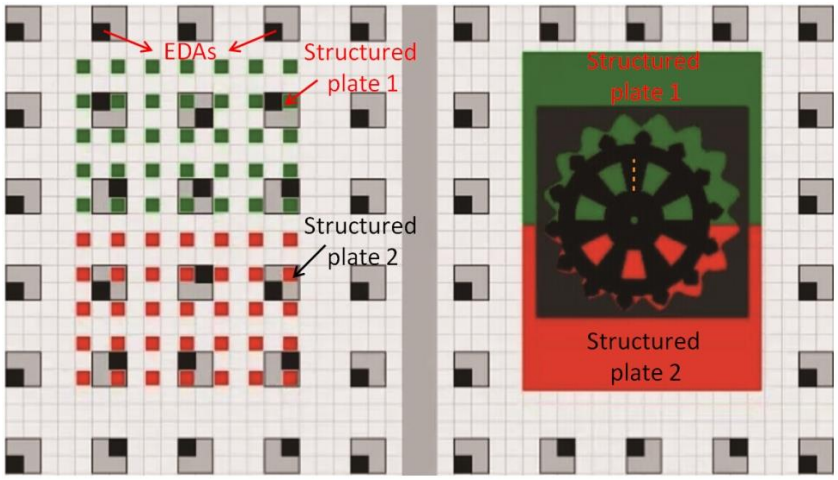

(a)

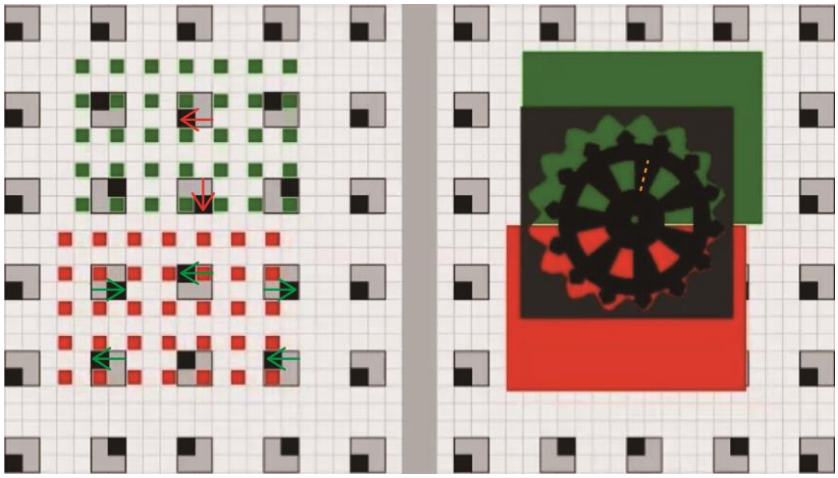

(b)

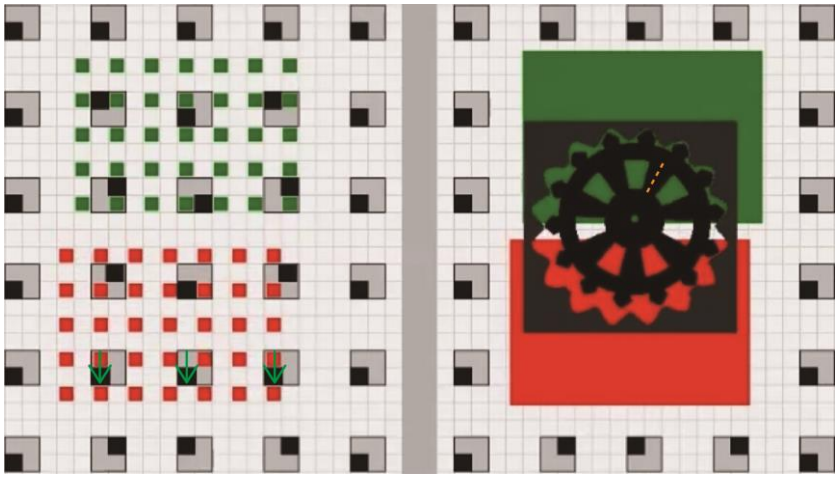

(c)

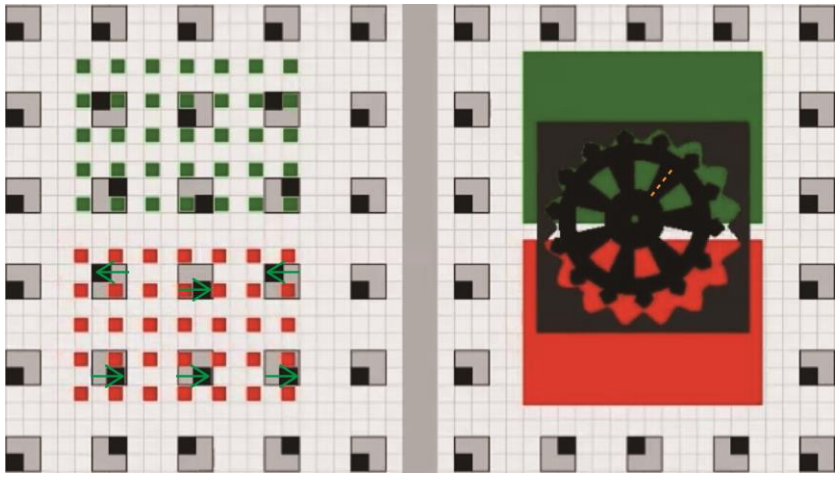

(d)

Figure V- 3: Rotation realized by two structured plates

V.2.1 Micro fabrication

During the characterization of the experimental device, it has been observed that the manufacturing errors can highly disturb the functioning of the device. The fabrication errors will result in bad engaging between MPM studs and structured plate. In order to minimize this effect, a structured plate and studs on the MPM have been micro-fabricated at ESIEE (Marne la Vallée). The proposed micro-fabrication process is detailed in Figure V- 4. The micro-fabrication process is separated into two steps. A 520 µm silicon wafer and a 500 µm glass wafer are used. In the first step, the silicon wafer and the glass wafer are firstly cleaned by HSO_3 and H_2O_2 during 10 minutes and by DI water during 5 minutes. Then, the two wafers are dried. Secondly, the silicon wafer and the glass wafer are anodic bonded (Figure V- 4 (a)). Thirdly, an aluminum layer is deposited on the surface of silicon wafer (Figure V- 4 (b)).

Fourthly, a photoresist resin is coated by spin on the top of aluminum layer (Figure V- 4 (c)). This is realized by PFR7790 coating during 30 seconds. The layers are then softly baked at 110 °C during 3 minutes. Fifthly, the layers are exposed under UV light with a mask during 3.5 seconds to etch resin, and then they are cleaned and dried (Figure V- 4 (d) and (e)). After that, the aluminum layer is etching at 30°C, and then the rest photoresist resin is removed (Figure V- 4 (f) and (g)).

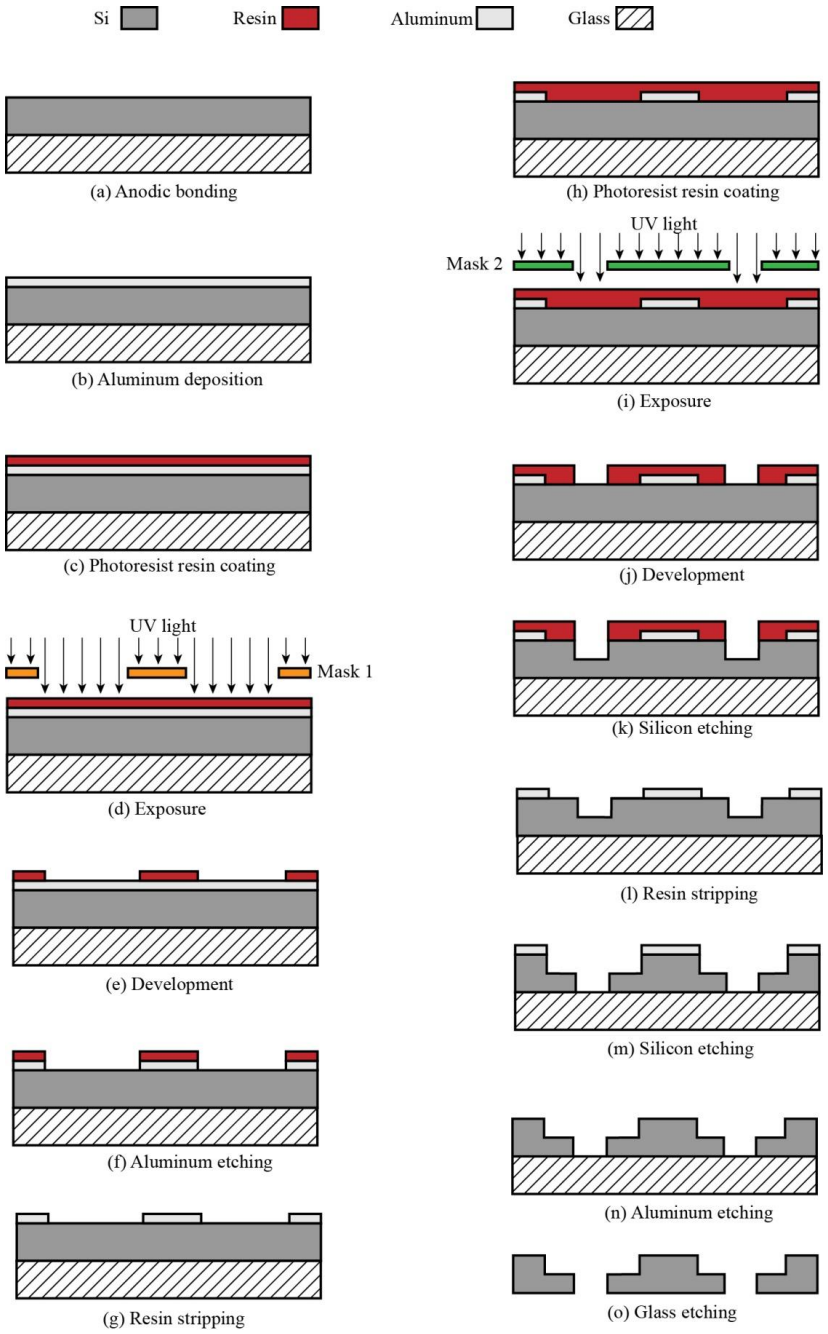

Figure V- 4: Micro fabrication process

In the second step, a new photoresist resin is firstly coated on the etched aluminum layer (Figure V- 4 (h)). Secondly, the layers are exposed under UV light with another mask to etch resin layer (Figure V- 4 (i) and (j)). Thirdly, 150 µm of the silicon layer is etched by Deep reactive-ion etching (DRIE) (Figure V- 4 (k)). Then, the resin layer is removed (Figure V- 4 (l)). Fourthly, 350 µm of the silicon layer is etched, then the aluminium layer is totally etched (Figure V- 4 (m) and (n)). At the end, the glass layer is removed and the structured plate is finally obtained (Figure V- 4 (o)). The obtained micro-fabricated parts are shown in Figure V- 5.

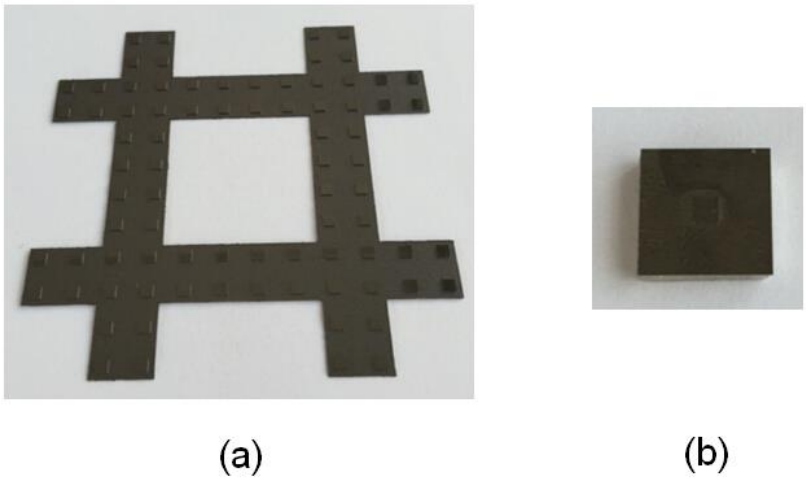

Figure V- 5: Prototype of the micro fabricated parts:
(a) Structured plate (b) Stud on MPM

In this thesis, the stroke of the DAA has been fixed at 4 mm. This value has been chosen considering the manufacturing capacity of the rapid prototyping techniques. Using micro-fabrication techniques, another group of geometrical values could be chosen (for example with 1 mm actuator stroke). With this stroke, the stud on the plate could be 0.5 mm. With a smaller stroke, the conveyance resolution of the proposed device will be directly reduced. Moreover, a DAA with an increase number of EDAs will be easily obtained in order to realize a long stroke conveyance device. The experiment with these pieces will be realized in the following work.

V.2.2 New support with holes

During the experiment, a sliding effect between the structured plate and the fixed part has been observed with high driving currents. This effect can generate studs engagement problems. To avoid this, a solution based on a new mechanical fixed support with hemispherical holes on the top side of the DAA can be proposed as represented in Figure V- 6. The structured plate should

also be modified with a hemispherical shape at the extremity of each stud. With these modifications, the manufacturing of the plate and of the mechanical support will be more complex but the positions of the structured plate will be indexed for each displacement step so that the sliding effect will be highly reduced.

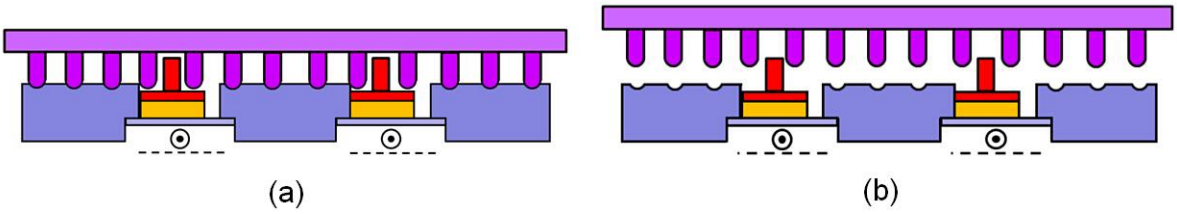

Figure V- 6: New support of DAA with structured plate

V.2.3 Control system

This part gives some perspectives to improve the positioning of the plate by acting on the control of the device in order to minimize the sliding effect or facilitate the realization of planar displacements.

V.2.3.1 Adapted control

To minimize the sliding effect of the structured plate, the control of the DAA can be adapted in order to reduce the acceleration of the MPM before it reaches the discrete position. For example, if a decreasing current pulse is used before arriving at the discrete position (Figure V- 7 (a)), the velocity of the MPM decreases, then the sliding between the MPM and the plate will be reduced. Another current pulse is also be used illustrated in Figure V- 7 (b), the input current changes to be negative before arriving at the stop, then the velocity of the MPM will be reduced immediately, the sliding will then be reduced.

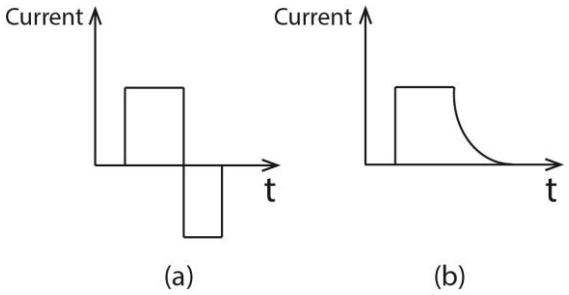

Figure V- 7: Different applications of current pulse

V.2.3.2 Control of structured plate displacement in two directions

In this thesis, the plate displacement has been experimented along one displacement axis and with only four EDAs. During experimentation, an electrical connection dedicated to the considered displacement axis has also been realized in order to simultaneously control two EDAs. These choices have been done due to experimental constraints as the limited number of available V-A converters. To realize plate displacements along x and y axes in a more flexible way and with a DAA composed of more EDAs, a multiplexer should be added between the V-A converters and the DAA (Figure V- 8). This multiplexer would be used to select (with digital outputs) the EDAs to be supplied and then the power signals (current signals) would be generated using two V-A converters (one for each displacement axis) [PETI 2014].

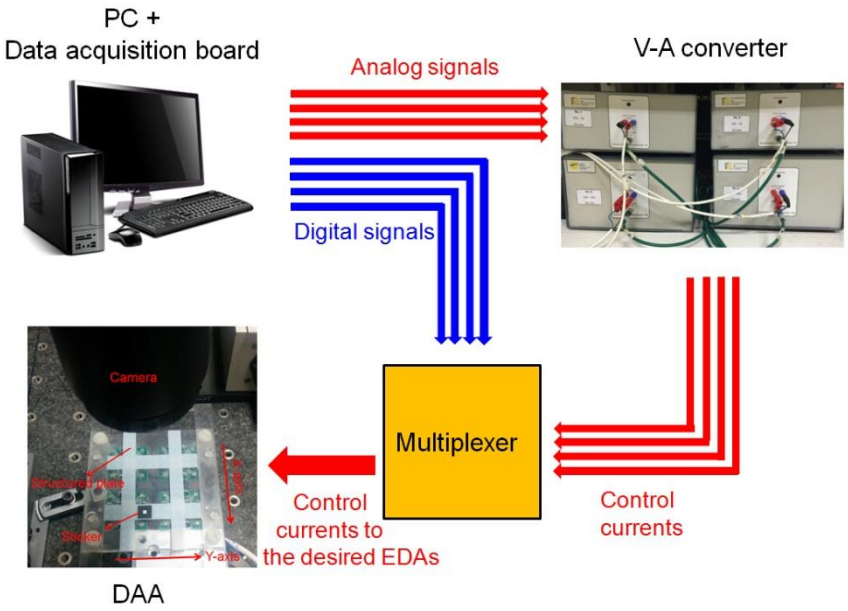

Figure V- 8: Control system with multiplexer

Annex: List of publications

[1] J. Xu, P. Huyan, L. Petit, F. Lamarque and C. Prelle, "Displacement modeling of a digital actuators array for 2D conveyance application", MECATRONICS 2014, Tokyo (Japan), November 27-30, 2014.

[2] P. Huyan, J. Xu, L. Petit and C. Prelle, "Modeling and optimization of a digital electromagnetic actuators array", IEEE/ASME International Conference on Advanced Intelligent Mechatronics (AIM), Besancon (France), July 8-11, 2014.

[3] J. Xu, L. Petit and C. Prelle, "Design and characterization of a digital actuators array with a structured plate for conveyance application", IEEE International Conference on Mechatronics and Automation (ICMA), Beijing (China), August 2-5, 2015.

[4] J. Xu, L. Petit, E. Dupon and C. Prelle, "Characterization of a conveyance device based on a digital actuators array and a structured plate", MECATRONICS – REM 2016, Compiègne (France), June 15-17, 2016.

Bibliography

[ABAD 2009] J. Abadie, N. Chaillet, C. Lexcellent, “Modeling of a new SMA micro-actuator for active endoscopy applications”. Mechatronics, International Federation of Automatic Control, 2009, vol.19(4), pp.437-442. 2008.

[AHNH 2014] H. Ahn, Y. Oh, K. Song, Y. Kim, H. Kho, M. Choi, S. Hahn, “Optimal Design of Permanent Magnetic Actuator for Permanent Magnet Reduction and Dynamic Characteristic Improvement Using Response Surface Methodology”, J. Electr. Eng. Technol., vol.10, pp.742-750, 2015.

[ATAK 2009] M. Ataka, B. Legrand, L. Buchaillot, D. Collard, H. Fujita, "Design, Fabrication, and Operation of Two-Dimensional Conveyance System With Ciliary Actuator Arrays," IEEE/ASME Transactions on Mechatronics, vol.14(1), pp.119-125, 2009.

[BENA 2007] M. Benali-Khoudja, M. Hafez, A. Kheddar, “VITAL: An electromagnetic integrated tactile display”, Displays, vol. 28(3), pp. 133-144, 2007.

[BERL 2000] A. Berlin, D. Biegelsen, P. Cheung, M. Fromherz, D. Goldberg, W. Jackson, B. Preas, J. Reich, L.-E. Swartz, “Motion control of planar objects using large-area arrays of MEMS-like distributed manipulators”, Micromechatronics’2000, 2000.

[BOHM 2000] S. Böhm, G.J. Burger, M.T. Korthorst, F. Roseboom, “A micromachined silicon valve driven by a miniature bi-stable electro-magnetic actuator”, Sensors and Actuators, vol.80, pp. 77-83, 2000.

[CARL 2000] E.T. Carlen, C.H. Mastrangelo, "Paraffin actuated surface micromachined valves," Thirteenth Annual International Conference on Micro Electro Mechanical Systems (MEMS 200), pp.381-385, 23-27 Jan, 2000

[CAZO 2008] P. Cazottes, A. Fernandes, J. Pouget, M. Hafez, “Actuation of bistable buckled beams with Macro-Fiber Composites”, IEEE/RSJ International Conference on Intelligent Robots and Systems (IROS 2008), vol. 6, pp.564-569, 2008.

[CHAL 2013] V. Chalvet, Y. Haddab, P. Lutz, “A Microfabricated Planar Digital Microrobot for Precise Positioning Based on Bistable Modules”, IEEE Transactions on Robotics, vol. 29(3), pp. 641-649, 2013.

[CHIA 2010] B.T. Chia, M. Cheng-Wen, L. Bo-Ting, S. Sun-Chih, Y. Yao-Joe, "Development of a 2×2 optical switch using bi-stable solenoid-based actuators," International Conference on Optical MEMS and Nanophotonics (OPT MEMS), pp.123-124, 9-12 Aug. 2010.

[CHEN 2005] W.-C. Chen, C. Lee, C.-Y. Wu, W. Fang, “A new latched 2 × 2 optical switch using bi-directional movable electrothermal H-beam actuators”, Sensors and Actuators A: Physical, vol.123–124(23), pp.563-569, 2005.

[COCH 2005] K.R. Cochran, L. Fan, D.L. DeVoe, “High-power optical microswitch based on direct fiber actuation”, Sensors and Actuators A, vol.119(2), pp.512-519, 2004.

[DIEP 2004] C. Dieppedale, B. Desloges, H. Rostaing, J. Delamare, O. Cugat, J. Meunier-Carus, “Magnetic bistable micro-actuator with integrated permanent magnets”, IEEE Sensors, October 24-27, 2004.

[DONG 2010] D. Lili, J. Edwards, "Closed-loop voltage control of a parallel-plate MEMS electrostatic actuator," American Control Conference (ACC), pp.3409-3414, June 30 - July 2, 2010.

[FREU 2004] M. Freudenreich, U. Mescheder, G. Somogyi, “Simulation and realization of a novel micromechanical bi-stable switch”, Sensors and Actuators A, vol.114(2-3), pp.451-459, 2004.

[FURL 2001] E.P. Furlani, “Permanent Magnet and electromechanical devices – Materials, analysis and applications”, Academic Press, San Diego, p.518, 2001.

[GIDD 2007] P. Giddings, C.R. Bowen, R. Butler, H.A. Kim, “Characterisation of actuation properties of piezoelectric bi-stable carbon-fibre laminates”, Composites Part A: Applied Science and Manufacturing, vol.39(4), pp.697-703, 2007.

[GOLL 1996] C. Goll, W. Bacher, B. Büstgens, D. Maas, W. Menz, W.K. Schomburg, “Microvalves with bistable buckled polymer diaphragms”, J. Micromech. Microeng., vol.6, pp. 77-79, 1996.

[HAGA 2005] Y. Haga, W. Makishi, K. Iwami, K. Totsu, K. Nakamura, M. Esashi, “Dynamic Braille display using SMA coil actuator and magnetic latch”, Sensors and Actuators A, vol.119(2), pp.316-322, 2004.

[HUWE 2010] H. Wei, H. Guoqing, X. Xin, X. Xiaozhu, "Modeling and Simulation of Electrostatic Comb-drive Actuators with Modelica", International Conference on Measuring Technology and Mechatronics Automation (ICMTMA), vol.2, pp.679-682, 13-14 March, 2010.

[HUSS 2014] H. Hussein, V. Chalvet, P. Le Moal, G. Bourbon, Y. Haddab, P. Lutz, "Design optimization of bistable modules electrothermally actuated for digital microrobotics”, IEEE/ASME International Conference on Advanced Intelligent Mechatronics (AIM), pp.1273-1278, July 8-11, 2014.

[HUYA 2014] P. Huyan, J. Xu, L. Petit, C. Prelle, "Modeling and optimization of a digital electromagnetic actuators array," IEEE/ASME International Conference on in Advanced Intelligent Mechatronics (AIM), pp.50-55, July 8-11, 2014.

[HUYA 2015] P. Huyan, “Réseau d’actioneurs électromagnétiques numérique : caractérisation d’une application de type convoyance et conception optimisée ”, PhD thesis, Laboratoire Roberval – Université de Technologie de Compiègne, 2015.

[JIA 2009] C. Jia, J. Zhou, W. Dong, W. Chen, “Design and fabrication of silicon-based 8×8 MEMS optical switch array”, Microelectronics Journal, vol.40(1), pp.83-86, 2008.

[KIM 2010] S.-W. Kim, J.-S. Koh, C. Maenghyo, K.-J. Cho, "Towards a bio-mimetic flytrap robot based on a snap-through mechanism," IEEE RAS and EMBS International Conference on Biomedical Robotics and Biomechatronics (BioRob), pp.534-539, Sept. 26-29, 2010.

[KHAN 2014] M.U. Khan, “Contribution to the design and fabrication of compact mechatronic systems: Application to an integrated micro-positioning

system", PhD thesis, Laboratoire Roberval – Université de Technologie de Compiègne, 2014.

[KHAZ 2010] JJ. Khazaai, M. Haris, H. Qu, J. Slicker, "Displacement amplification and latching mechanism using V-shape actuators in design of electro-thermal MEMS switches", IEEE Sensors, pp.1454-1459, Nov. 1-4, 2010.

[LIAO 2010] B.T. Liao, B.T. Chia, S.C. Shih, K.C. Fan, Y.J. Yang, "A 2 x 2 Split Cross-Bar Optical Switch Using a Hybrid Actuation Configuration", Journal of lightwave technology, vol. 28(20), 2010.

[LIU 2015] X. Liu, H. Al Hajjar, F. Lamarque, E. Doré, O. Carton, A. Zeinert, S. Charvet, "An optical wireless bistable micro-actuator," IEEE International Conference on Mechatronics and Automation (ICMA), pp.1624-1629, 2015.

[LUHA 2008] R. Luharuka, P.J. Hesketh, "A bistable electromagnetically actuated rotary gate microvalve", J. Micromech. Microeng., vol.18(3), 2008.

[MAO 2010] S. Mao, H. Wang, Y. Wu, J. Tang, G. Ding, "A latching bistable microswitch using dual-beam electrothermal actuation", IEEE International Conference on Nano/Micro Engineered and Molecular Systems (NEMS), pp.732-735, Jan. 20-23, 2010.

[MATS 2013] T. Matsunaga, K. Totsu, M. Esashi, Y. Haga, "Tactile display using shape memory alloy micro-coil actuator and magnetic latch mechanism", Displays, vol.34(2), pp.89-94, 2013.

[MENE 2006] P. Meneroud, G. Magnac, G. Patient, F. Claeyssen, "Bistable micro actuator for energy saving", ACTUATOR 2006, 10th International Conference on New Actuators, June 14-16, 2006.

[SUMA 2012] N. Suma, V.S. Nagaraja, S.L. Pinjare, K. N. Neethu, K.M. Sudharshan, "Design and characterization of MEMS thermal actuator," International Conference on Devices, Circuits and Systems (ICDCS), pp. 638-642, 2012.

[OBER 2006] J. Oberhammer, M. Tang, A.Q. Liu, G. Stemme, "Mechanically tri-stable, true single-pole-double-throw (SPDT) switches", J. Micromech. Microeng., vol.16, pp.1-8, 2006.

[PETI 2009] L. Petit, "Contribution aux techniques d'actionnement numérique Cas d'un système électromagnétique 2D", PhD thesis, Laboratoire Roberval – Université de Technologie de Compiègne, 2009.

[PETI 2014] L. Petit, A. Hassine, J. Terrien, F. Lamarque, C. Prelle, "Development of a Control Module for a Digital Electromagnetic Actuators Array," IEEE Transactions on Industrial Electronics, vol.61(9), pp.4788-4796, 2014.

[PLOT 2001] F. Plötz, S. Michaelis, R. Aigner, H.-J. Timme, J. Binder, R. Noé, "A low-voltage torsional actuator for application in RF-microswitches", Sensors and Actuators A, vol. 92, pp. 312-317, 2001.

[PORT 2008] P. Portela, P. Camanho, P. Weaver, I. Bond, "Analysis of morphing, multi stable structures actuated by piezoelectric patches", Computers & Structures, vol. 86(3–5), pp.347-356, 2008.

[RADI 1997] http://www.esrf.eu/Accelerators/Groups/InsertionDevices/Software/Radia

[ROOD 2008] B. Roodenburg, B.H. Evenblij, "Design of a fast linear drive for (hybrid) circuit breakers – Development and validation of a multi domain simulation environment", Mechatronics, vol. 18, pp. 159-171, 2008.

[SARA 2007] E. Sarajlic, D. Collard, H. Toshiyoshi, H. Fujita, "Design and Modeling of compliant Micromechanism for Mechanical Digital-to-Analog Conversion of Displacement" IEEE Transactions on Electrical and Electronic Engineering, vol.2(3), pp.357-364, 2007.

[SING 2014] Y. Singh, R.K.N.D. Rajapakse, E. Kjeang, D. Mumford, "Performance of piezoelectric actuators in a hydrogen environment: Experimental study and finite element modelling", International Journal of Hydrogen Energy, vol.40(8), pp.3370-3380, 2014.

[SONG 2007] G.-E. Song, K.-H. Kim, Y.P. Lee, "Simulation and experiments for a phase-change actuator with bistable membrane", Sensors and Actuators A, vol.136, pp.665-672, 2007.

[STAA 2011] M. Staab, H.F. Schlaak, "Novel electrothermally actuated magnetostatic bistable microrelay for telecommunication applications", IEEE 24th International Conference Micro Electro Mechanical Systems (MEMS), pp.1261-1264, Jan. 23-27, 2011.

[VITU 2009] R. Vitushinsky, S. Schmitz, A. Ludwig, "Bistable Thin-Film Shape Memory Actuators for Applications in Tactile Displays," Journal of Microelectromechanical Systems, vol.18, no.1, pp.186-194, 2009.

[WANG 2009] D.-A. Wang, H.-T. Pham, Y.-H. Hsieh, "Dynamical switching of an electromagnetically driven compliant bistable mechanism", Sensors and Actuators A, vol.149, pp.143-151, 2009.

[WUYI 2010] Y. Wu, G. Ding, C. Zhang, J. Wang, S. Mao, H. Wang, "Design and implementation of a bistable microcantilever actuator for magnetostatic latching relay", Microelectronics Journal, vol. 6, pp. 325-220, 2010.

[WIJN 2006] W. Van der Wijngaart, D. Chugh, E. Man, J. Melin, G. Stemme, "A Low-Temperature Thermopneumatic Gas Bubble Valve," IEEE International Conference on Micro Electro Mechanical Systems (MEMS), pp.198-201, 2006.

[ZAID 2011] S. Zaidi, F. Lamarque, J. Favergeon, O. Carton, C. Prelle, "Wavelength-Selective Shape Memory Alloy for Wireless Microactuation of a Bistable Curved Beam", IEEE Transactions on Industrial Electronics, vol.58(12), pp.5288-5295, 2011.

[ZHAN 2007] Y. Zhang, G. Ding, S. Fu, B. Cai, "A fast switching bistable electromagnetic microactuator fabricated by UV-LIGA technology", Mechatronics, vol.17(2–3), pp.165-171, 2007.